The mesoscale organization of Syntaxin 1A and SNAP25 at the plasma membrane

Dissertation

zur

Erlangung des Doktorgrades (Dr. rer. nat.)

der

Mathematisch-Naturwissenschaftlichen Fakultät

der

Rheinischen Friedrich-Wilhelms-Universität Bonn

vorgelegt von

Jasmin Mertins

aus

Oberhausen

Bonn 2023

Angefertigt mit Genehmigung der Mathematisch-Naturwissenschaftlichen
Fakultät der Rheinischen Friedrich-Wilhelms-Universität Bonn

1. Gutachter: Prof. Dr. Thorsten Lang

2. Gutachter: Prof. Dr. Sven Burgdorf

Tag der Promotion: 17.01.2023

Erscheinungsjahr: 2023

Eidesstattliche Erklärung

Hiermit versichere ich, dass ich die vorliegende Dissertation eigenständig und ohne unerlaubte Hilfe angefertigt habe. Es wurden keine anderen als die angegebenen Hilfsmittel verwendet. Direkt oder indirekt übernommenes Gedankengut wurde nach bestem Wissen und Gewissen kenntlich gemacht. Die Arbeit liegt in dieser oder ähnlicher Form keiner anderen Prüfungsbehörde vor.

(Datum) (Unterschrift)

Anmerkung

Teile dieser Arbeit wurden bereits in folgender Publikation veröffentlicht:

Mertins, J., Finke, J., Sies, R., Rink, M. K., Hasenauer, J., Lang, T. (2021). "The mesoscale organization of syntaxin 1A and SNAP25 is determined by SNARE-SNARE interactions." *eLife*, 2021 Nov 15; DOI: 10.7554/eLife.69236

Table of contents

List of Figures

List of Tables

Abbreviations

a.u.	arbitrary units
BSA	bovine serum albumin
ddH_2O	double distilled water
DMEM	Dulbecco's modified eagle's medium
DMSO	dimethylsulfoxid
DPBS	Dulbecco's phosphate-buffered saline
DTT	dithiothreitol
EDTA	ethylenediaminetetraacetic acid
EGTA	ethylene glycol-bis(2-aminoethylether)-N,N,N,N-tetraacetic acid
ER	endoplasmic reticulum
FRAP	fluorescence recovery after photobleaching
FWHM	full width at half maximum
GFP	green fluorescent protein
GPI	glycosylphosphatidylinositol
GPL	glycerophospholipid
HS	heparan sulfate
HSPG	heparan sulfate proteoglycan
IF	immunofluorescence
MCS	membrane contact sites
min	minute
NA	numerical aperture
PBS	phosphate buffered saline
PC	phosphatidylcholine
PCC	Pearson correlation coefficient
PFA	paraformaldehyde
PI(4,5)P_2	phosphatidylinositol-4,5-bisphosphate
PLL	poly-L-lysine

PM	plasma membrane
RFP	red fluorescent protein
ROI	region of interest
RT	room temperature
s.d.	standard deviation
SDS-PAGE	sodium dodecyl sulphate-polyacrylamide gel electrophoresis
SL	sphingolipid
SM	sphingomyelin
SNARE	soluble N-ethylmaleimide-sensitive-factor attachment receptor
STED	stimulated emission depletion
TEM	tetraspanin enriched microdomain
TIRF	total internal reflection fluorescence
TM	transmembrane
WB	western blot
YFP	yellow fluorescent protein

1 Summary

The plasma membrane is a highly crowded place consisting of a plethora of proteins and lipids, which show a high degree of micropatterning. Most proteins are not homogeneously distributed but concentrated in clusters. Moreover, clusters of different proteins group together by a yet not understood mechanism.
The two classical SNARE-proteins Syntaxin 1A and SNAP25 are one example of such proteins. Together with Synaptobrevin, they are known to catalyze neuronal exocytosis. Even though they need to form complexes for this process, they are largely segregated in the plasma membrane. Syntaxin 1A is concentrated in clusters, occupying only a small part on the plasma membrane. The more abundant SNAP25 on the other hand can be found in rather large, more widespread crowds. The cytosolic protein Munc18-1 is a key regulator of neuronal exocytosis and binds tightly to Syntaxin 1A.

In this study, we wanted to determine the relationship between Syntaxin 1A clusters and SNAP25 crowds at the plasma membrane of PC12 cells. To this end, we combined quantitative western blot for stoichiometric analysis, epitope accessibility to probe for molecule crowding and high-resolution microscopy to localize protein clusters/crowds.
Furthermore, using epifluorescence and high-resolution microscopy, we found that Syntaxin 1A is capable to redistribute the more abundant SNAP25 crowds on the plasma membrane. In particular, raising the Syntaxin 1A concentration at the plasma membrane lead to an expected increase in its cluster size and number on the membrane, whereas SNAP25 crowds interestingly became darker and more clustered. A Syntaxin 1A deletion variant where the N-terminal part of the SNARE-motif was deleted did not show this effect. By comparing different SNAP25 deletion variants we could further determine that the N-terminal motif of SNAP25 was the main facilitator of interaction with Syntaxin 1A. We conclude that Syntaxin 1A clusters

and SNAP25 crowds group together (organizing on the mesoscale) via a SNARE-SNARE-motif interaction.
Additionally, the effect of Munc18-1 on the mesoscale distribution of SNARE-proteins was analyzed as well. Experiments using recombinant Munc18-1 showed binding towards Syntaxin 1A, yet we could not detect any significant effect on the mesoscale distribution of the two SNARE-proteins.

All in all, in this study we showed that the SNARE-motif not only play an important role in the fusion of membranes, yet it also facilitates a strong protein-protein interaction which is capable organizing Syntaxin 1A clusters and SNAP25 crowds at the plasma membrane.

2 Introduction

2.1 Cellular membranes

Cellular membranes are only a couple of nanometers in width, yet without them, there would be no cell at all. The basis of all cellular membranes is a lipid bilayer. Prokaryotes (Bacteria and Archaea) only possess an outer cell membrane, they do not show any internal membranous organelles. Compared to that, Eukaryotes contain membrane-bound organelles with distinct functions and a specialized nucleus (Figure 2.1). This enhances their overall physiological efficiency, because due to compartmentalization, different biochemical reactions can take place simultaneously and in close proximity within the cell.

The plasma membrane encloses the cell from its external surrounding. Even though it is a physical barrier that encapsulates the cell, it is not a rigid structure, but highly flexible. The plasma membrane is semi-permeable, allowing for diffusion of small, uncharged molecules. It also allows for passive transport (along a concentration gradient) or active transport (energy dependent) across the membrane of charged and/or larger molecules. Next to its function as a barrier, the plasma membrane is also a place of communication. It receives and transmits signals from one side to the other, enabling the cell to react and adapt to its surroundings.

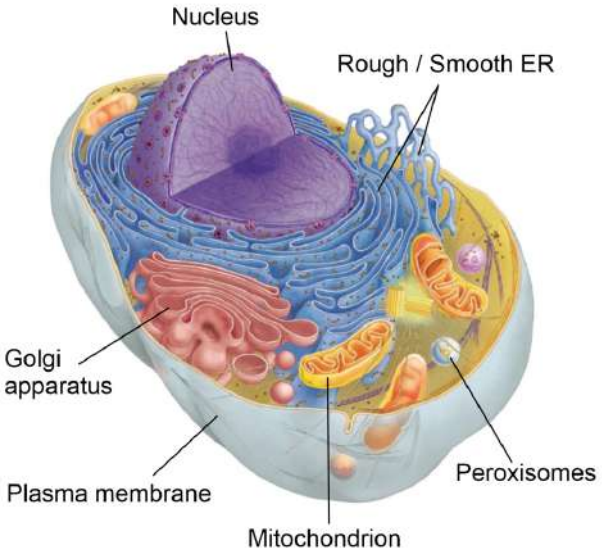

FIGURE 2.1: **Compartmentalization in the eukaryotic cell.** Schematic overview of an eukaryotic cell, with key organelles highlighted, all encapsulated by a lipid bilayer. This creates specific micro environments in the cell, leading to simultaneous biochemical reactions inside the cell. Membranes also allow active communication with the extracellular environment, which is crucial for the survival of the cell and subsequently the whole organism (modified from: Campbell et al., 2010).

2.1.1 Basic components of the membrane

Even though the functions of membranes are manifold, overall they contain only a few classes of biomolecules. The principal components of each biological membrane are lipids and proteins, as well as carbohydrate groups attached to some of them.

2.1.1.1 Lipids

Amphipathic lipids are the main structural component of the membrane. They have a small, polar headgroup and a non-polar tail. Overall, the specific lipid composition of membranes defines and changes their physical properties. We can see an asymmetric distribution of lipids between the inner and outer leaflet of the membrane. This asymmetric distribution is maintained at all times, regulating biological processes such as signal transduction. Acyl-chains from one lipid can protrude from one leaflet into the other, leading to interleaflet coupling (Nickels et al., 2015), which can affect leaflet composition (Fowler et al., 2016).

We can distinguish three major classes of lipids in eukaryotes (mentioned in decreasing order of frequency): **(i)** Glycerophospholipids (GPLs); **(ii)** Sphingolipids (SLs) and **(iii)** Sterols.

(i) Glycerophospholipids (GPLs) contain a glycerol backbone that is linked to two hydrophobic fatty acids. The fatty acid chains can vary in length and their number in double bonds. GPLs can be distinguished by their different headgroups, which are attached to the glycerol backbone via a phosphate linker. The headgroups can vary, influencing the properties of the lipid itself. Some of the most common headgroups are choline, serine, glycerol or inositol. The dominant membrane lipid in most species (except E. coli) is Phosphatidylcholine (PC), which is zwitterionic.

(ii) SLs have a similar composition as GPLs, yet they differ in their backbone. Here, the backbone is a sphingosine, where one fatty acid and a polar headgroup are linked to. The most common SLs are sphingomyelins, which contain either a phosphocholine or a phosphoethanolamine headgroup. The membranous myelin sheath that surrounds the axons of nerve cells for insulation purposes is especially rich in sphingomyelins. Furthermore, SLs can also be glycosylated to yield glycosphingolipids. Glycosphingolipids are found almost exclusively in the outer leaflet of the membrane (Fujimoto et al., 2017).

(iii) Sterols differ to GPLs and SLs in the way that their general basic structure is a four-fused-ring structure, that is nearly planar. Its derivative cholesterol is the major component in animal plasma membranes. Additionally, cholesterol is also an important precursor to other steroid hormones. Its ring-system structure makes it more rigid than other membrane lipids, therefore making it an important factor influencing the properties, specifically fluidity, of membranes.

2.1.1.2 Proteins

Proteins are the most abundant component of the plasma membrane, they constitute up to half of the overall membrane area (Lindén et al., 2012). One can generally

distinguish between two types of proteins in the membrane: **(i)** Integral or **(ii)** peripheral proteins.

(i) Integral proteins are tightly associated with the membrane by hydrophobic forces. They are either embedded into the lipid core of the membrane, with one or several membrane spanning domains (transmembrane regions, TMRs), or they are only embedded into one layer of the membrane.

(ii) Peripheral proteins only interact with the surface of the cell membrane. They can be anchored to the membrane via electrostatic interactions with lipid headgroups, hydrophobic interactions or post-translational modifications (i.e. a glycosylphosphatidylinositol (GPI) anchor).

2.2 Lateral organization of the membrane

The first model describing the organization of cellular membranes was proposed 50 years ago by Singer and Nicolson (Singer et al., 1972, Figure 2.2). In this model, the biological membrane is described as a homogeneous mixture of "proteins in a sea of lipids".
Coming from the basic fluid-mosaic model, the "lipid-raft-hypothesis" (Simons et al., 1997) changed the view of the membrane. According to Simons and colleagues, cholesterol and sphingolipids form liquid ordered phases, so-called “lipid rafts", which represent an interaction surface for proteins to attach. Rafts themselves were experimentally defined as detergent-resistant membranes (DRMs), because they survived solubilization with Triton-X 100 at 4 °C and could be isolated by density gradient centrifugation. Over the years, many controversies came up regarding the lipid-raft-hypothesis. Finally, DRMs have been shown to most likely be post-solubilization artifacts (Munro, 2003; Heerklotz, 2002; Schuck et al., 2003).
As a result of the controversies, the term “lipid raft” was re-defined by leading researchers at a 2006 symposium (Pike, 2006). This lead to a shift from speaking about "lipid rafts" to "membrane rafts". Membrane rafts were collectively defined

as highly transient, heterogeneous accumulations that compartmentalize cellular processes. Per definition, they are highly enriched in sterol- and sphingolipids and can vary in size from around 10 to 200 nm.

Still, even considering the above discussed controversies and the re-definition of the term, the phenomenon of micropatterning on the membrane is beyond debate (Figure 2.2). A different model that tries to explain the lateral in-homogeneity and movement of proteins is the "picket-fence-model". It suggests that transmembrane proteins ("pickets") are anchored to the cytoskeleton-network ("fences") thus representing barriers, which could explain hop diffusion of molecules (Kusumi et al., 1993; Kusumi et al., 2010).

When talking about micropatterning, studies also show that membrane rafts/domains exhibit a specific lateral organization between themselves, termed "mesoscale organization" (Lillemeier et al., 2006; Saka et al., 2014). Important work from Lillemeier and colleagues showed by using transmission electron microscopy of membrane sheets from T-cells that proteins assemble in certain areas (which they call "protein islands"), surrounded by protein-free regions. Protein-islands showed enrichment of cholesterol, in contrast to protein-free regions (Lillemeier et al., 2006). Later on, Saka et al. employed metabolic labeling and click chemistry in live cells as well as on membrane sheets to study the distribution of proteins on the membrane. They found that proteins were not homogeneously distributed on the membrane, yet found proteins in larger assemblies, and those assemblies were stabilized by cholesterol (supporting Lillemeier´s results). Additionally, they observed that proteins seem to prefer a specific location inside of multi-protein assembly (Saka et al., 2014).

At the moment, it can be safely concluded that most, if not all, proteins are segregated in specific areas on the membrane. The biological implications of this spatial organization can be diverse.

Using super-resolution microscopy combined with steady-state cross-correlation showed that the B-cell receptor (BCR) and the Lyn kinase (Src- family tyrosine kinase) transiently co-localize upon antigen presentation in intact cells (Stone et al.,

2015). It was further shown that BCR clustering stabilizes ordered membrane domains and enhancing the local concentration of BCRs can influence downstream signaling (Stone et al., 2017).

Accumulation of proteins have long been suggested to play a role in the infection of viruses, one example for that are Tetraspanins (Tspans). Tspans constitute a conserved family of four-span transmembrane proteins, capable of forming interactions with themselves and other membrane proteins, giving rise to so-called "Tspan-enriched microdomains (TEMs)" (Monk et al., 2012). It has been shown that Tspan CD151 and its integration into TEMs (in association with laminin-binding integrins) plays an essential role in Human papillomavirus type 16 (HPV 16) endocytosis (Scheffer et al., 2013).

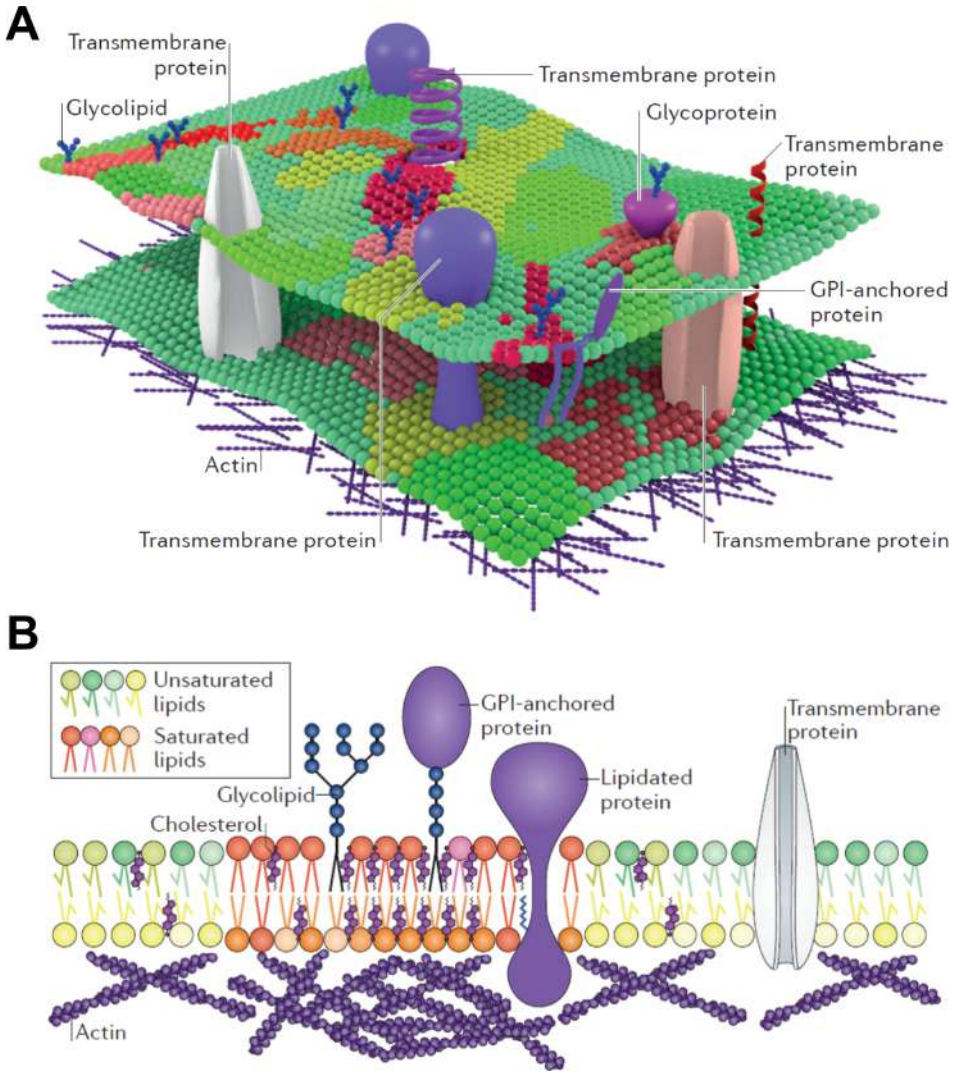

FIGURE 2.2: **Lateral organization of the plasma membrane. (A)** Lateral heterogeneity of the plasma membrane. Depicted are the main components of the membrane, lipids and proteins. **(B)** Different types of proteins (GPI-anchored protein, Lipidated protein) are enriched in domains on the membrane. They are small, highly dynamic and transient in their composition. They are enriched in saturated lipids (red to orange) which leads to changes in their physical properties such as decreased fluidity, tighter packing of molecules and specific organization (here: exclusion of a transmembrane protein). Cortical actin is also depicted, which plays a role in the lateral organization of the plasma membrane (modified from: Sezgin et al., 2017).

2.2.1 Biophysical and biochemical consequences of high protein concentrations

A characteristic property of cells is that the intracellular environment contains a very high concentration of macromolecules. Up to 40 % of the total volume inside the cell is made up of macromolecules (Chebotareva et al., 2004) (Figure 2.3 A). This very high concentration can have serious consequences on the thermodynamic activity of macromolecules due to the so-called "excluded volume" effect. This describes the phenomenon that upon tight packing of bigger macromolecules, the physical space in between them becomes unavailable for other molecules due to steric exclusion. An overview of theoretical and in-vitro studies suggested consequences of molecular crowding on the general activity of macromolecules, promotion of molecule assembly, diminishing of diffusion rates and limitation of steric accessibility (Zhou et al., 2008).

Also the plasma membrane itself has been recognized as a place of high molecular crowding more than 30 years ago (Ryan et al., 1988). As mentioned earlier (see section 2.1), the membrane is constituted of a plethora of proteins embedded in lipids, more precisely proteins occupy up to 50 % of the overall plasma membrane area (Lindén et al., 2012) (Figure 2.3 B). Consequences of this crowded environment inside the cell also hold true for the cell membrane. Crowding effects on membrane proteins have been studied with a variety of different experimental approaches. For example when using FRAP analysis in COS-7 cells, the lateral diffusion of proteins was slowed down when the total protein concentration in the membrane was increased (Frick et al., 2007). This shows that the mobility of proteins in membranes is influenced by protein-protein interactions. This result can also be observed in GUV membranes. Here, FCS measurements revealed a lowered lateral diffusion constant when increasing the protein density on the membrane (Ramadurai et al., 2009). The behaviour of isolated proteins can be described by Brownian motion (Block, 2018). Diffusion of a molecule in any bilayer is dependent on its viscosity and thickness.

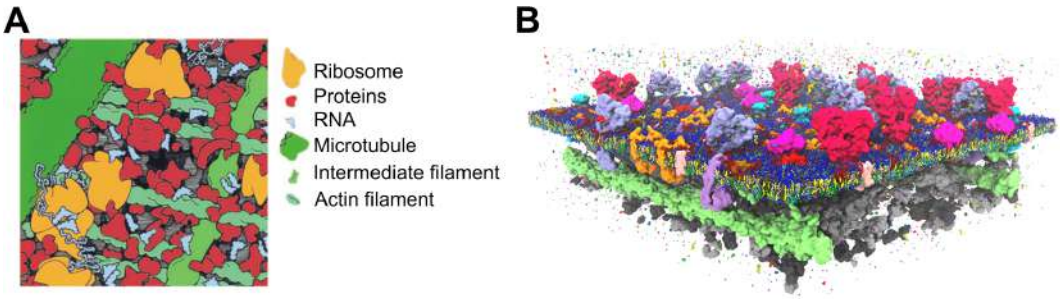

FIGURE 2.3: **Molecular crowding inside the cell and the plasma membrane.** The cell interior is filled with a plethora of different macromolecules: proteins in general, organelles of the cell (i.e. ribosomes), RNA as well as cytoskeletal elements (microtubules, actin and intermediate filaments). A significant portion of the space is occupied, making it unavailable for other molecules, leading to exclusive volume effects (modified from: Goodsell, 1992). **(B)** Modified view of the composition of the cell membrane. The principle structure remains the same, yet the amount of proteins embedded in the membrane is much higher than initially estimated (modified from: Marrink et al., 2019).

2.3 SNARE-proteins

A suitable example to study the clustering behaviour and lateral organization of proteins on the plasma membrane are proteins from the soluble N-ethylmaleimide-sensitive factor attachment protein receptor (SNARE)-family. The first SNARE-genes were identified in *Saccharomyces cerevisiae* already in 1980 (Novick et al., 1980). Since then, conserved forms of SNARE-proteins have also been found in mammals, *Arabidopsis thaliana* (Jahn et al., 2012), *Drosophila* (Littleton, 2000) and *Caenorhabditis elegans* (Richmond et al., 2002).

After their initial discovery, they were quickly found to play a key role in almost all membrane fusion steps. Structurally, all SNARE-proteins share a conserved stretch of 60-70 amino acids, termed the SNARE-motif. Membrane fusion itself is catalyzed by the assembly of SNAREs localized in opposing membranes into coiled-coil structures ("SNAREpins") to form *trans* -SNARE complexes. Assembly starts at the N-terminus of the SNARE-motifs and continues towards the C-terminus. This process is described as "zipper-like", pulling the opposing membranes into

close proximity until fusion occurs (Weber et al., 1998; Jahn et al., 2006). SNARE-pins constitute the "minimal membrane fusion machinery" as shown by experiments reconstituting SNARE-proteins into lipid bilayer vesicles and examine their mixing behavior (Weber et al., 1998).

2.3.1 Neuronal SNAREs

The neuronal SNAREs that catalyze Ca^{2+}-triggered exocytosis of secretory and small synaptic vesicles are the vesicle protein Synaptobrevin (also: VAMP; vesicle-associated membrane protein) and the plasma membrane proteins Syntaxin 1A and SNAP25 (synaptosomal-associated protein of 25kDa) (Figure 2.4 A). The fusion process involving these three proteins has been researched intensively over the last decades.

The crystal structure of the neuronal SNARE core-complex reveals a twisted formation of the four SNARE-motifs contributed from Syntaxin 1A, SNAP25 and Synaptobrevin (Sutton et al., 1998). This alpha-helical complex is largely hydrophobic, the core itself is polar. The arginine side chains extend into the asymmetric arrangement and form hydrogen bonds. The amino acids found in this layer are conserved in almost the entire SNARE-superfamily (Ossig et al., 2000).

Neuronal SNARE-proteins can further be categorized according to their central aminoacid in the fully zippered SNARE-complex, which is either glutamine (Q-SNAREs) or arginine (R-SNAREs), depending on which they contribute to the full SNARE-complex (Fasshauer et al., 1998) (Figure 2.4 B). Q-SNARE proteins are further categorized into Q_a, Q_b and Q_c-SNAREs (Bock et al., 2001). Alternatively, they can be categorized according to their membrane location: R-SNAREs are located at the vesicle membrane, giving them also the name v-SNAREs. Q-SNAREs on the other hand can be found at the target membrane, hence they are also called t-SNAREs. Yet, this does not apply in the case of homotypic fusion, where fusion occurs between membranes from the same origin (Delgado Cruz et al., 2019). The majority of t-SNAREs are anchored to the membrane via a transmembrane domain located towards the C-terminus. Alternatively, post-translational modifications facilitate membrane docking. Some SNAREs also have an independently

folded coiled-coil domain located N-terminally to the SNARE-motif.

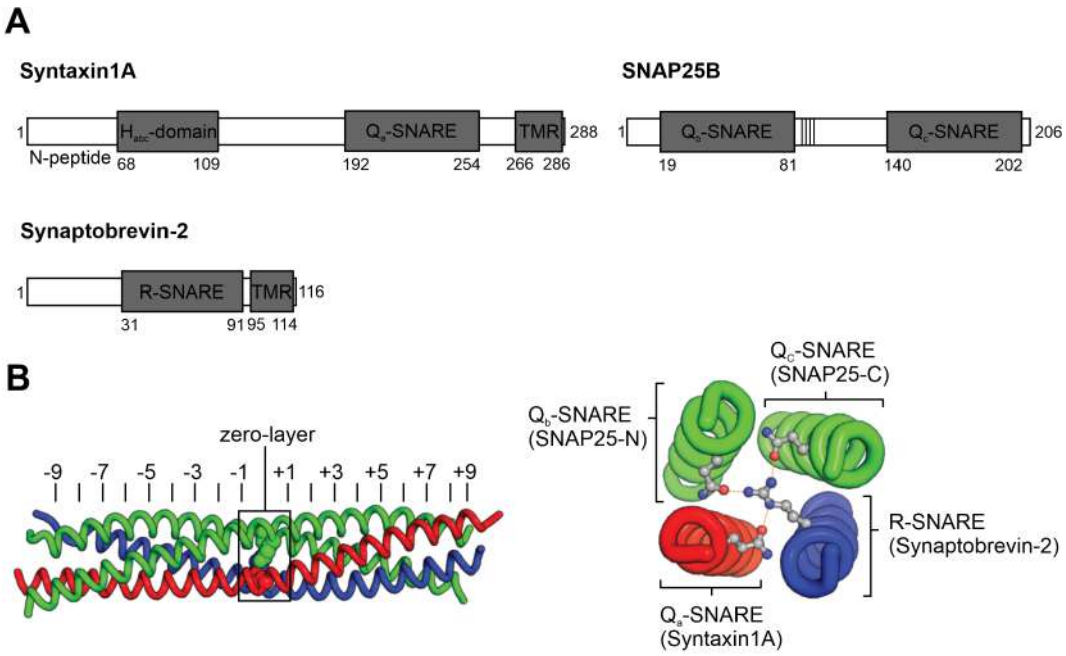

FIGURE 2.4: **Domain topology of neuronal SNAREs and assembled SNARE core-complex. (A)** The neuronal SNAREs Syntaxin 1A (Uniprot #Q16623), SNAP25 (Uniprot #P60880) and Synaptobrevin-2 (Uniprot #P63027) show a very similar topology. Each of them contains one SNARE-motif, with SNAP25 even containing two SNARE-motifs. SNAP25s palmitoylated cysteine-cluster (which is important for membrane anchoring) is shown as vertical dashes. Amino acid sequence and domain positioning according to Uniprot. Displayed is the human form of each protein. **(B)** The SNARE core-complex exhibits a twisted formation. SNAP25 (green) contributes two SNARE-motifs with one glutamine each, Syntaxin 1A (red) contributes one SNARE-motif with a central glutamine and lastly Synaptobrevin-2 (blue) contributes one motif with an arginine. From N- to C-terminus, the layers are labeled from -9 up to +9, with the zero-layer in the middle (modified from: Baker et al., 2016).

2.3.2 Syntaxin 1A

The syntaxin-family consists of 15 known genes in mammals, with a total of 18 syntaxin proteins. They were first described in 1992 as two 35-kDa proteins involved in the docking of synaptic vesicles (Bennett et al., 1992). They turned out to be Syntaxin 1A and 1B, which are located at the plasma membrane and are expressed in neuronal and secretory cells. The remaining members of the syntaxin family show a ubiquitous distribution (Teng et al., 2001).

Characteristic structural features include their C-terminal transmembrane region (TMR), with no extracellular part. The TMR is followed by a short poly-basic linker and the SNARE-motif. Another linker connects the SNARE-motif to the N-terminus end is comprised of several hydrophobic segments, which can independently fold into coiled-coil α-helical structures (Teng et al., 2001) (Figure 2.5). Some members of the family also display an additional small N-terminal peptide (Dulubova et al., 2003).

In Syntaxin 1A, the N-terminal domain is known as the H_{abc}-domain (Fernandez et al., 1998) and folds back onto the SNARE-motif when its isolated (Dulubova et al., 1999). This so-called "closed conformation" renders the protein inaccessible for further interactions with SNAP25 and consequently SNARE-complex assembly. A later study specified that isolated Syntaxin 1A switches independently between open and closed states on a sub-millisecond time scale (Margittai et al., 2003) (Figure 2.5, left side). This conformational change apparently plays a key role in the regulation of synaptic transmission.

Syntaxin 1A can also be found in tightly packed clusters on the plasma membrane, containing roughly several dozens of molecules with a cluster diameter of around 70 nm (Figure 2.5, right side). These assemblies are highly dynamic with single syntaxin-molecules entering and exiting a cluster (Sieber et al., 2007).

2.3.3 SNAP25

Shortly after its initial discovery (Oyler et al., 1989), SNAP25 was isolated as part of the SNARE-complex confirming its importance in exocytosis (Söllner et al., 1993). It is the founding member of the sub-family of proteins which can mostly be found in the post-Golgi secretory pathway (Kádková et al., 2019). In vertebrates, SNAP23, SNAP25, SNAP29 and SNAP47 could be identified to be expressed in neurons (Arora et al., 2017).

Compared to other SNARE-proteins, SNAP25 contains two SNARE-motifs which it contributes to the SNARE-complex necessary for membrane fusion. When not engaged in a complex, the SNARE-motifs are largely unstructured and only become

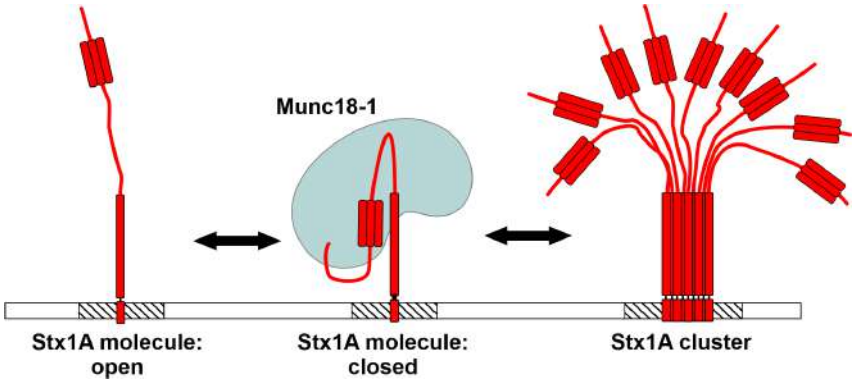

FIGURE 2.5: **Syntaxin 1A conformations and clustering.** Diagram showing the different conformations that Syntaxin 1A is able to adapt. **Left side:** Syntaxin 1A in its open conformation. In isolation, Syntaxin 1A switches independently between the open and closed conformation. **Middle part:** The single molecule is shown bound by Munc18-1, locking it into the closed conformation. **Right side:** When engaged in a cluster, Stx1A is in its open conformation. Striped rectangles represent cholesterol-enriched membrane regions. Black arrows in between diagrams represent the fact that all conformations are reversible.

alpha-helical upon association with Syntaxin 1A (Fasshauer et al., 1997b). Almost all of SNAP25 resides in the plasma membrane, only 20 % is found in a perinuclear recycling endosome-trans-Golgi network (Aikawa et al., 2006). Attachment to the membrane is mediated by palmitoylation of four cysteines close to the N-terminal SNARE-motif (C85, C88, C90 and C92; see vertical dashes in Figure 2.4 A) (Hess et al., 1992). The two existing splice variants SNAP25A and SNAP25B differ only in nine amino acids (Bark et al., 1994). SNAP25A is the main isoform in adrenal chromaffin cells (Grant et al., 1999), whereas SNAP25B is developmentally regulated and the main isoform in the adult brain (Boschert et al., 1996).

SNAP25 is organized in clusters on the membrane that are dependent on cholesterol (Chamberlain et al., 2002). Estimates of SNAP25 per cluster range between 40-50 (Rickman et al., 2010) and 50-70 molecules (Knowles et al., 2010).

2.3.4 Regulatory SM-proteins

Other proteins involved in the fusion of membranes are the so-called Sec1/Munc18-like (SM) proteins, whose different members can be found in all eukaryotes (Toonen et al., 2003). They are hydrophilic proteins and located in the cytoplasm. Structural

information is available for eight members, which show a highly conserved topology. Each one consists of three distinct domains (Domains 1, 2, 3a and b) which arrange into an arch-shaped form (Archbold et al., 2014) (Figure 2.5, middle part).

2.3.4.1 Munc18-1

The best characterized member of this family is Munc18-1, also known as STXBP1 (syntaxin binding protein) or n-Sec1. Initial studies showed that Munc18-1 is able to bind tightly to Syntaxin 1A in its closed conformation, where the H_{abc}-domain is folded over onto the SNARE-motif and the central cavity of Munc18-1 clasps around it with dissociation constants in the nanomolar range (Pevsner et al., 1994; Misura et al., 2000). This lead to the hypothesis of Munc18-1 being a negative regulator of exocytosis by inhibiting the assembly of the SNARE-complex (Wu et al., 2001). Surprisingly, this was in contrast to another study, which showed that a complete knock-out of Munc18-1 lead to a total loss of synaptic transmission in neurons, without affecting brain development (Verhage et al., 2000).
In-vivo studies proved that Syntaxin 1A is still able to assemble into SNARE-complexes even in the complete absence of Munc18-1 (Toonen et al., 2005), suggesting a function further downstream. For example, studies showed that Munc18-1 is important in the docking of LDCV (large dense core vesicles) to the membrane (Voets et al., 2001; Toonen et al., 2006).
A multitude of studies examined the binding of these two proteins in detail: Additionally to binding a closed conformation of Syntaxin 1A, Munc18-1 is also able to bind to Syntaxin 1A in its open conformation (Burkhardt et al., 2008, Colbert et al., 2013) via a conformational adjustment of domain 3 (Munch et al., 2016), most likely by interacting with its N-peptide (Shen et al., 2010; Pertsinidis et al., 2013). Furthermore, Munc18-1 also seems to be able to bind to Syntaxin 1A when it is already engaged in a fully assembled SNARE-complex (Syntaxin 1A / SNAP25 / Synaptobrevin) (Dulubova et al., 2007; Shen et al., 2007), even though it was shown that the binding affinity from Munc18-1 to an assembled SNARE-complex is significantly reduced in isolation (Burkhardt et al., 2008). The specific regions of interaction of Munc18-1 and Syntaxin1A have been examined in detail (for a detailed

overview of important mutations that influence Syntaxin 1A- and/or its interaction with Munc18-1, see Figure 2.6).

Although the interaction and function of Munc18-1 has been studied in detail (and in various different experimental systems such as *in-vivo* mouse models, liposome reconstitution or proteins in isolation), there is yet no conclusive answer. Most recent studies propose a function of Munc18-1 (in close collaboration with Munc13) in stabilizing the *trans*-SNARE-complex against dissociation via NSF/αSNAP (He et al., 2017; Prinslow et al., 2019). Taken together, Munc18-1 binding of Syntaxin 1A could stabilize SNARE-complexes and thus influence exocytosis.

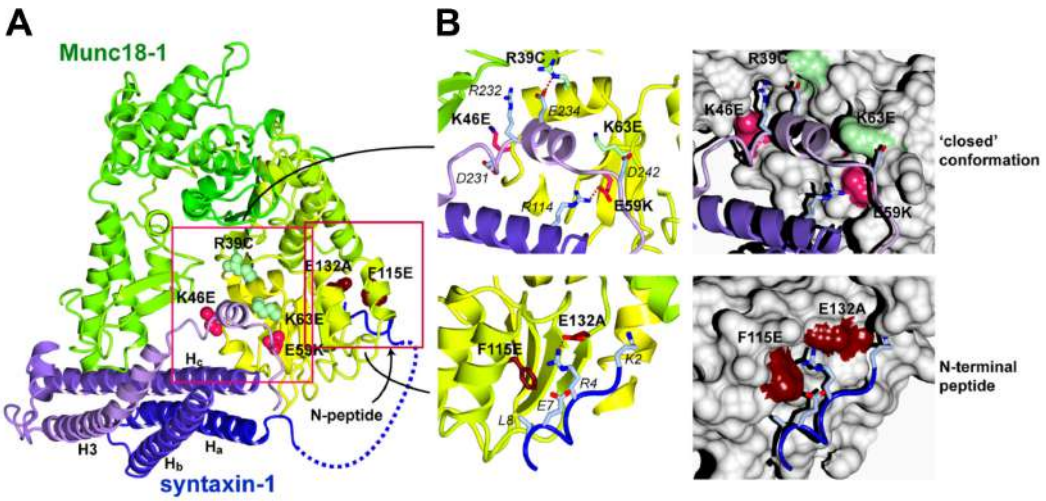

FIGURE 2.6: **Munc18-1/Syntaxin 1A complex structure. (A)** Ribbon representation of Munc18-1/Syntaxin 1A complex structure. Syntaxin 1A is shown in different shades of blue, the connecting loop between the H_{abc}-domain and the N-peptide is shown as a dashed line. Munc18-1 is shown in different shades from green (N-terminus) to yellow (C-terminus). **(B)** Ribbon and surface representation of the interaction surfaces between Munc18-1 and Syntaxin 1A, studied mutations in Munc18-1 are written in bold letters. **Upper panel:** Closed conformation; Double mutation K46E/E59K (magenta) inhibits binding with syntaxin´s closed conformation and reduces plasma membrane localization of Syntaxin 1A. Point mutations R39C and K63E (mint) do not seem to influence binding to Syntaxin 1A, even though R39 forms a salt bridge with syntaxin´s H_{abc}-domain and K63 interacts with syntaxin´s H3-helix. **Lower panel:** N-terminal peptide interaction in the hydrophobic pocket on the outer surface of Munc18-1; Double mutation F115E/E132A (dark red) dramatically reduces Munc18-1 binding to Syntaxin 1A in a SNARE-complex, yet only reduces the binding slightly to free syntaxin-molecules (Malintan et al., 2009). (Figure and legend modified from: Han et al., 2009)

2.3.5 SNARE-cycle

The meticulous interplay between Synaptobrevin, Syntaxin 1A and SNAP25 to form a tight complex is important to bring two membranes together and ultimately leads to the release of neurotransmitter or peptide hormones into the synaptic cleft. This process is strictly regulated by several other accessory proteins.

The process starts with an acceptor-complex at the plasma membrane (Figure 2.7 A). *In-vitro* studies suggest that SNARE-complex assembly probably starts with an at least partially arranged Q-SNARE acceptor-complex on the plasma membrane (Jahn et al., 2006). Other resources argue that a complex between closed Syntaxin 1A and Munc18-1 is the starting point (Rizo et al., 2015). Even though there has been a lot of research regarding the starting point, it is not conclusively known (hence why Figure 2.7 A illustrates both conformations).

Yet, continuing from the acceptor-complex, according to the zipper-hypothesis (Hanson et al., 1997), the SNARE-complex assembly starts at the N-terminus of the SNARE-motif, first leading to a loose *trans*-complex association (Figure 2.7 B). Once the reaction grows further towards the C-terminus, the full *trans*-complex (Figure 2.7 C) is formed and the opposing membranes are pulled closer together until fusion. The *cis*-SNARE complex is present post-fusion and is characterized by the TMR from Syntaxin 1A and Synaptobrevin being located in the same bilayer (Stein et al., 2009).

After fusion (Figure 2.7 D), the complex is disassembled by the ATPase n-ethylmaleimide-sensitive factor (NSF) together with several molecules of the adaptor protein soluble NSF attachment protein (here: isoform α-SNAP) (Block et al., 1988; Weidman et al., 1989), the SNARE-proteins are recycled and used for another fusion round (Jahn et al., 2006).

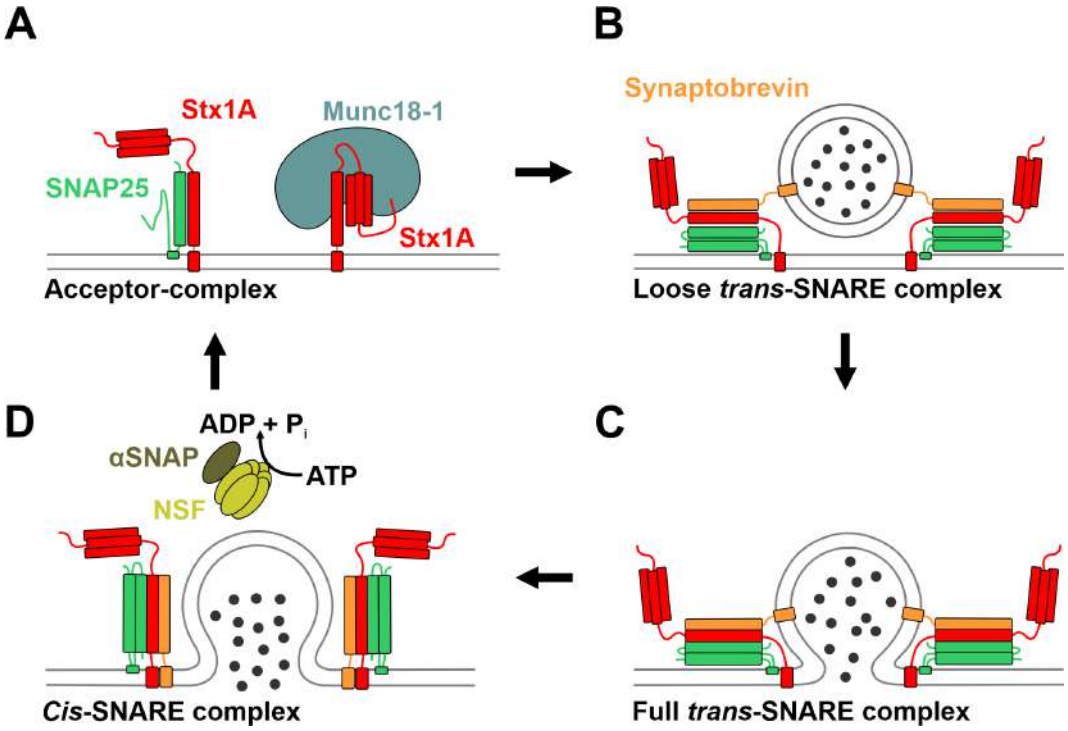

FIGURE 2.7: **Schematic model of the SNARE-cycle. (A)** Before synaptic vesicle exocytosis takes place, an acceptor complex is formed. Here, two proposed alternatives are shown side by side (see section 2.3.5). **(B)** Proceeding from the acceptor-complex, a partially arranged, loose *trans*-SNARE complex is formed. With the help of regulatory proteins the synaptic vesicle is primed for fusion. **(C)** Upon Ca^{2+}-influx (Synaptotagmin-1 acts as the Ca^{2+}-sensor (Fernández-Chacón et al., 2001)), the full *trans*-SNARE complex is assembled and pulls the membranes into close proximity until fusion. The fusion pore opens and expands, releasing neurotransmitter into the synaptic cleft. **(D)** Afterwards, the *cis*-SNARE complex is disassembled by the ATPase NSF and its partner αSNAP by an ATP-dependent mechanism. The vesicle is recycled as well. For reasons of simplicity, not all regulatory proteins are shown in detail here.

2.3.6 SNARE-clustering on the membrane

SNARE-proteins are highly abundant proteins in the presynaptic membrane of synapses (Wilhelm et al., 2014) as well as in the plasma membrane of neuroendocrine PC12 cells (Sieber et al., 2007; Knowles et al., 2010).
Specific molecule numbers of SNAREs on the plasma membrane have been examined by different groups. For Syntaxin 1A, values from 540 molecules/μm^2 (Knowles et al., 2010) up to around 1800 molecules/μm^2 (Sieber et al., 2007) at the plasma membrane of PC12 cells are reported. Differences in numbers are most likely due to different experimental approaches in determining the plasma membrane surface area of PC12 cells. In their 2010 study, Knowles et al. also determined the number of SNAP25 molecules at the plasma membrane, which where around 7500 molecules/μm^2, resulting in a roughly 14-fold surplus of SNAP25 at the plasma membrane. Interestingly, at synaptic boutons of rats, the SNAP25 to Syntaxin 1A ratio is only 1.3 (Wilhelm et al., 2014).

Regarding their lateral distribution on the plasma membrane, Syntaxin 1A and SNAP25 can be found in clusters or crowds, respectively (Chamberlain et al., 2001; Lang et al., 2001).
For Syntaxin 1A clustering, the most information is available in the literature. It is located in tightly packed clusters (Figure 2.5, right side) comprised of several dozens of molecules with a diameter of 70 nm (Sieber et al., 2007; Knowles et al., 2010; Rickman et al., 2010), showing an internal density gradient (Bar-On et al., 2012). Homo-oligomerization occurs mainly via tight interactions from the SNARE-domain itself (Merklinger et al., 2017), which also facilitates the interaction with SNAP25 in the plasma membrane. Syntaxin 1A molecules are very dynamic, exchanging between clusters (Sieber et al., 2007) and reversibly accumulating underneath docked granules (Barg et al., 2010).

For SNAP25 on the other hand, less information is available regarding its distribution on the plasma membrane. Clustering is generally cholesterol dependent (Chamberlain et al., 2001) and independent from its SNARE-motifs (Halemani et al., 2010). Studies found that SNAP25-crowds are larger than that of Syntaxin 1A (SNAP25 mean diameter 130 nm vs Stx1A mean diameter 93 nm) and were also more elliptical shaped when employing TIRF-microscopy combined with dSTORM-imaging of PC12 cells. Additionally, SNAP25-crowds showed more overlap with other SNAP25-crowds than reported for Syntaxin 1A clusters (Bar-On et al., 2012). They are also highly dynamic (as already mentioned for Syntaxin 1A), with freely diffusing molecules in the membrane in balance with clustered molecules (Bar-On et al., 2012). Furthermore, crowds of SNAP25 are observed changing in their size or even completely disappearing (Antoku et al., 2015).

In solution, Syntaxin 1A and SNAP25 are interacting, exhibiting different complex configurations. Earliest studies found that a 2:1 $(Stx1A)_2$:SNAP25 complex can form, where each of SNAP25´s SNARE-motifs interacts with one Syntaxin 1A (Fasshauer et al., 2004). In this configuration, Synaptobrevin binding is inhibited. This "dead-end-complex" is probably an off-pathway of the fusion reaction. In a later study employing liposome fusion assays, this kinetic dead-end-complex was avoided by increasing the ratio of SNAP25 to Syntaxin 1A. Additionally, stabilizing the 1:1 hetero-complex with a small fragment of Synaptobrevin increased fusion rates (Pobbati et al., 2006).
FRET-studies at the plasma membrane of living PC12 cells detected two types of Syntaxin 1A/SNAP25 complexes. A two-helix complex between the N-terminal SNARE-motif of SNAP25 and syntaxin´s SNARE-motif has been reported or a three helix complex between Syntaxin 1A and SNAP25´s SNARE-motifs (thus the previous mentioned 1:1 Syntaxin 1A/SNAP25 heterodimer). Interestingly, these two complexes were spatially separated in different cluster populations (Rickman et al., 2010). Until now, no conclusive evidence was found for the existence of the 2:1 $(Stx1A)_2$:SNAP25 dead-end-complex in native membranes of PC12 cells.

2.3.6.1 Physiological role of clusters

The function and underlying nature of the organization of the clusters/crowds has been topic of research for quite some time. Different functions especially of syntaxin-clusters are debated in the literature (Bogaart et al., 2013).

Some early studies suggested that Syntaxin 1A clusters define vesicle docking and fusion sites (Lang et al., 2001; Ohara-Imaizumi et al., 2004). It was also found to reversibly cluster underneath docked granules (Barg et al., 2010). Efficient fusion was found to require at least three assembled SNARE-complexes (Mohrmann et al., 2010; Heo et al., 2021). Tight syntaxin-clusters could also enhance the recycling of *cis*-SNARE complexes leading to faster re-establishing of the fusion site (Bar-On et al., 2008).

Another thought is that clustering of Syntaxin 1A in homo-oligomeric clusters might be a way to promote the reactive 1:1 heteromeric complex and avoid the dead-end-complex, by shielding syntaxin´s reactive SNARE-motif inside of the tightly packed cluster (Figure 2.5, right side). Thus, molecules inside the cluster are inaccessible for SNAP25.

A lot of the research regarding syntaxin-clustering was done in PC12 cells, where exocytosis can theoretically occur all over the plasma membrane. In comparison to that, exocytosis at synapses is mainly confined to a specialized membrane, the so-called "active zone" (AZ). Studies looking directly at syntaxin´s localization and mobility at the AZ and outside of it (using the NMJ of Drosophila), found syntaxin-clusters to be larger in diameter (increase up to around 25 %) as well as a slower diffusion rate (Ullrich et al., 2015). They conclude from this, that syntaxin-clusters outside of the AZ might act as "reserve pools" from where more syntaxin molecules could be recruited to the AZ. A similar observation regarding the decrease in mobility of Syntaxin 1A was already made in FRAP-experiments at the AZ in rat spinal cord neurons (Ribrault et al., 2011).

2.3.6.2 Mechanisms of clustering

Regarding the formation of clusters/crowds of Syntaxin 1A and SNAP25, several mechanisms are thought to likely play a role, which will be exemplified in the following:

Role of cholesterol

Earlier studies employing different cell lines suggested enrichment of SNAREs in detergent-resistant membranes (DRMs) (Lafont et al., 1999; Chamberlain et al., 2001; Chamberlain et al., 2002; Salaün et al., 2005). Over the years, the general believe in DRMs has been questioned, due to a lot of controversies in the literature and the relative unspecific parameters that define DRMs. Cholesterol specifically is an important regulator of SNARE-cluster integrity. In neuronal PC12 cells, depletion of cholesterol dissolves SNARE-clusters and inhibits exocytosis (Lang et al., 2001). The same effects could also be observed in lung epithelial cells (Chintagari et al., 2006) and endothelial cells (Predescu et al., 2005). However, it is not completely clear whether disruption of SNARE-clusters due to cholesterol depletion and inhibition of exocytosis directly correlate.

On the other hand, using different experimental parameters, other studies could show that SNAREs could not be associated with classical raft markers such as Thy-1 (also: CD90; Glycoprotein attached to the outer surface of the PM) (Lang et al., 2001) or Flotillin-1 (peripheral membrane protein) (Ohara-Imaizumi et al., 2004). Yet, reconstitution of SNAREs into giant unilamellar vesicles showed that they preferentially aggregated in the liquid-disordered/non-raft phase (Bacia et al., 2004). Interestingly, Syntaxin 4 (important for constitutive exocytosis) organizes in clusters distinct form Syntaxin 1A (Sieber et al., 2006) which are still intact after depletion of cholesterol (Low et al., 2006). Separation of syntaxin´s into different clusters can in part be explained by local hydrophobic mismatch in the membrane due to a slightly longer TMD from Syntaxin 4 (1-2 residues longer depending on the species) (Milovanovic et al., 2015). Taken together, cholesterol is in general important for membrane micropatterning (Saka et al., 2014), thus probably also affecting

SNARE-protein behaviour.

Protein-protein interactions

Yet, clustering is also dependent on homophilic protein-protein interactions. Especially in syntaxin-clusters, the interaction between the SNARE-motif is crucial for homophilic clustering (Sieber et al., 2006). Raising the calcium concentration in PC12 cells leads to a significant increase in Syntaxin 1A clustering on the membrane (Zilly et al., 2011). SNAP25 also clusters in an ion concentration dependent manner on the plasma membrane (Batoulis et al., 2016).

Syntaxin 1A is connected to actin via the adaptor protein Myosin-Va in chromaffin cells (Watanabe et al., 2005). SNAP25 organization is influenced by the actin cytoskeleton as well (Torregrosa-Hetland et al., 2013).

Additionally, heterophilic interactions mediate the sorting of proteins into spatially distinct clusters on the mesoscale. In non-polarized MDCK cells, Syntaxin 3 has been shown to interact with microtubules, whereas Syntaxin 4 is dependent on actin filaments (Low et al., 2006).

Protein-lipid interactions

Ionic interactions between macromolecules and lipids also influence the clustering behaviour of SNAREs. In PC12 cells and reconstituted lipid bilayers, Syntaxin 1A is clearly associated with PI(4,5)P_2 enriched regions in the membrane via a cluster of positively charged amino acid residues (^{260}KARRKK^{265}) located close to the TMD (Van Den Bogaart et al., 2011; Murray et al., 2011).

2.3.7 Technical approach to study membranes

Studying plasma membrane components is not as straightforward as one might expect. As mentioned before, the plasma membrane is a highly crowded place with protein-protein and protein-lipid interactions, which are important for the integrity and function of the membrane itself.

A detergent-based approach to study the plasma membrane and its components has the disadvantage that it disrupts the overall structure and is also able to induce ordered domains (Heerklotz, 2002). Regarding structural analysis at high resolution, membrane proteins are also harder to crystallize due to their hydropbic nature, flexibility and instability. Only around 4 % of all deposited structures in protein databases belong to membrane proteins (see entries in PDB; //www.rcsb.org/ and PDBTM; //pdbtm.enzim.hu/).

Imaging proteins in the plasma membrane using microscopic methods has become very popular because it leaves the membrane environment intact and also gives important spatial information. However, one major disadvantage of this approach is the intracellular fluorescence of the cell. One approach to overcome this, is the use of confocal microscopy. Here, a pinhole in front of the detector blocks light from outside of the focal plane. This eliminates unwanted background signal, i.e. from the inside of the cell. Another microscopy approach is "Total internal reflection microscopy" (TIRF) microscopy, which achieves less background signal by restricting the illumination only to the plasma membrane itself.

One approach that leaves the physiological environment intact, yet still allows us to visualize membrane proteins at a high signal-to-noise ratio, is the so-called "cell unroofing" technique.

Additionally, the lateral size of membrane domains requires a technique that is able to resolve such small structures. For this study, we combined the approach of native plasma membrane sheets with sub-diffraction STED-microscopy to analyze the mesoscale distribution of SNARE-proteins.

2.3.7.1 Plasma membrane sheets

Because we are focusing on proteins primarily located at the plasma membrane, we can use plasma membrane sheets to study the localization and behaviour of SNARE-proteins in their physiological environment. This techniques leaves weak and transient interactions intact.

This approach was first used in the 70s for electron microscopy experiments (Vacquier, 1975) and improved over the following years. Generally, a mechanical force is used to rip-off the apical part of the cell, leaving behind only the basal plasma membrane attached to the substrate (Figure 2.8). Employing plasma membrane sheets has several different advantages. Generating membrane sheets only takes seconds and is achieved without any other detergents. Thus, it shows a physiological snapshot with no disruptions. Furthermore, the cytoplasmic side of the basal membrane is exposed and thus readily available for subsequent labeling or other treatments. Lastly, background fluorescence is completely absent which makes it easy to use for microscopy studies. Membrane sheets in combination with fluorescence microscopy have been used extensively studying exocytosis of secretory granules at the plasma membrane from PC12 cells (Avery et al., 2000; Holroyd et al., 2002) or examining the lateral distribution of proteins in general (Lang et al., 2002).

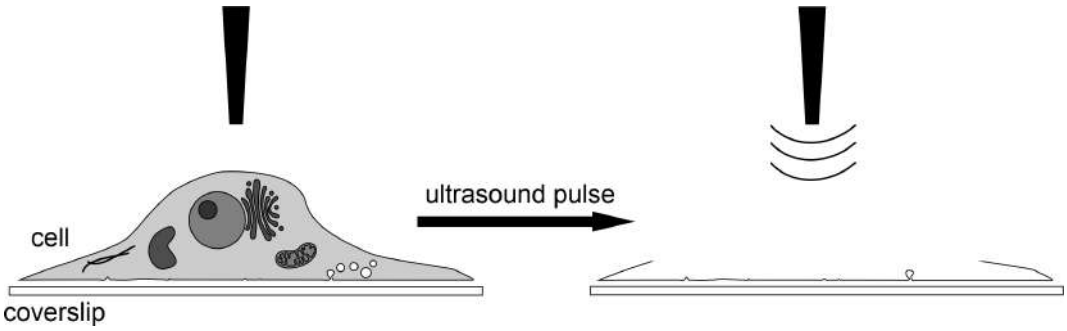

FIGURE 2.8: **Generating plasma membrane sheets.** To generate native plasma membrane sheets for microscopy, cells are first seeded on a coverslip prior to the experiment (left side). Then a short ultrasound pulse is applied to the top of the cell, subsequently ripping off the top part of the cell (right side). The cytoplasm with its organelles are removed, leaving behind only the basal plasma membrane. Proteins and lipids embedded in the basal plasma membrane are now readily accessible for either further experiments or direct fixation and subsequent immunostaining.

2.3.7.2 STED-microscopy to visualize nanodomains

In order to visualize nanodomains on the plasma membrane, we need to employ high-resolution microscopy. Conventional diffraction limited microscopy is not able to properly resolve the lateral dimensions of nanodomains.

The concept of Stimulated Emission Depletion (STED) microscopy (Wichmann et al., 1994) (for more technical details see Figure 2.9) was the first successful approach to overcome the physical diffraction limit in optical microscopy set by Ernst Abbe over 100 years ago. This achievement was even honored by the Nobel Prize committee in 2014 due to its far reaching impact in the scientific community.

Since then, more and more groups are routinely using STED-microscopy to analyze biological structures and processes beyond the diffraction limit, leading to new insights from cellular components, such as organelles or cytoskeletal elements (Sahl et al., 2017) to imaging live brain tissues (Calovi et al., 2021).

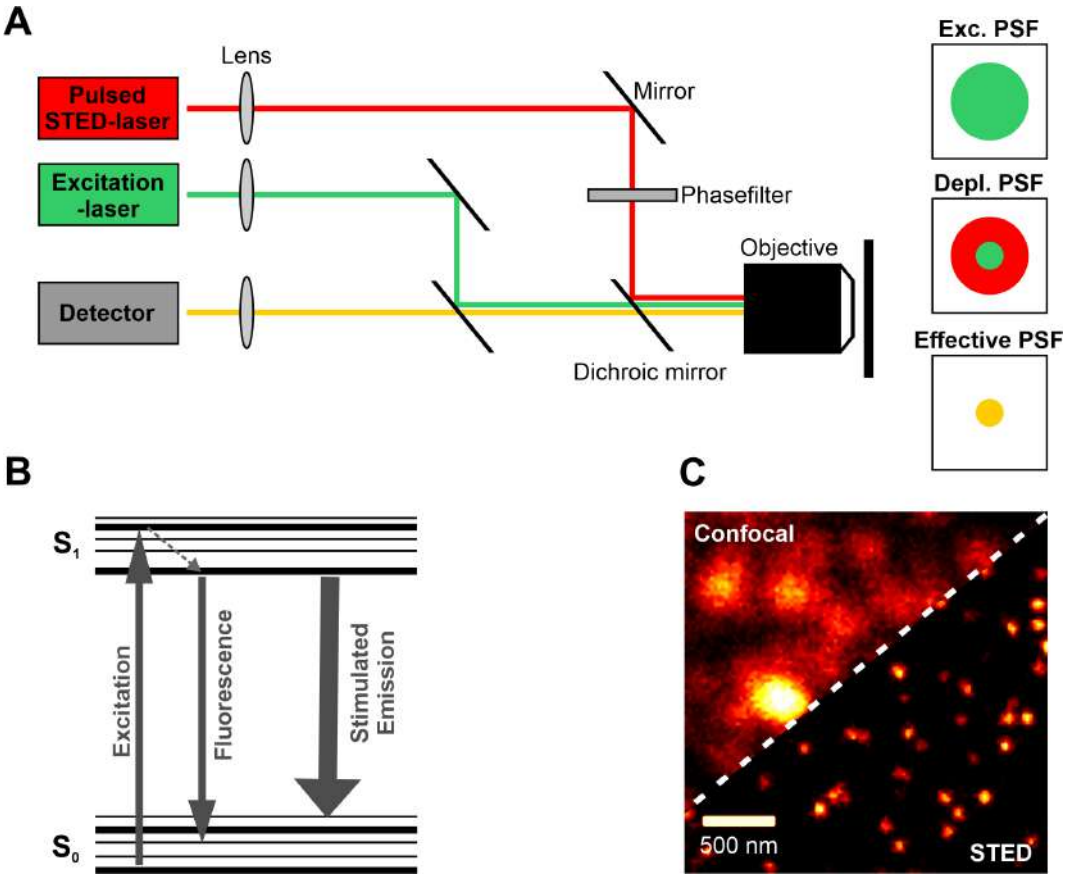

FIGURE 2.9: **Overview of STED-microscopy.** The general principle behind STED-microscopy is to prevent peripheral fluorophores from participating in image formation and thereby enhancing the lateral resolution. **(A)** Diagram of a STED-microscope light path, based on a confocal microscope (left side). The excitation spot (green) which is still diffraction limited, the doughnut-shaped depletion laser (red) which reduces the lateral PSF size by depleting exited states at the periphery of the excitation spot and the remaining effective PSF (yellow), now beyond the diffraction limit (right side). **(B)** Simplified Jablonski diagram of the electronic states of a molecule. Fluorescence in general occurs when a fluorophore is excited from its electronic ground state into a higher energy level (S_0 to S_1, arrow "Excitation") induced by the excitation laser. After initial vibrational relaxation (dotted arrow), the fluorophore relaxes and thereby emits detectable light (S_1 back to S_0, arrow "Fluorescence"). The high energetic depletion laser disrupts this process and forces the photons to be released in a red-shifted state, allowing it to be spectrally separated (S_1 to slightly higher energy level of S_0, arrow "Stimulated emission"). **(C)** Example image of a PC12 plasma membrane sheet stained for endogenous Syntaxin 1A (employing αHPC-1 antibody coupled with AF594), highlighting the achieved improvement in resolution.

3 Aim of the study

Micropatterning of proteins on the plasma membrane is a scientifically accepted concept. However, very little is known about the mechanisms underlying mesoscale organization. Using the two classical SNARE-proteins Syntaxin 1A and SNAP25 as an example, we examined how protein clusters/crowds mutually influence each other. Furthermore, the influence of other accessory proteins such as Munc18-1 on the lateral distribution is also undetermined.

(i) The first aim was to study the Syntaxin 1A-SNAP25 mesoscale network on the plasma membrane of PC12 cells. In order to do this, epifluroescence and high-resolution microscopy was employed to characterize the lateral distribution on membrane sheets. Deletion constructs of Syntaxin 1A and SNAP25 were characterized to further specify interacting domains.

(ii) The second aim was to identify which role the accessory protein Munc18-1 plays on the mesoscale distribution of SNARE-proteins on the plasma membrane.

4 Material and Methods

4.1 Material

4.1.1 Technical appliances

Equipment	Manufacturer	Application
Spectrophotometer: NanoDrop2000	ThermoFisher Scientific, Waltham, USA	measuring DNA concentration
Gel imager: Odyssey® CLx Imaging System	LiCor,Lincoln, USA	Western blot imaging
Sonicator: Sonopuls HD 2070	Bandelin, Berlin, Germany	Generating PM sheets
NEON™ Transfection System	ThermoFisher Scientific Waltham, USA	Transfection of cells
Inverted bright-field microscope: ECLIPSE TS100, CFI60 Infinity Optical System	Nikon, Tokyo, Japan	Cell culture
Inverted Olympus IX-81-ZDC, MT20E illumination system	Olympus, Tokyo, Japan	Epifluorescence Imaging
STED-module in combination with Olympus IX-83 confocal microscope	Abberior Instruments, Göttingen, Germany / Olympus, Tokyo, Japan	Confocal and STED micros-copy

TABLE 4.1: Technical appliances.

4.1.2 Cell lines

PC12 cells

PC12 cells are derived from a rat pheochromocytoma (Greene et al., 1976) and are a neuroendocrine cell line. The cells used in this study are a generous gift from Rolf Heumann (Bochum) and show similarities to PC12 cell clone 251 (Heumann et al., 1983). Cells were usually kept at a high confluency. They were passaged every three to four days. They were used for experiments up to a maximum passage of

35, unless morphological changes were observed earlier.

HepG2 cells

HepG2 cells are a human liver carcinoma cell line. In comparison to PC12 cells, they do not endogenously express neuronal SNARE-proteins. Cells used in this study were purchased from Cell Line Services (CLS, #300198) and passaged every three to four days.

4.1.3 Cell culture media and reagents

Medium/Reagent	Supplier	Composition
Dulbecco´s PBS (DPBS)	PAN Biotech, #P04-36500	PBS without Ca^{2+} and Mg^{2+}
Fetal bovine serum (FBS)	PAN Biotech, #PP30-3306	see manufacturer
Horse serum (HS)	BioWest, #S0900-500	see manufacturer
Penicillin/streptomycin (P/S)	PAN Biotech, #S0900-500	10,000 U/ml Penicillin and 10 mg/ml Streptomycin
DMEM (used as PC12 starving media)	PAN Biotech, #P04-04515	see manufacturer
DMEM with Supplements (PC12 growth media)	PAN Biotech, #P04-04515	supplemented with 5 % (v/v) FBS, 10 % (v/v) HS and 1 % (v/v) P/S
MEM Eagle with Supplements (HepG2 growth media)	PAN Biotech, #PP04-08509	MEM Eagle with 10 % (v/v) FBS and 1 % (v/v) P/S
Trypsin	PAN Biotech, #P10-0231SP	Trypsin (0.05 %) with 0.02 % EDTA/PBS, w/o Ca^{2+} and Mg^{2+}

TABLE 4.2: Cell culture media and reagents.

4.1.4 Buffers and Solutions

Name	Composition
Phosphate buffered saline (PBS)	137 mM NaCl, 2.7 mM KCl, 1.76 mM KH_2PO_4, 10 mM Na_2HPO_4, pH 7.4
Sonication buffer	20 mM HEPES-KOH, 120 mM potassium glutamate, pH 7.2 20 mM potassium acetate, 10 mM EGTA
Munc18-1 incubation buffer	Sonication buffer supplemented with 1mM DTT
Ionomycin incubation buffer	PC12 starving medium suppl. with 20 mM HEPES, 3.2 mM Ca^{2+} and freshly added 20 µM Ionomycin
Paraformaldehyde (PFA) solution (4 %)	16 % PFA stock solution in PBS
Blocking buffer	3% bovine serum albumin (BSA) in PBS
Poly-L-Lysine (PLL) stock solution (20x)	2 mg/ml PLL in ddH_20
Tris-Acetat-EDTA (TAE) buffer	40 mM Tris, 1 mM EDTA, 0.11% (v/v) acetic acid
Towbin buffer	25 mM Tris, 192 mM glycine, 20 % (v/v) methanol, pH 8.3
Sodium dodecyl sulfate (SDS) running buffer	25 mM Tris, 0.1 % (w/v) SDS, 192 mM glycin, pH 8.3
4x Laemmli buffer (reducing)	10 % (w/v) SDS, 40 % (w/v) glycerol, 0.008 % (w/v) bromophenol blue, 300 mM Tris HCl, 10 % (v/v) beta-mercaptoethanol, pH 6.8

TABLE 4.3: Buffers and solutions.

4.1.5 Antibodies

Primary Antibodies

IF: Immunofluorescence; WB: Western blot

Target/ Name	Host species	Supplier/ Catalognumber	Application/ Dilution
Syntaxin 1A (HPC-1)	mouse	Sigma, #S0664	IF (1:500), WB (1:1000)
SNAP25 (Cl. 71.1)	mouse	Synaptic Systems, #111 011	IF (1:200), WB (1:1000)
β-Actin (9E10)	mouse	Cell Signaling, #3700	WB (1:5000)
Myc-tag (A7)	mouse	Invitrogen, #MA1-21316	IF (1:200), WB (1:1000)
SNAP25	rabbit	Synaptic Systems, #111 002	IF (1:200)
Myc-tag (71D10)	rabbit	Cell Signaling, #2278S	IF (1:200)
α-Tubulin	rabbit	Cell Signaling, #2144S	WB (1:500)
β-Actin (13E5)	rabbit	Cell Signaling, #4970	WB (1:5000)
GFP	rabbit	Chromotek, #PABG1-100	WB (1:2000)
Munc18-1	rabbit	Synaptic Systems, #116 002	IF (1:500)

TABLE 4.4: Primary antibodies.

Secondary Antibodies

IF: Immunofluorescence; WB: Western blot

Target/ Species	Host species	Coupled fluorophore	Supplier/ Catalognumber	Application Dilution
GFP	alpaca/ nanobody	ATTO647N	Chromotek, #gba647n-100	IF (1:200)
GFP	alpaca/ nanobody	ATTO594	Chromotek, #gba594-100	IF (1:200)
mouse	donkey	AlexaFluor594	Invitrogen, #A21203	IF (1:200)
mouse	goat	ATTO647N	Sigma, #20185	IF (1:200)
rabbit	goat	StarGreen	Abberior, #STGREEN-1002-500	IF (1:200)
mouse	goat	IRDye 800CW	LiCor, #925-32210	WB (1:10,000)
rabbit	goat	IRDye 680CW	LiCor, #925-68071	WB (1:10,000)

TABLE 4.5: Secondary antibodies.

4.1.6 Plasmids

Name	Tag	Resistance	Origin	Additional information
Syntaxin 1A-full-myc (Stx-full)	C-terminal 3xmyc-tag	Kan.	Merklinger et al., 2017	Full rat Syntaxin 1A sequence based on NP_446240.2 (aa 1-288)
Syntaxin 1A-ΔS-myc (Stx-ΔS)	C-terminal 3xmyc-tag	Kan.	Merklinger et al., 2017	Rat Syntaxin 1A deletion construct (aa 191-218 missing)
Syntaxin 1A-full-GFP (Stx-GFP)	C-terminal mEGFP	Amp.	Sieber et al., 2006	Full rat Syntaxin 1A sequence based on NP_446240.2 (aa 1-288)
Syntaxin 1A-ΔS-GFP (Stx-ΔS-GFP)	C-terminal mEGFP	Amp.	Merklinger et al., 2017	Rat Syntaxin 1A deletion construct (aa 191-218 missing)
GFP-SNAP25-WT	N-terminal mEGFP	Amp.	Halemani et al., 2010	Rat SNAP25B sequence based on NP_112253.1 (aa 1-206)
GFP-SNAP25-ΔN	N-terminal mEGFP	Amp.	Halemani et al., 2010	Rat SNAP25B deletion construct (aa 14-79 missing)
GFP-SNAP25-ΔC	N-terminal mEGFP	Amp.	Halemani et al., 2010	Rat SNAP25B deletion construct (aa 143-202 missing)
GFP-SNAP25-ΔN/C	N-terminal mEGFP	Amp.	Halemani et al., 2010	Rat SNAP25B deletion construct (aa 14-79 and 143-202 missing)
Munc18-1-GFP	C-terminal mEGFP	Amp.	Nikolas Reppert (AG Lang)	Munc18-1 human, based on pEGFP-C1 backbone

TABLE 4.6: Plasmids.

4.1.7 Recombinant Munc18-1

Recombinant Munc18-1 was a kind gift from Kerstin M. Rink, group of Prof. Thomas Söllner, Heidelberg University Biochemistry Center (BZH).

Munc18-1: Stock concentration: 9.2 µM; used concentration is given in each individual experiment.

4.1.8 Kits

Name	Supplier
NucleoBond Xtra Midi	Macherey and Nagel, #740410
NEON Transfection System Kit	ThermoFisher Scientific, #MPK10096
GFP-Trap Agarose (for Co-IP)	Chromotek, #gta-20

TABLE 4.7: Kits.

4.1.9 Software

Software	Supplier/Developer	Application
Microsoft Office Excel	Microsoft corporation	Primary data analysis, statistical analysis and organization
GraphPad Prism 6.01	GraphPad Software	Further data organization and visualization
CorelDraw Graphics	Corel Corporation	Illustration, layout and visualization of data
ImageJ (FIJI bundle)	Wayne Rasband (NIH)	Image analysis
BioEdit	Thomas A. Hall	DNA sequence analysis
Overleaf	John Hammersley	LaTex editor

TABLE 4.8: Software.

4.2 Methods

4.2.1 Cell culture

All cells were cultured in a cell incubator (Binder, Tuttlingen, Germany) at 37 °C and 5 % CO_2. General handling and transfections were performed under a sterile Laminarflow hood (BDK, Sonnenbühl, Germany). PC12 and HepG2 cells were grown to around 80-90 % confluency before passaging them into a new 75 cm^2 cell culture flask. PC12 cells were always kept at a high cell density. For cell passaging, cells were washed with DPBS once and then incubated with trypsin at 37 °C until all cells were detached. Growth medium (according to the cell type) was then added and the cell suspension was centrifuged for 3 min at 26 rcf. The supernatant was removed and new medium was added. To triturate larger PC12 cell clumps more efficiently, a 20 ml syringe with a 21-gauge needle was used twice. For transfection (see section 4.2.3), cells were counted using a Neubauer chamber. For further cultivation, cells were directly transferred into a new cell culture flask.

4.2.2 Preparation of coverslips

Glass coverslips (high precision, 1.5H, Menzel) were placed under agitation in 1 M HCl, followed by another round in 1 M NaOH. In between the incubation steps, coverslips were thoroughly washed with deionized water. Clean coverslips were kept in 100 % ethanol until further use. For coating, coverslips were taken out of 100 % ethanol and placed into 6-well plates. After excess ethanol has evaporated, 500 µl of PLL solution was added onto each coverslip and incubated for 30 min. Afterwards, the PLL solution was removed, coverslips were dried overnight under the Laminarflow hood and sterilized for 20 min by UV-light exposure.

4.2.3 Transfection

For the transfection of PC12 and HepG2 cells, the NEON Transfection eelctroporation system was used acccording to the manufacturer´s instructions. For preparation, the cells were detached from the flask, centrifuged and resuspended in new growth medium before counting. The appropriate amount of cells (1.5-2 x 10^6) were

resuspended in 125 µl of R-buffer or DPBS (for PC12 or HepG2 cells respectively) and mixed with 10 µg of plasmid DNA (per construct), unless stated otherwise. HepG2 cells were transfected using a single 50 ms pulse at 1200 V, for PC12 cells a single 30 ms pulse at 1410 V was used. Transfected cells were immediately transferred into antibiotics-free medium and cultivated for 16-24 h. As a control, cells not undergoing electrophoresis were used, which were seeded at a density of 2-3 x 10^5 cells per coverslip.

4.2.4 Ionomycin incubation of whole cells

For experiments in Figure 5.6, around 16 h after transfection, PC12 cells were washed twice with starving medium and equilibrated in it for 2 h at 37 °C. Afterwards, the medium was exchanged with either starving medium supplemented with 3.2 mM Ca^{2+} (+ already present Ca^{2+} in the cell medium of 1.8 mM, which then adds up to a total of 5 mM Ca^{2+} in the solution) or starving medium with 10 mM EGTA to chelate Ca^{2+}. Intact PC12 cells were incubated for 5 min at 37 °C before proceeding to generate membrane sheets and fixation.

4.2.5 Membrane sheet preparation and Munc18-1 incubation

For membrane sheet preparation, cells were briefly washed in ice-cold PBS before subjecting them to a 100 ms ultrasound pulse in ice-cold sonication buffer. The distance of the sonication tip was adjusted due to experience. Plasma membrane sheets were either subjected to incubation with different treatments or directly fixed in 4 % PFA in PBS for 30-45 min.

For Munc18-1 incubation experiments, coverslips with PM sheets were incubated on parafilm to which a volume of 150 µl incubation buffer (composition see table 4.3) or a specified concentration of Munc18-1 protein diluted in incubation buffer was diluted. Experiments in Figure 5.16 used an incubation period of 15 min at 37 °C, incubation time in experiments shown in Figure 5.15 were reduced to 10 min

at 37 °C. Afterwards, excess Munc18-1 was removed with a thorough DPBS wash, followed by fixation in 4 % PFA.

4.2.6 Immunostaining

Cells or PM sheets were fixed with 4 % PFA in PBS for 30-45 min followed by quenching in 50 mM NH_4Cl for 15 min. Cells were also permeabilized with 0.2 % Triton-X in PBS for 1 min. Coverslips were washed briefly with PBS and blocked with 3 % BSA in PBS for at least 1 h. Primary antibody and secondary antibody/nanobody incubation was performed in 1 % BSA in PBS for 1 h at RT, respectively. In between primary and secondary antibody/nanobody incubation steps, the samples were washed three times with 0.5 % BSA in PBS. At the end, excessive secondary antibody/nanobody was washed off with PBS. Samples were embedded in ProLong Gold Antifade Mountant (Invitrogen, #P36930) on microscopy slides, sealed and stored at 4 °C prior to imaging.

4.2.7 Co-Immunoprecipitation

For immunoprecipitation, 24 h after transfection HepG2 cells were scraped, suspended in ice-cold PBS and pelleted. Cells were lysed in ice-cold Tris buffer (150 mM NaCl, 0.5 mM EDTA, 10 mM Tris, pH 7.5) containing 1 % Triton-X 100. Immunoprecipitation was done according to the manufacturer's manual using αGFP-Agarose beads (Chromotek, #gta-20). In brief, the cell lysate was incubated for 1 h at 4 °C with αGFP-nanobodies covalently bound to agarose beads. Beads were collected, washed, and for protein detachement heated for 10 min at 95 °C in 2xSDS-sample buffer (120 mM Tris/Cl, 20 % Glycerol, 4 % SDS, 0.04 % bromphenol blue, 10 % beta-mercaptoethanol). Beads were removed from the supernatant by centrifugation. Samples were then subjected to SDS-PAGE.

4.2.8 Western Blot and SDS-PAGE

Western blot was employed for Co-IP analysis and for the quantification of expression levels. In the latter case, transfected cells were used 24 h after transfection, unless stated otherwise. Cells were washed once with PBS and then lysed by adding 4xLämmli buffer and heated for 10 min at 95 °C. They either were used directly afterwards or stored at -20 °C until further use.
For SDS-PAGE, a 4 % stacking gel and 10 % running gel was used to separate the proteins. The gel was run in SDS running buffer for 20-30 min at 70 V and then for 60-90 min at 120 V. To transfer the proteins from the gel onto the nitrocellulose membrane, a wet blotting system (BioRad) was employed. Transfer took place in ice-cold Towbin buffer for 1 h at 100 V. Membranes were quickly rinsed with PBS and blocked with Intercept Odyssey Blocking buffer (LiCor, #927-60001) for 1 h. Primary and secondary antibodies were diluted in Odyssey Blocking buffer supplemented with 0.1 % Tween-20. Primary antibodies were incubated overnight at 4 °C, secondary antibodies for 1 h at RT. Between primary and secondary antibody incubation membranes were washed with PBS containing 0.1 % Tween20 (PBS-T) and finally with PBS before imaging using a Li-Cor Odyssey Classic Imaging System. Blots were analyzed using ImageJ, measuring the integrated band intensity and correcting for background.

4.2.9 Epifluorescence microscopy

For epifluorescence imaging, an inverted Olympus IX-81 microscope equipped with an ImagEM C9100-13 16-bit EM CCD camera (Hamamatsu Photonics, Shizuoka, Japan) in combination with a MT20E illumination system (Olympus, Tokyo, Japan), an Apochromat NA 1.49 60x oil objective was used, yielding a pixel size of 266.67 nm. In some cases, an additional 1.6x lens was used as well, decreasing the pixel size to 166.67 nm. The microscope is equipped with filter sets for GFP (F36-525, GFP), AlexaFluor594 (F36-503, Cy3) and AlexaFluor647/StarRed (F46-009, Cy5) (all from AHF Analysentechnik).

Images in Figure 5.14 and 5.15 were acquired with a new illumination system, employing photodiode lasers. GFP was excited with a 493 nm laser, Cy3 with a 561 nm laser and Cy5 with a 638 nm photodiode laser. The filter sets did not changed from the ones previously used. Lasers were always set to 100 % illumination power and only the illumination time (in ms) was changed. All images were acquired using the CellR (Olympus) software.

4.2.10 Confocal and STED microscopy

Confocal and super-resolution images were taken with a four-channel STED microscope (Abberior Instruments, Goettingen, Germany) module in combination with an Olympus IX-83 confocal microscope (Olympus, Tokyo, Japan), equipped with an UPlanSApo 100× (1.4 NA) objective (Olympus, Tokyo, Japan). GFP-fluorescence was excited with a 488 nm laser and emission recorded with a 500 - 520 nm filter. AlexaFluor594/ATTO594 were excited with a 561 nm laser and emission recorded with a 580–630 nm filter. ATTO647N/StarRed was excited with a 640 nm laser and emission recorded with a 650–720 nm filter. A pulsed STED laser 775 nm was used for depletion of the 561 nm and 640 nm laser. STED images were recorded via time-gated detection with 0.96 ns delay and 8 ns gate width. The pinhole size was set to 1 AU. Pixel size in all recordings was set to 25 nm.

For analysis of the plasma membrane fraction of GFP-SNAP25 (Figure 5.4), the equatorial plane of cells was imaged. For all other experiments, the focal plane was adjusted to the basal plasma membrane.

4.2.11 Image analysis

All image analysis was performed using the program ImageJ. If not stated otherwise, a rectangular/square ROI was placed in one channel and propagated (if necessary) to the other channel. This ROI was used for calculation of the Pearson Correlation Coefficient, mean intensity and specific maxima analysis.

Average fluorescence intensity

The average fluorescence intensity of a sheet was calculated by measuring the mean intensity of a ROI placed onto a membrane sheet and onto the background, and subsequently subtracting the latter from the former.

For the calculation of the GFP-SNAP25 plasma membrane fraction (Figure 5.4), three ROIs were manually drawn. The most outer ROI outlined the border of the cell ("outer rim"), the cytoplasm ("inner rim") and the nucleus ("nucleus"). They were background corrected, the integrated density was determined (mean intensity * size) and subsequently used to calculate the plasma membrane and cytoplasmic fractions: "outer rim" - "inner rim" = "plasma membrane signal"; "inner rim" - "nucleus" = "cytoplasm signal". The plasma membrane fraction was then determined by: "plasma membrane fraction" = "plasma membrane signal" / ("cytoplasm signal + "plasma membrane signal").

For epifluroescence images in Figure 5.7, specific ROIs were used. Due to the small size of PC12 cells and the low magnification, up to 12 sheets were imaged with one recording. From ROIs, "binary masks" were created in ImageJ. First, raw images were smoothed using a Gaussian blur (σ = 3), then a binary mask was created and saved individually. The binary masks, which specifically outlined the membrane sheets, were overlayed with the raw image and the mean intensity in the regions defined in the binary mask, was measured. Lastly, they were background corrected.

Relative standard deviation of the mean (rSDM)

The rSDM was calculated by measuring the standard deviation of the mean intensity of the pixel values of a ROI using ImageJ and dividing it by the mean intensity of the ROI.

Maxima analysis

A custom ImageJ macro (Merklinger et al., 2017) was used to determine maxima fluorescence intensity, size, density or distances. For each individual sheet, maxima

intensity, size and distance were averaged. GFP-SNAP25 images generally show a lower signal-to-noise ratio and so to improve maxima detection, a Gaussian blur with σ = 0.5 was employed before analysis. A specific threshold was set for maxima detection, which varied between experiments. In general, the cluster analysis macro uses the "Find maxima" function from ImageJ and extracts certain parameters which are used for further analysis. Maxima density was calculated by relating the number of all detected maxima to the size of the ROI. Maxima fluorescence intensity is calculated by placing a circular ROI with a diameter of 5 pixels centered on the maxima and measuring the average intensity. Distance between maxima is determined by taking each maxima position and determine its nearest neighbouring maxima, either in the same or in the other channel. Maxima size is measured by placing a vertical and horizontal line scan (31 x 3 pixels) in the center of a detected maxima, then a Gaussian function was fitted on the intensity profile of each line. The maxima size was then determined by the full-width at half maxima (FWHM) of the Gaussian fit. Maxima with a fit quality of $R^2 < 0.8$ and a non-centered peak (not in the middle third of the linescan) were excluded from size analysis.
For Figure 5.11 for Syntaxin 1A, a total number of 26266, 7252 and 11214 maxima were analysed per condition Control, Stx-full and Stx-ΔS, respectively. For SNAP25 maxima size distribution, a total number of 3026, 3814 and 2822 maxima were analysed per condition Control, Stx-full and Stx-ΔS, respectively.

Pair distribution functions in Figure 5.9 were kindly done by Prof. Jan Hasenauer (Computational Life Sciences, LIMES Institute, University of Bonn), using the program MATLAB. Calculations were done using the specific coordinates determined by the custom ImageJ macro used for the maxima analysis.

Pearson correlation coefficient (PCC)

The PCC was used as a parameter to determine the overlap between two channels and describes the linear relationship between two values. It was determined in ImageJ using a custom macro (written by Dr. Gero Schloetel, AG Lang). As a co-localization control, to generate a non-related distribution of the channels,

one channel was flipped vertically and horizontally before determining the PCC ("flipped PCC").

5 Results

5.1 Mesoscale organization of Syntaxin 1A and SNAP25

In this study, the mechanisms underlying mesoscale organization of Syntaxin 1A and SNAP25 at the plasma membrane are investigated. SNARE-proteins are highly abundant at the plasma membrane, with values ranging from 540 up to 1800 molecules/μm^2 and $\sim$7500 molecules/μm^2 for Syntaxin 1A and SNAP25, respectively (Sieber et al., 2007; Knowles et al., 2010).

Syntaxin 1A is found in small, tightly packed cluster with a size of $\sim$65 nm in diameter (Sieber et al., 2007). Its size tends to increase with the syntaxin concentration (Sieber et al., 2006) (section 2.3.2). SNAP25 on the other hand, shows a more widespread pattern with a larger area occupancy on the membrane (section 2.3.3). Despite their important interaction with one another to catalyze fusion, we find find them in close proximity to each other, but in principle largely segregated in the plasma membrane.

This study tries to illuminate the underlying mechanism of this organization by employing microscopic analysis on fixed membrane sheets. This has the advantage that we can observe the proteins in their physiological environment which is important because, compared to in-vitro studies with reconstituted proteins, the plasma membrane is an environment that shows molecular crowding due to its high density of proteins and lipids. Molecular crowding could influence several parameters regarding protein behaviour (section 2.2.1). On the other hand, labelling of proteins can be a challenge in highly crowded and densely packed protein clusters on the plasma membrane posing certain experimental challenges.

5.1.1 Labelling strategy to visualize Syntaxin 1A and SNAP25

Due to the fact that SNARE-proteins are present at a very high copy number at the plasma membrane of PC12 cells (Sieber et al., 2007; Knowles et al., 2010), labelling for correct visualization is technically difficult. In order to visualize both proteins reliably, a co-expression system of Syntaxin 1A and SNAP25 (both labelled with a tag) was established and characterized.

For Syntaxin 1A, an antibody is commercially available that visualizes the protein´s distribution reliably (Zilly et al., 2011), called HPC-1, which is raised against the N-terminal domains of Syntaxin 1A. When overexpressing Syntaxin 1A, we use a construct that also contains a C-terminal 3xmyc-tag (Figure 5.1, middle) (Merklinger et al., 2017), which can be labelled with an antibody as well, enabling us to visualize only overexpressed Syntaxin 1A. Using the myc-tag, we have to deal with a staining gradient towards the middle of the membrane sheet, because the myc-antibody needs to diffuse underneath the sheet. However, we can ignore this problem by choosing a ROI for analysis at the well stained periphery of the membrane sheet. To uncover a role of syntaxin´s SNARE-motif in the organization of SNARE-proteins on the membrane, we also used a deletion construct where the N-terminal part of the SNARE-motif is deleted (Figure 5.1, right side).

Labelling SNAP25 presents a challenge. Despite the fact that several antibodies are available, they visualize the distribution of SNAP25 only imperfectly (Zilly et al., 2011). Thus, SNAP25 is genetically labelled by attaching GFP to its N-terminus. The GFP-tag and SNAP25 are almost the same molecular size (27 and 25 kDa, respectively), yet it has been shown to not interfere with the protein´s function (Delgado-Martínez et al., 2007). We aimed for only a moderate overexpression of GFP-SNAP25, to not push the protein-ratio too far off the physiological point. Furthermore, this approach requires the use of an αGFP nanobody labelled with ATTO647 applicable for high-resolution microscopy, which is smaller than the conventional primary and secondary antibodies used for Syntaxin 1A visualization (Figure 5.1, left side).

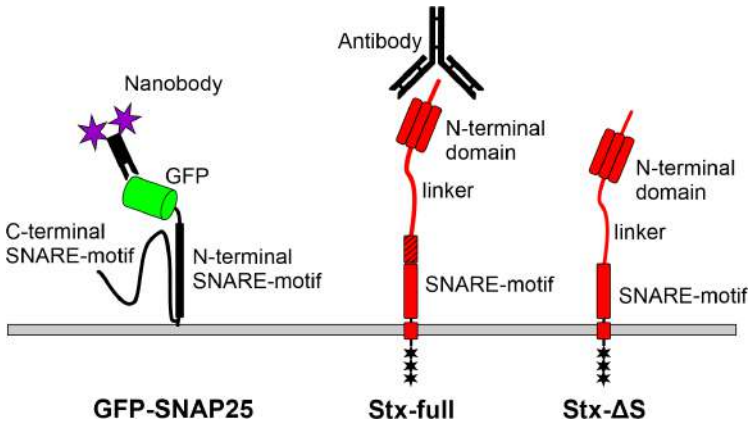

FIGURE 5.1: **SNARE-constructs primarily used in this study and labelling approach.** Cartoons of the Syntaxin 1A and SNAP25 constructs. **Left side:** SNAP25 with its N-terminal GFP-tag. The GFP is visualized with an αGFP nanobody coupled with a STED-appropriate fluorophore. **Middle:** Syntaxin 1A full-length (Stx-full) and the primary antibody used for its visualization (HPC-1). **Right side:** Deletion variant of Syntaxin 1A (Stx-ΔS), which is lacking the N-terminal part of the SNARE-motif (lined box). Both syntaxin-constructs also contain a 3xmyc-tag at the C-terminal end, facing the extracellular site of the plasma membrane.

5.1.2 Co-expression system of GFP-SNAP25 in combination with Stx-full or Stx-ΔS

In the following, we establish and characterize the co-expression of the above established constructs. GFP-SNAP25 is expressed alone or together with the two Syntaxin 1A constructs to determine any possible effect on the endogenous protein level and consequently the SNARE-protein ratio.

5.1.2.1 Characterization of SNARE-protein expression in PC12 cells

To determine the protein expression levels, western blot analysis was employed (Figure 5.2). Moreover, the samples were split for parallel epifluroescence microscopy analysis (Figure 5.7). For western blot analysis, an antibody raised against the N-terminus of Syntaxin 1A or the N-terminal SNARE-motif of SNAP25 was used, thus not distinguishing between endogenous and overexpressed protein, yet they can be distinguished by size.

Analyzing expression levels in whole cells (Figure 5.2 A), we find that the endogenous expression level of SNAP25 is not significantly influenced by the co-expression

of either syntaxin construct (Figure 5.2 B). We see that the overexpression of GFP-SNAP25 roughly increases the total level of SNAP25 by around 50 % in all conditions, independent from co-expression of syntaxin constructs. We see a slight drop in total SNAP25 in condition Stx-full + GFP-SNAP25 (Figure 5.2 C).

Analyzing syntaxin levels (Figure 5.2 D), the endogenous level of Syntaxin 1A is also not significantly changed by co-expression with GFP-SNAP25 (Figure 5.2 E), expression of additional Stx-full or Stx-ΔS increased the total protein level by around 150 %. Furthermore, we observe a high variety in syntaxin expression levels (Figure 5.2 F, compare with standard deviation´s in SNAP25 expression levels in C).

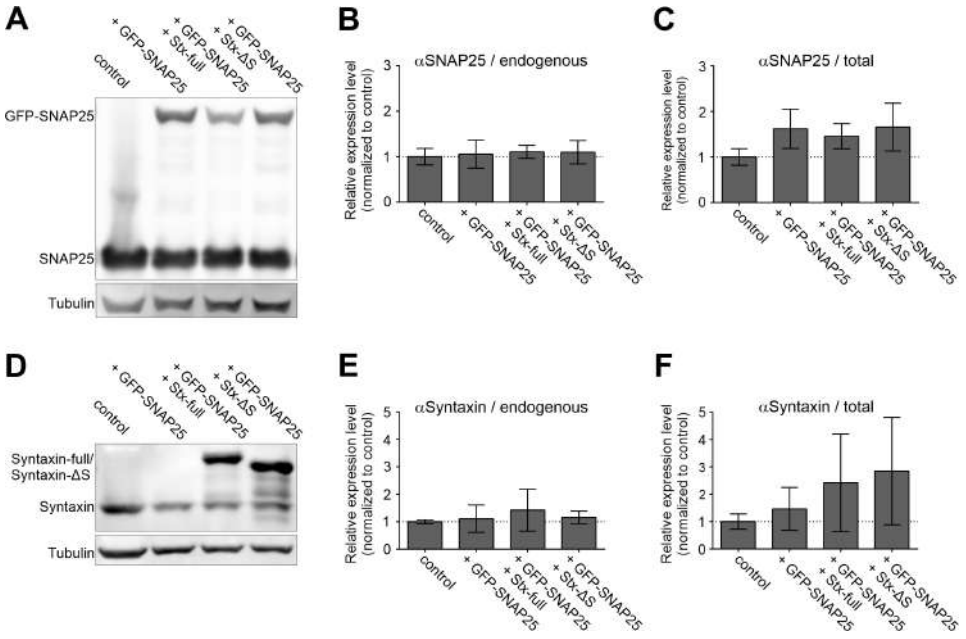

FIGURE 5.2: **Expression levels of endogenous SNAREs and overexpressed GFP-SNAP25, Stx-full and Stx-ΔS.** Western blot analysis comparing endogenous and overexpressed protein levels of Syntaxin 1A and SNAP25. **(A)** Analysis of the expression level of endogenous SNAP25 (25 kDa) or overexpressed GFP-SNAP25 (52 kDa) using an antibody against SNAP25´s N-terminal SNARE-motif. Tubulin (50 kDa) was used for normalization. **(B)** Quantification of endogenous SNAP25 (25 kDa band) and **(C)** endogenous + overexpressed GFP-SNAP25 (52 kDa band). **(D)** Endogenous and overexpressed Syntaxin 1A-variants were visualized using an antibody against its N-terminal part. **(E)** Quantification of endogenous Syntaxin 1A (33 kDa) and **(F)** endogenous + overexpressed variants Stx-full (38 kDa) and Stx-Stx-ΔS (35 kDa). Values are given as means ± SD. Statistical analysis showed no significant difference between any of the conditions (n = 3 experiments; two-tailed unpaired t-test, not significant = $p > 0.05$) (Figure taken from: Mertins et al., 2021).

5.1.2.2 Ratio of endogenous and overexpressed SNAREs in PC12 cells

The amount of SNARE-proteins and the Syntaxin 1A/SNAP25 ratio is a crucial point in the process of exocytosis. In PC12 cells, the ratio of endogenous Syntaxin 1A to SNAP25 at the plasma membrane is around 1:14 (Knowles et al., 2010). To make sure that we do not diminish or even invert the ratio of SNAP25 to Syntaxin 1A in our approach using overexpressed proteins, we needed to estimate the endogenous SNARE-concentration in the here used PC12 cells on the level of whole cells and further determine the ratio after overexpression directly at the plasma membrane.

5.1.2.2.1 Ratio of endogenous SNAREs in whole cells To determine the ratio of endogenous Syntaxin 1A and SNAP25, western blot analysis was performed. In order to quantify the endogenous ratio, we opted for an expression of GFP-tagged constructs (Syntaxin 1A-GFP or GFP-SNAP25) and used the respective GFP-signal for normalization.

For this, PC12 cells were used untransfected (Figure 5.3, left lane) or transfected either with Syntaxin 1A-GFP or GFP-SNAP25 (Figure 5.3, middle or right lane, respectively). The western blot was first immunostained with an antibody directly raised against Syntaxin 1A (HPC-1, binding to its N-terminal domain), visualizing endogenous Syntaxin 1A (Figure 5.3, upper red arrow) and overexpressed Syntaxin 1A-GFP (Figure 5.3, left band in red box #1). SNAP25 was stained with an antibody directly raised against itself (binding to its N-terminal domain), visualizing endogenous SNAP25 (Figure 5.3, lower red arrow) and overexpressed GFP-SNAP25 (Figure 5.3, right band in red box #1). For normalization, Actin was stained as well. After this staining, the western blot membrane was stripped and subsequently immunostained again. This time, an antibody directly against GFP was employed (which has the same staining affinity for both constructs), only visualizing the GFP-tag of overexpressed Syntaxin 1A-GFP or GFP-SNAP25 (Figure 5.3, red box #2).

For analysis, the band staining intensity of the respective overexpressed SNARE-protein construct (Syntaxin 1A-GFP or GFP-SNAP25 in Figure 5.3 red box #1) was

divided by the GFP-tag staining intensity (Figure 5.3, red box #2), after normalization to actin. In this way we can calculate the so-called "GFP-conversion factor" to determine the endogenous protein ratio band in GFP-unit equivalents. Here, we obtain a GFP-conversion factor of 1.85 and 2.49 for Syntaxin 1A and SNAP25, respectively. Now dividing the staining intensity of the endogenous bands from Syntaxin 1A or SNAP25 (Figure 5.3, red arrows) by the corresponding conversion factor, we get their GFP-intensity equivalents (Figure 5.3, quantification on the right side). Consequently, we can determine an endogenous ratio of Syntaxin 1A to SNAP25 in our PC12 cells of around 1:12.
It should be noted that we observe a strong degradation band for Syntaxin 1A-GFP which we do not observe for the myc-tagged syntaxin constructs used in later experiments (compare with Stx-myc overexpression in Figure 5.2 D). This points to degradation of Syntaxin 1A-GFP at a very high expression level, which however does not affect the conversion factor because it is not used for analysis.

As determined by the western blot analysis shown in Figure 5.2, we need to take into account that we elevate Syntaxin 1A by $\sim$150 % and SNAP25 only by $\sim$50 %, considering untransfected and transfected cells. This leads to a diminished average ratio of only 7-fold more SNAP25 in comparison to Syntaxin 1A.
At the plasma membrane, this ratio changes further according to publications which assume that all Syntaxin 1A (Sieber et al., 2007, Knowles et al., 2010) but only 80 % of SNAP25 (Knowles et al., 2010) localizes to the plasma membrane. As for our further planned experiments, we study SNAREs specifically in the plasma membrane from overexpressing PC12 cells, thus we wondered what the Syntaxin 1A/SNAP25 ratio is in this preparation.

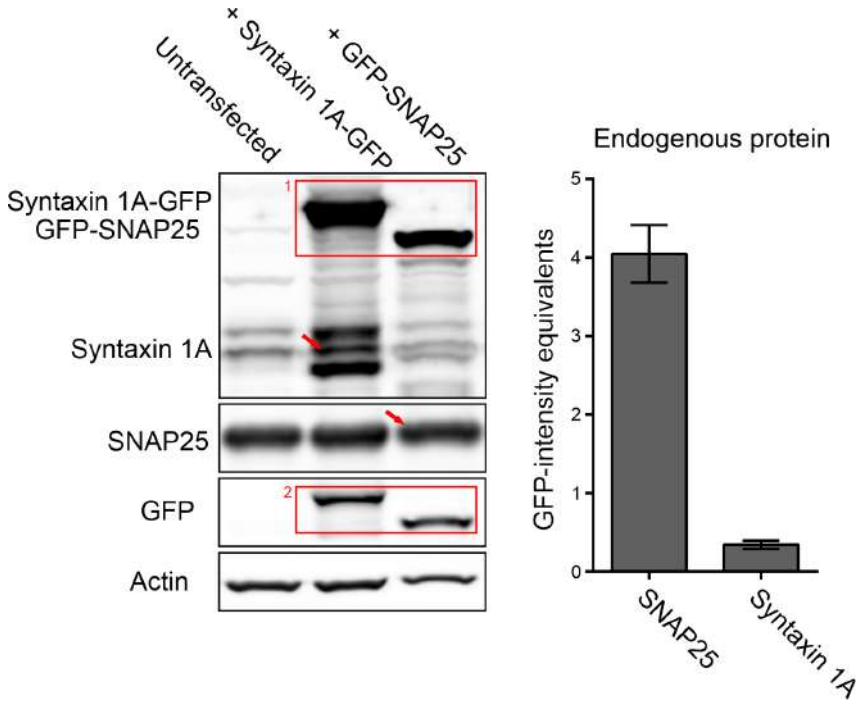

FIGURE 5.3: **Ratio of endogenous Syntaxin 1A and SNAP25 in PC12 cells.** *Western Blot analysis immunostaining syntaxin 1A-GFP/GFP-SNAP25 bands with an antibody raised against the respective SNARE (red box #1) and stained again after stripping the membrane with an anti-GFP antibody (red box #2). From the band intensities, we obtain a conversion factor allowing us to express the endogenous band intensities in GFP-signal equivalents, and by this determine the SNAP25:syntaxin 1A ratio.* ***(A)*** *Representative Western Blot from PC12 cells expressing either no construct (left lane), syntaxin 1A-GFP (middle lane) or GFP-SNAP25 (right lane), using for syntaxin 1A and SNAP25 the same mouse monoclonal antibodies as in Figure 5.2, for actin a polyclonal rabbit antibody and for GFP a polyclonal rabbit anti-GFP antibody. Different from Stx-full expression (compare to Figure 5.2), we observe degradation bands of syntaxin 1A-GFP (see above and below the endogenous syntaxin 1A band indicated by a red arrow). For the conversion factor only non-degraded syntaxin 1A-GFP is taken into account. The SNARE-antibody band intensity from the overexpressed construct (red box #1; syntaxin 1A-GFP ∼60 kDa; GFP-SNAP25 ∼52 kDa) is normalized to actin and then divided by the respective actin normalized GFP-band intensity (red box #2), which yields GFP-conversion factors of 1.85 and 2.49 for syntaxin 1A and SNAP25, respectively.* ***(B)*** *Quantification of GFP-intensity equivalents. The band intensities of the endogenous SNARE-proteins (red arrows) are divided by the respective conversion factors, yielding their GFP-intensity equivalents. The ratio of the GFP-equivalents equals the ratio of the endogenous SNARE-proteins, resulting in a 12-fold excess of SNAP25 over Syntaxin 1A. Values are given as means ± SD (n = 3 experiments) (Figure and legend in italics taken from: Mertins et al., 2021).*

5.1.2.2.2 Localization of GFP-SNAP25 in PC12 cells Next, we checked if the overexpression would lead to altered trafficking to the membrane. Merklinger et al. already showed similar trafficking rates from the constructs Stx-full and Stx-ΔS

to the plasma membrane (Merklinger et al., 2017). For GFP-SNAP25, we did not expect any difference in the membrane targeting as well, because the trafficking of SNAP25 has been shown to be independent of syntaxin (Loranger et al., 2002) and GFP-tagged SNAP25 shows no difference in function to untagged SNAP25 (Delgado-Martínez et al., 2007).

But to confirm this assumption and determine the specific amount of GFP-SNAP25 at the plasma membrane, PC12 cells were transfected, either with GFP-SNAP25 alone or in combination with Stx-full or Stx-ΔS. Employing confocal microscopy, the GFP-intensity of whole cells was recorded at the cell´s equatorial plane (Figure 5.4), followed by analysis of the GFP-intensity at the plasma membrane (for details regarding the analysis see Figure 5.4 and section 4.2.11). When only GFP-SNAP25 is overexpressed, we find around 56 % of the overall intensity at the membrane. This number decreases slightly when Stx-full is co-expressed (around 50 %), yet the difference is non-significant. In the presence of Stx-ΔS this number rises again to roughly 56 %, showing that the trafficking to the membrane is not different whether GFP-SNAP25 is expressed alone or in combination with one of the Syntaxin 1A-variants. The value of around 56 % is lower than the previously reported 80 % (Knowles et al., 2010), which may be due to underestimation of the plasmalemmal fraction, because GFP-SNAP25 intensity at the membrane seems to self-quench (see Figure 5.7).

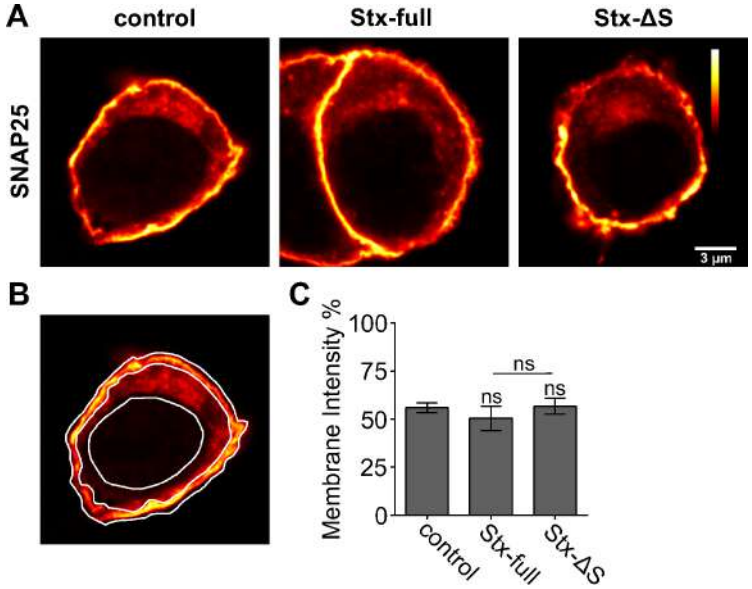

FIGURE 5.4: **Localization of GFP-SNAP25 in PC12 cells. (A)** PC12 cells were either transfected with GFP-SNAP25 alone, or in combination with Stx-full or Stx-ΔS. Whole cells were fixed and imaged using confocal microscopy. Focusing on the cell´s equatorial plane, the fluorescence intensity of the GFP-tag was recorded. **(B)** The plasma membrane fraction was quantified by manually drawing three ROIs: (i) around the whole cell, (ii) on the cytoplasmic part of the membrane and (iii) around the nucleus. For details regarding the calculation of the plasma membrane fraction and background correction see section 4.2.11. **(C)** Quantification of the GFP-intensity at the plasma membrane in each of the three conditions. Values are given as means ± SD (n = 3 experiments; 20 cells per condition and experiment; two-tailed t-test compares (i) control to Stx-full/Stx-ΔS and (ii) Stx-full to Stx-ΔS; ns = $p > 0.05$) (Figure taken from: Mertins et al., 2021).

5.1.2.2.3 Ratio after overexpression of SNAREs directly at the plasma membrane To determine the ratio of Syntaxin 1A/SNAP25 specifically at the plasma membrane after overexpression, Stx-full or GFP-SNAP25 was expressed in PC12 cells. Membrane sheets were stained for endogenous + overexpressed Syntaxin 1A ("Total Stx1A" in Figure 5.5 A) with an antibody against syntaxin´s N-terminal domain (HPC-1) and simultaneously against overexpressed Stx-full ("OE Stx1A" in Figure 5.5 A) using an antibody against the C-terminal myc-tag. Endogenous + overexpressed SNAP25 ("Total SNAP25" in Figure 5.5 B) was visualized using an antibody against SNAP25 and overexpressed GFP-SNAP25 ("OE SNAP25" in Figure 5.5 B) was visualized directly via the GFP-tag.

Plotting the values of "Total Stx1A/SNAP25" versus "OE Stx1A/SNAP25", we can see that, on the level of single membrane sheets, Syntaxin 1A is elevated up to

9-fold, but in the majority of membrane sheets it is elevated around 3- to 6-fold. SNAP25 on the other hand is elevated up to 4-fold, with the majority of membrane sheets showing a 2- to 3-fold elevation. This exemplifies the high variety of expression levels between cells.

In later experiments (see Figures 5.7 to 5.12), membrane sheets were usually taken from a middle expression range because in the highest expression states it was not possible to distinguish between single maxima anymore. We rarely observed membrane sheets with different relative levels of overexpression, meaning when SNAP25 was highly elevated, Syntaxin 1A was as well. Therefore, in those membrane sheets from the middle expression range, we estimate that we still deal with roughly 5-fold more SNAP25 over Syntaxin 1A.

Thus we can safely conclude that we usually deal with a several fold surplus of SNAP25 in all imaged plasma membrane sheets.

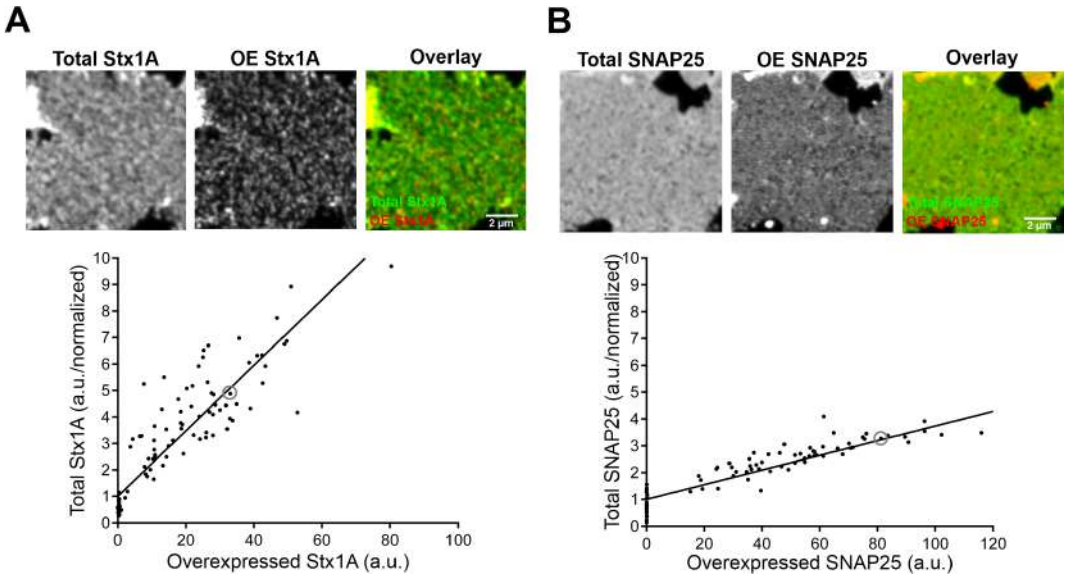

FIGURE 5.5: **Ratio of Syntaxin 1A and SNAP25 after overexpression directly at the plasma membrane.** Immunostaining directly at the plasma membrane of unroofed PC12 cells reveals different elevation levels. **(A and B)** Stx-full or GFP-SNAP25 is expressed and stained for endogenous + overexpressed (Total Stx1A/SNAP25) and overexpressed (OE Stx1A/SNAP25) protein. Specific single sheet intensities are plotted against each other and a regression line is fitted through the respective data, yielding slopes of 0.03 for Syntaxin 1A and 0.12 for SNAP25, respectively. Y-axis intercepts from regression lines represent the average signal of endogenous protein, used for normalization of the total protein intensities. Circled dots show two representative sheets which were typically used for further detailed analysis regarding cluster organization. Images are shown at arbitrary scaling. Values from three biological replicates are pooled, each including at least 30 membrane sheets (Figure taken from: Mertins et al., 2021).

5.1.3 Epitope accessibility of GFP-SNAP25

Before turning towards high-resolution microscopy, we examined the syntaxin-dependent distribution of SNAP25 at the plasma membrane of PC12 cells by epi-fluorescence microscopy. GFP-SNAP25 was either overexpressed alone or in combination with one of the syntaxin-constructs. Previous studies showed that epitope accessibility of SNAP25 was dependent on the conformational state of the protein itself. Staining with an antibody was significantly reduced when (YFP-)SNAP25 is forced in a highly clustered state. Furthermore, when looking at the intensity of the GFP-tag itself, it was also drastically decreased after Ca^{2+}-treatment (Zilly et al., 2011). This is an effect most likely due to GFP self-quenching resulting from GFPs coming into close proximity, a phenomenon already described in GFP-labelled protein oligomers (Ochiishi et al., 2016, Schneider et al., 2021).
Here, the epitope accessibility towards GFP of the GFP-SNAP25 construct was probed by comparing the GFP-intensity itself to a staining with a corresponding αGFP nanobody, to determine the influence of Syntaxin 1A on the lateral organization/packing of SNAP25.

5.1.3.1 Artificially increasing the clustering degree of SNARE-proteins to investigate changes in epitope accessibility

Zilly et al. argue that the change in SNAP25 staining intensity in membrane sheets is due to a change in packing density and consequentially a decrease in epitope accessibility. To proof whether this concept can be employed to the accessibility of the GFP-tag, we wanted to force the proteins at the plasma membrane into a highly clustered state and assess the staining intensity as well as epitope accessibility for the GFP-tag itself using an αGFP-nanobody, the GFP-intensity and additionally the conventional antibody HPC-1 to stain Syntaxin 1A. For the conventional antibody HPC-1, the binding accessibility is expected to decrease (Zilly et al., 2011).
To drive the molecules into a highly clustered state, we raised the calcium concentration in intact PC12 cells using the ionophore "Ionomycin". Ionomycin is capable of forming a complex with divalent cations, preferentially Ca^{2+}. In order to see

whether Syntaxin 1A influences epitope accessibility, PC12 cells were transfected with GFP-SNAP25 alone or in combination with Stx-full or Stx-ΔS.

Intact PC12 cells were incubated with a buffer containing Ionomycin and extracellular Ca^{2+} or, as a control, EGTA was added to the buffer to chelate calcium-ions in the extracellular environment. After a 5 min treatment at 37°C, native membrane sheets were generated, fixed and stained.

Figure 5.6 shows representative images from the three conditions and analysis of the ROI staining intensity and degree of clustering (rSDM, the value increases when the observed protein pattern is less homogeneous thus more clustered; see also section 4.2.11). Values are normalized to the control (no Ca^{2+}) per condition and experiment. It is set to 100 % and shown as a dotted line in the graphs. In this way we can focus on the change in staining intensity and degree of clustering as a direct result of an increased calcium concentration.

Figure 5.6 A and B show the GFP-tag fluorescence (488 channel) and the corresponding αGFP-nanobody coupled with ATTO647 (647 channel). The same membrane sheet was imaged in both channels for better comparison. Without raising the intracellular calcium concentration, GFP-SNAP25 shows a very widespread distribution all over the membrane (Figure 5.6 A, upper row; no Ca^{2+}). Looking at the corresponding nanobody-staining, the staining pattern looks identical.

Upon elevation of intracellular calcium, the staining intensity and degree of clustering drastically change for the GFP-fluorescence and nanobody staining (lower row; + Ca^{2+}). The intensity of the GFP-fluorescence decreases to roughly 30 - 50 % of the initial intensity, the rSDM increases 2.5 - 4-fold. Looking at the visualization with the nanobody, the effect is even shown for both parameters (please note different scaling of y-axis in rSDM plot, Figure 5.6 A-C). When looking at the GFP-fluorescence itself, in comparison to the control, the Stx-full condition shows a 2.5-fold increase in clustering compared to Stx-ΔS, which shows an almost 4-fold increase. This points to the fact that GFP-SNAP25, in the presence of Stx-full, is already more tightly clustered than GFP-SNAP25 together with Stx-ΔS. Yet, the effect of Syntaxin 1A on the accessibility of the GFP-tag is not clear from this experiment,

because the changes between the control and Stx-full/Stx- after calcium-elevation are not significant. Therefore, we wanted to turn to single sheet analysis (Figure 5.7). Thus we conclude that tight clustering induced by Ca^{2+} is most likely responsible for GFP-self quenching and also for an inaccessibility of the αGFP nanobody to its epitope.

The staining of syntaxin-clusters with a conventional antibody is displayed in Figure 5.6 C. In line with previous reports, we observe a decrease in staining intensity upon tighter packing of syntaxin molecules when employing the HPC-1 primary antibody. Here, the difference in the rSDM upon calcium incubation is even more pronounced. In the control and Stx-full condition the rSDM rises around 4 to 6-fold, yet Stx-ΔS increases up to 9-fold. The rSDM increase of Stx-ΔS upon calcium elevation is probably stronger, because it is much less clustered in the absence of Ca^{2+}.

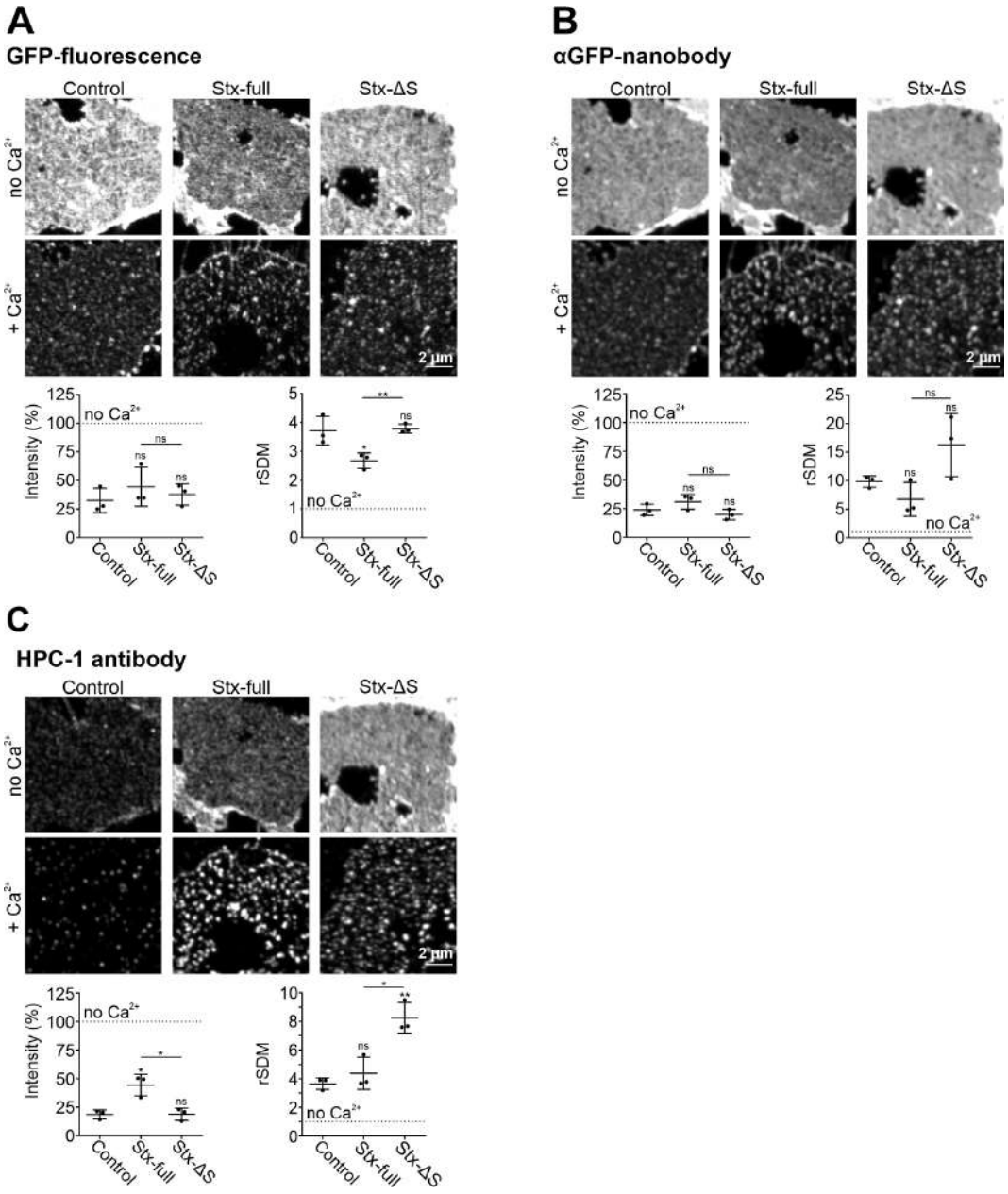

FIGURE 5.6: **Influence of intracellular elevated calcium concentration on epitope accessibility comparing nanobody and conventional antibody. (A)** Confocal imaging of GFP-fluorescence from GFP-SNAP25 imaged in the 488-channel, **(B)** corresponding αGFP-nanobody ATTO647 and **(C)** Syntaxin 1A visualized with a conventional antibody HPC-1 coupled with AF594. Upper row always shows membrane sheets which were incubated without extracellular Ca^{2+} (chelated by EGTA) in comparison to increased calcium-concentration (lower row). Values are related to no Ca^{2+}, set to 100 % (dotted line). Images from one channel are shown at the same scaling, employing a linear lookup table. Values are given as means ± SD (n = 3 experiments; 20 sheets per condition and experiment; two-tailed t-test compares (i) control to Stx-full/Stx-ΔS and (ii) Stx-full to Stx-ΔS.

5.1.3.2 Accessibility towards the GFP-tag probed directly in membrane sheets

After establishing that the staining with an αGFP-nanobody is able to detect different packing densities, we tested the accessibility of GFP-SNAP25 directly in PC12 plasma membrane sheets.

Images in Figure 5.7 A show membrane sheets from PC12 cells, visualizing the GFP-tag and the corresponding nanobody-intensity. Upper row shows membrane sheets only expressing GFP-SNAP25 (control), in the middle row membrane sheets with GFP-SNAP25 + Stx-full are shown (Stx-full), lastly the lower row shows the membrane sheets expressing the Syntaxin 1A-deletion variant (Stx-ΔS). Looking at the overall average sheet intensity (Figure 5.7 B), upon co-expression with Stx-full, the GFP- and nanobody-intensity both decrease. The GFP-intensity decreases to around 77 % and the ATTO647-intensity arising from the nanobody is even lower with only 47 % .The Pearson Correlation Coefficient (PCC, measures the overlap between two channels; section 4.2.11) shows the same pattern, in the way that upon Stx-full co-expression the PCC decreases and subsequently increases upon co-expression with the variant Stx-ΔS (Figure 5.7 C). As a control, the GFP-channel was flipped horizontally and vertically, mimicking a non-related distribution, before measuring the PCC again ("flipped" condition in Figure 5.7 C).

Plotting the single membrane sheet intensities from the GFP-tag against the αGFP-nanobody without additional syntaxin, we can observe that the binding shows a positive correlation to the expression level (control shown in black, Figure 5.7 D). Compared to that, when Stx-full is present, we have less ATTO647-intensity per GFP-tag intensity (Stx-full shown in red, Figure 5.7 D). Again, upon expression of Stx-ΔS, the nanobody per GFP-tag ratio increases slightly (Stx-ΔS shown in green, Figure 5.7 D) compared to Stx-full, but does not reach the control level. This is in accordance with the overall average membrane sheet intensity in Figure 5.7 B and excludes that effects in Figure 5.7 B are due to the inclusion of unrepresentative populations of membrane sheets or differences in expression levels.

Taken together, the data suggests that Syntaxin 1A mediates a state of SNAP25 in which it is packed more densely.

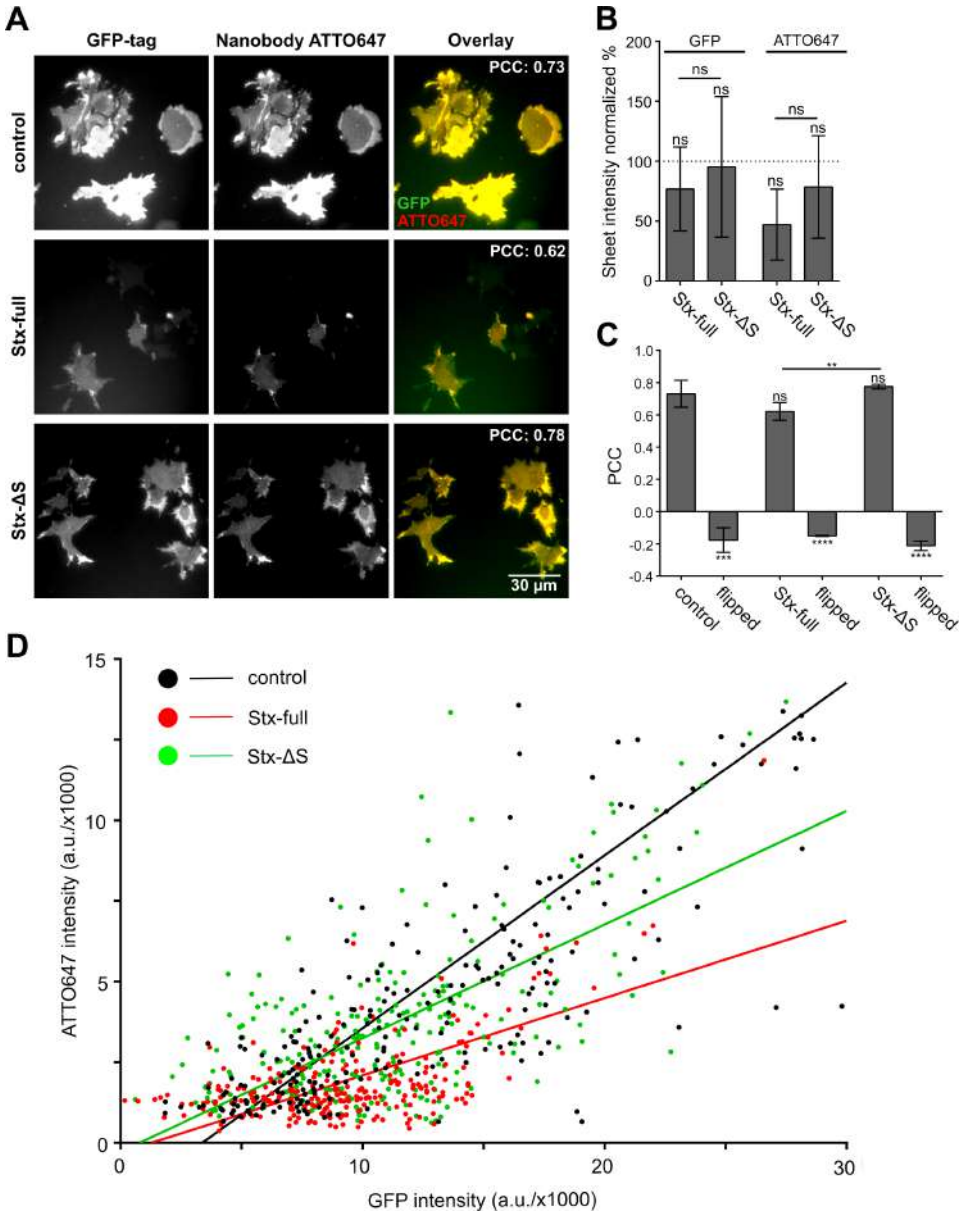

FIGURE 5.7: **Accessibility of the GFP-epitope at the plasma membrane changes upon syntaxin overexpression.** Plasma membrane sheets from PC12 cells expressing GFP-SNAP25 alone or in combination with one of the syntaxin-constructs were fixed and stained as described in section 4.2. **(A)** Epifluorescence images showing GFP- (left column) or ATTO647 labelled nanobody-staining (middle column) as well as the overlay (right column). Images from one channel are shown at the same scaling, employing a linear lookup table. **(B)** Average ROI sheet intensity from the GFP-tag and αGFP-nanobody ATTO647 per condition, normalized to control (set to 100 %). **(C)** PCC and flipped control. **(D)** ATTO647 intensity from individual membrane sheets is plotted against their corresponding GFP intensity values. Then, a linear regression line is fitted through the data, yielding slopes of 0.54 (control), 0.24 (Stx-full) and 0.35 (Stx-ΔS). Two-tailed t-test shows a p-value < 0.0001 between control and Stx-full/Stx-ΔS and between Stx-full and Stx-ΔS slopes. Per condition, membrane sheets from 3 independent experiments are pooled (control: n = 245; Stx-full: n = 266; Stx-ΔS: n = 269 membrane sheets) (Figure taken and modified from: Mertins et al., 2021).

5.1.4 Interaction between SNAP25 and Stx-full/Stx-ΔS probed by Co-Immunoprecipitation

The previous experiment where the epitope accessibility was analysed, showed that upon expression of additional Stx-full, we observe a diminished accessibility for the nanobody towards GFP-SNAP25. Expression of Stx-ΔS did show a weaker effect, which suggests that this change in accessibility might be dependent on a complete SNARE-motif. Previous studies already reported that the Stx-ΔS construct is less efficient in homomeric clustering due to its shortened SNARE-motif (Merklinger et al., 2017), thus it might also have a weakened interaction with SNAP25. To assess the interaction strength between SNAP25 and Stx-full/Stx-ΔS, we employed Co-Immunoprecipitation.

For this experiment we used HepG2 cells because they do not express endogenous SNARE proteins and endogenous Syntaxin 1A would compete for binding to SNAP25. This allows us to only focus on the interaction of GFP-SNAP25 and Stx-full or Stx-ΔS. GFP-SNAP25 was pulled down from Lämmli-lysed cells using anti-GFP agarose beads, analysed by western blot and stained against the myc-tag of the syntaxin-constructs. Figure 5.8 shows that the pull-down of GFP-SNAP25 was essentially complete and a large fraction of Stx-full was co-immunoprecipitated (compare weak band in flow-through and strong band in pull-down). Compared to that, the interaction with Stx-ΔS is almost completely abolished (Figure 5.8), obvious by the weak myc-staining in the pull-down. Quantification shows that only around 10 % of Stx-ΔS is co-immunoprecipitated in comparison to Stx-full.

This diminished interaction supports the view that the difference in epitope accessibility (Figure 5.7) when overexpressing Stx-full compared to the variant with a shortened SNARE-domain is due to a Syntaxin 1A-SNAP25 interaction.

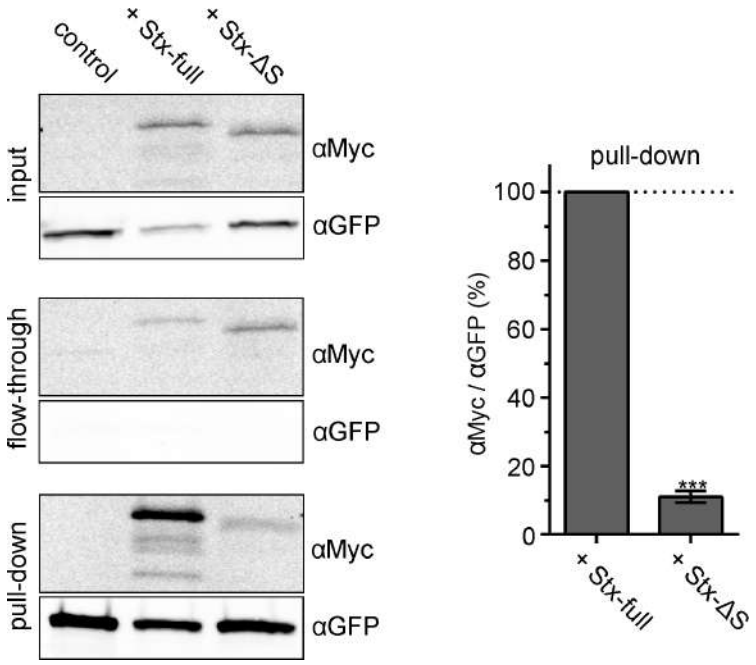

FIGURE 5.8: **Co-IP reveals diminished interaction between GFP-SNAP25 and Syntaxin 1A with a shortened SNARE-motif.** Expression of GFP-SNAP25 alone (control) or together with Stx-full or Stx-ΔS in HepG2 cells (which lack endogenous SNARE-proteins) and subsequent immunoprecipitation of GFP-SNAP25 with αGFP agarose beads. Left, Stx-full or Stx-ΔS visualized using an αMyc-tag antibody and GFP-SNAP25 using an αGFP antibody in the input (whole cell lysate), flow-through and pull-down. Right, band quantification of pull down. The αMyc band intensity is related to the αGFP band intensity and Stx-full is set to 100 %. Values are given as means ± SD (n = 3 experiments). Two-tailed t-test compares Stx-full to Stx-ΔS; ***$p < 0.001$. Transfection, lysis and pull-down of HepG2 cells was done by Jérôme Finke (Figure taken from: Mertins et al., 2021).

5.1.5 High-resolution STED microscopy to study mesoscale organization of SNARE-proteins at the plasma membrane

Subsequently, we analysed the lateral distribution of SNARE-proteins at the plasma membrane using high-resolution light microscopy. For this, the same samples as in the previous experiment employing epifluorescence imaging see (Figure 5.7) were recorded.

The high-resolution imaging data was further analysed employing a custom-written ImageJ macro, capable of extracting high-volumes of data describing distinct parameters of the two proteins of interest as cluster density, intensity and distances to each other. The custom-written ImageJ macro (for more information see section 4.2.11) determines the specific size of each detected maxima individually. Depending on the expression level and the ROI size of that particular sheet, we end up with up to several hundreds of analysed maxima for each sheet. For the specific maxima size, values were only included if they showed a R^2-value > 0.8 and if the peak of the gaussian fit was located close to the middle of the line scan. This selection was used to exclude maxima which were so close to each other that they already merged, leading to abnormal large maxima sizes.

Again, we examined the previously established overexpression conditions with either GFP-SNAP25 alone or in combination with Stx-full or Stx-ΔS. Given the tight interaction between Stx-full and GFP-SNAP25 (see Co-IP in Figure 5.8) and the diminished epitope accessibility (see epifluorescence imaging in Figure 5.7), Stx-full was hypothesized to influence the lateral distribution of SNAP25 in the plasma membrane. As stated before (see section 5.1.3.1), syntaxin-constructs were visualized employing conventional primary and secondary antibody staining (αHPC-1 coupled with AF594), whereas GFP-SNAP25 was visualized with an αGFP-nanobody coupled with ATTO647.

Visually, it is already obvious that the Syntaxin 1A staining is much more punctuate and consistent regarding the shape of the maxima. It is concentrated in sharply defined clusters with a diameter of $\sim$80 nm for the endogenous syntaxin control (control condition, Figure 5.9 A, top left image). Overexpression of Stx-full increases

the average staining intensity by ∼5-fold. The number of maxima triples and the specific maxima size increases by 40 % (Figure 5.9 B). Overexpression of the deletion construct Stx-ΔS leads to an even larger increase in staining intensity by up to 11-fold. Compared to Stx-full, the number and size of maxima increases even further (∼400 % and ∼180 % increase, respectively). This is to be expected, because at the same molecule copy number, Stx-ΔS clusters are stained more efficient due to their less tight packing (Merklinger et al., 2017).

Compared to that, the SNAP25 staining (αGFP-nanobody coupled with ATTO647), is present in diffuse structures spread out all over the plasma membrane (Figure 5.9 A). Because nanobodies are directly linked to a fluorophore, they do not produce the same signal amplification as primary and secondary antibody staining. The lower signal-to-noise ratio might also lead to a diffuser signal appearance and thus influences the counting of maxima, which will most likely be overestimated. This is the reason why the analysis of maxima sizes is not presented here for SNAP25, because the results are presumably not very reliable given the weak staining. Therefore, we opted for the analysis of the degree of clustering, rSDM.

As shown in Figure 5.7 and Figure 5.9 A, expression of Stx-full decreases the ROI intensity of SNAP25 (quantification of ATTO647 intensity). Together with that, the rSDM increases (Figure 5.9 C), which can also be observed as a less abundant staining in the images (compare upper and middle row in Figure 5.9 A). As already seen in Figure 5.7, the expression of Stx-ΔS does not influence SNAP25 in the same way when looking at the parameter ROI intensity or the additional parameters rSDM and maxima density.

A detailed analysis of the overlap of both proteins (Figure 5.9 D) shows an expected increase in overlap when raising the overall syntaxin level by adding Stx-full (See Figure 5.9 A as well). Interestingly, the increase in overlap is even stronger when Stx-ΔS is overexpressed. Yet, given our expectation that Stx-ΔS clusters form less efficiently and hence Stx-ΔS is more homogeneously distributed all over the membrane, a larger overlap between Syntaxin 1A and SNAP25 is expected.

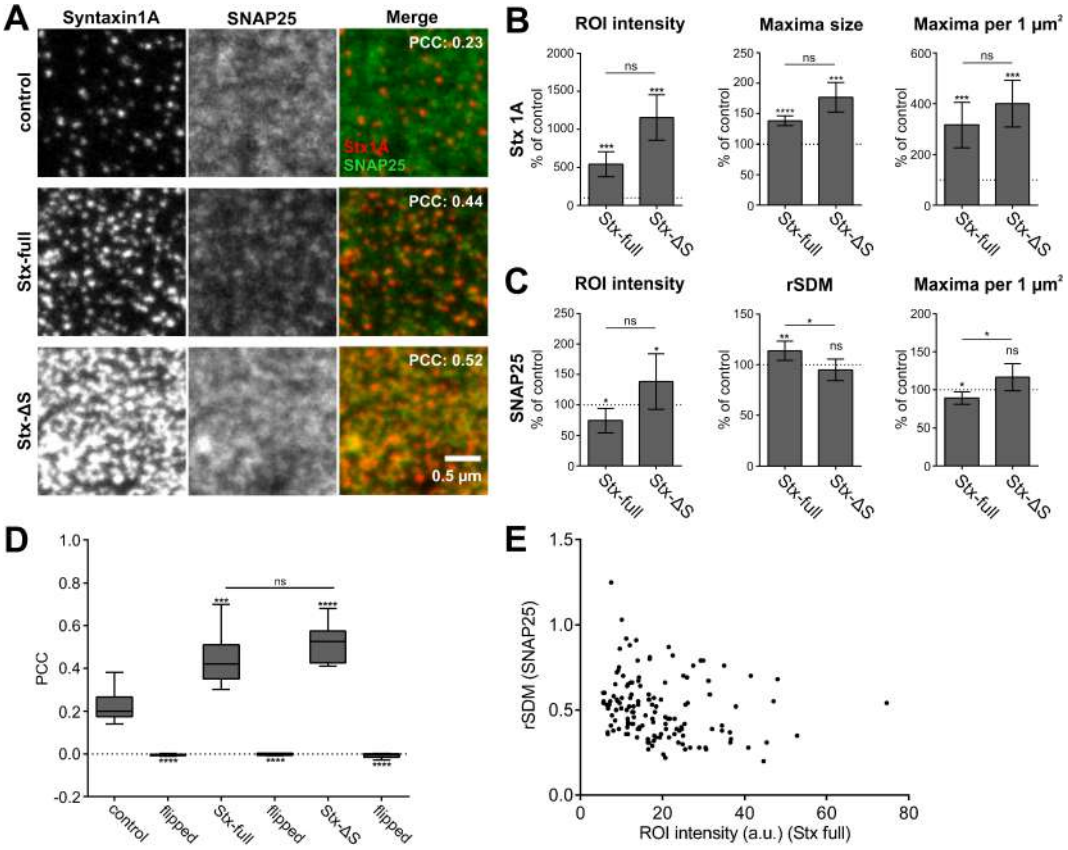

FIGURE 5.9: **Syntaxin 1A clusters change the distribution of SNAP25.** Membrane sheets are generated from PC12 cells expressing GFP-SNAP25 alone (control) or together with Stx-full or Stx-ΔS. Endogenous Syntaxin 1A/Stx-myc constructs are visualized by an antibody raised against the molecule's N-terminus, coupled an AF594-coupled secondary antibody; GFP-SNAP25 is visualized by an ATTO647-labelled αGFP nanobody. **(A)** Representative images from the Syntaxin 1A or SNAP25 channel for each condition, PCC is given in the top right corner (for more details see D). **(B)** Analysis of Syntaxin 1A ROI staining intensity, maxima size and maxima density; control was used for normalization and set to 100 %. **(C)** For SNAP25, the ROI intensity, clustering degree (rSDM) and maxima density were analysed. Again, control value was used for normalization and set to 100 %. **(D)** PCC quantification and corresponding flipped control. (n = 6 to 9 experiments, including the three experimental preparations used in Figure 5.7; at least 15 membrane sheets were imaged per condition and experiment. Two-tailed student´s t-test compare (i) control to Stx-full/Stx-ΔS and (ii) Stx-full to Stx-ΔS; ns = not significant, $p > 0.05$; *$p < 0.05$; **$p < 0.01$; ***$p < 0.001$). **(E)** Individual membrane sheet intensity of Stx-full plotted against the rSDM of SNAP25. 139 single sheets from the Stx-full condition are shown (Figure taken and modified from: Mertins et al., 2021).

To rule out the possibility that the less homogeneous SNAP25 distribution and staining is an effect of a very high Stx-full expression level, individual sheet intensities of this condition were plotted against the clustering degree of SNAP25 (Figure

5.9 E). In fact, we do not observe an increase in the rSDM with the expression level. Furthermore, this shows that the ratio of the two proteins is also not the most important factor.

Finally, Figure 5.10 shows a magnified view of a few syntaxin-clusters and SNAP25. SNAP25 is located closely around clustered syntaxin. In general, we do not observe concentric clusters of Syntaxin 1A and SNAP25.

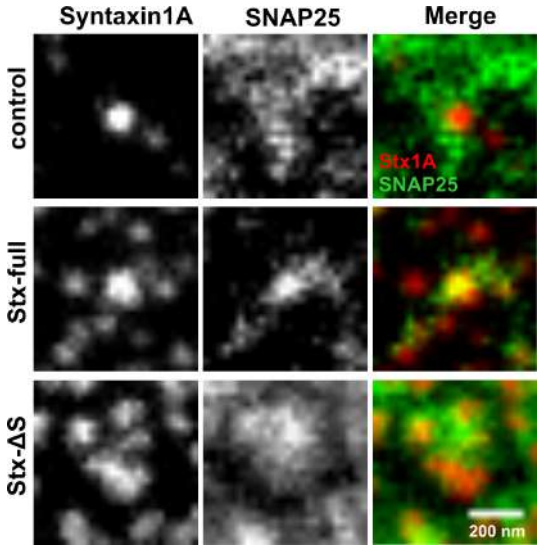

FIGURE 5.10: **Magnified view of Syntaxin 1A-clusters and SNAP25-crowds.** A magnified view shows that SNAP25 accumulates around Syntaxin 1A-clusters, the two proteins do not mix inside the cluster (Figure taken from: Mertins et al., 2021).

5.1.5.1 Maxima size distribution

To further characterize how SNAP25 maxima depend on the interaction with Syntaxin 1A, we looked more closely at the size distribution of the maxima. As already mentioned in the previous section 5.1.5, due to the lower signal-to-noise ratio of the SNAP25 staining with the αGFP-nanobody, maxima size analysis for this channel was not as decisive compared to the one for Syntaxin 1A maxima. Nevertheless, we wanted to take a closer look at the data, to see whether the SNAP25 maxima size may change overall, or if different populations can be distinguished with regards to the co-expression of Stx-full or Stx-ΔS. In addition, we analysed the size distribution of endogenous Syntaxin 1A, Stx-full and Stx-ΔS maxima.

Maxima sizes were determined on the basis of high-resolution images presented

in Figure 5.9 employing the previously mentioned custom-written ImageJ macro (see section 4.2.11 and section 5.9). Figure 5.9 B already shows the average maxima size of Syntaxin 1A in each condition (control, Stx-full and Stx-ΔS). In the following analysis, all maxima sizes from each independent experiment and sheet were pooled and sorted into 10 nm steps.

Figure 5.11, upper graph shows the maxima size distribution of endogenous Syntaxin 1A (red bars, control) and upon expression of Stx-full (black bars, Stx-full) and Stx-ΔS (grey bars, Stx-ΔS) in percentages. When looking at endogenous Syntaxin 1A only, the maxima size peaks at around 60 - 70 nm. Overall, around a third of all analysed maxima show this size. This is close to previously found average syntaxin-cluster sizes of ∼65 nm in STED-microscopy (Sieber et al., 2007) and ∼50 nm in PALM (Rickman et al., 2010).

Upon expression of the Stx-full construct, maxima sizes increase over the whole spectrum, peaking at around 70 - 80 nm. This is to be expected when raising the syntaxin concentration at the plasma membrane, because it was already reported that overexpression leads to a higher cluster density, which are not much bigger (Sieber et al., 2006; Merklinger et al., 2017). Expression of Stx-ΔS shifts the distribution of maxima sizes even further towards bigger maxima. The peak is lower, but still located at a maximum diameter of 70 - 80 nm, yet with only 15 % of all maxima. Maxima sizes from 120 nm upwards is dominated by Stx-ΔS maxima.

SNAP25 on the other hand shows a very different maxima size distribution (Figure 5.11, lower graph). Maxima cover a wider range of sizes, with overall less pronounced peaks compared to Syntaxin 1A maxima distribution. As already stated previously, due to the more diffuse staining of GFP-SNAP25, we most likely overestimate the maxima sizes. Keeping that in mind, in comparison to the control, we can still see a very prominent shift of SNAP25 maxima sizes towards smaller values when Stx-full is expressed, with a peak at 60 - 70 nm. This presents a stark contrast to the expression of Stx-ΔS that does not induce such a change, but it looks more similar to the observed maxima sizes when no additional syntaxin is expressed (control).

Hence, the syntaxin-variant with the shortened SNARE-motif (Stx-ΔS) does not

seem to have the ability to change the distribution of SNAP25, like Stx-full has altogether.

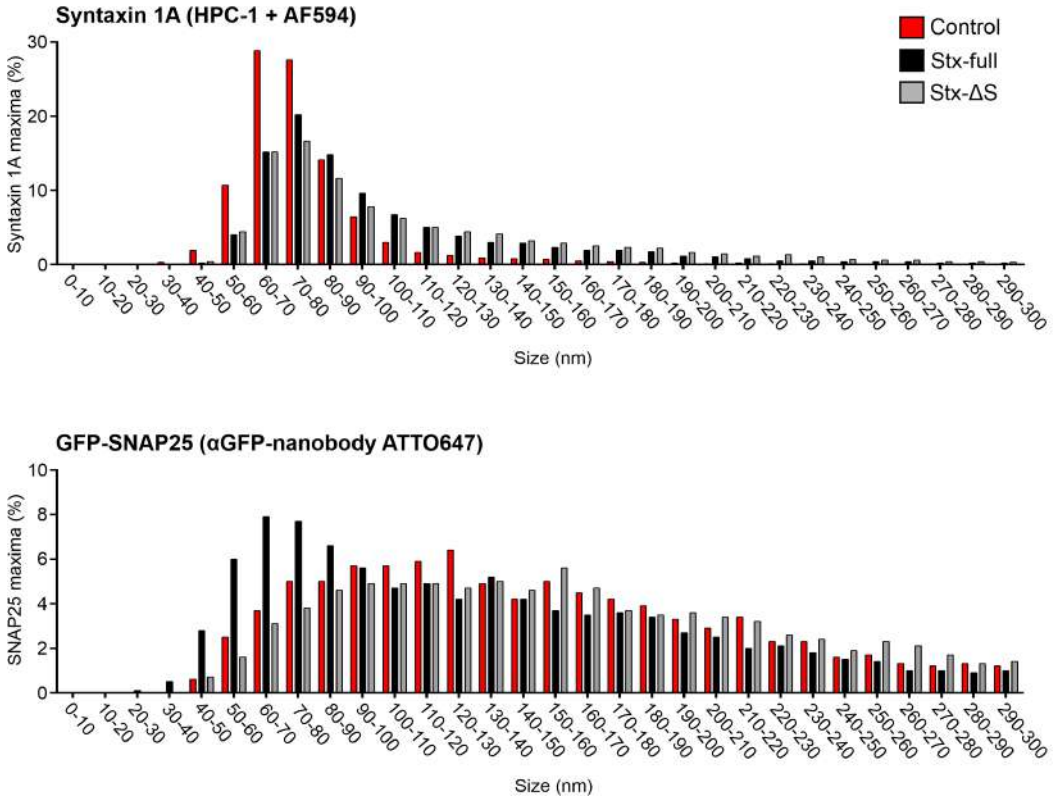

FIGURE 5.11: **Maxima size distribution of Syntaxin 1A and SNAP25.** Histogram of maxima sizes from Syntaxin 1A and SNAP25 in the control (red bars, endogenous Syntaxin 1A) and after expression of Stx-full (black bars) or Stx-ΔS (grey bars). Given is the percentage of clusters found in a bin with a size of 10 nm. This graph only shows maxima sizes up to 300 nm, for a complete maxima size distribution up to 1000 nm, see Suppl. Figure 7.1.

5.1.6 Imaging with exchanged spectral properties to assure that SNAP25 staining is less defined

As mentioned before, we observe a rather diffuse staining pattern with a low signal-to-noise ratio for GFP-SNAP25 when using the αGFP-nanobody coupled with ATTO647, which is in contrast to the defined staining of Syntaxin 1A with the HPC-1 primary antibody and secondary antibody coupled to AF594. We argue that this difference in staining pattern is due to the organization of the protein itself on the membrane and not influenced by the chosen fluorophore. To determine that the spectral properties of the fluorophores do not influence the outcome of the analysis, the fluorophores were exchanged and the analysis repeated.

For this,PC12 cells were transfected with GFP-SNAP25 alone or in combination with either Stx-full or Stx-ΔS and treated as mentioned before. To visualize Syntaxin 1A, the HPC-1 antibody was now visualized with a secondary antibody coupled with ATT0647. For SNAP25 on the other hand, an αGFP-nanobody coupled with ATTO594 was employed. Please note that we could not use a nanobody coupled with AF594 because it is not commercially available. However, AF594 and ATTO594 have very similar spectral properties, which makes ATTO594 a suitable replacement for this experiment.

After switching the spectral properties, example images from membrane sheets (5.12 A) show a very similar staining pattern as already observe in Figure 5.9. Regarding the staining of Syntaxin 1A (control and Stx-full) and its deletion-variant Stx-ΔS, we still see a defined cluster-staining, cluster size and density (compare Figure 5.9 B and Figure 5.12 B). We can also still observe that Stx-full influences SNAP25-distribution compared to Stx-ΔS (see decrease in SNAP25 staining intensity and maxima density as well as an increased clustering degree, Figure 5.12 C). Furthermore, even in the other channel, the staining from GFP-SNAP25 still looks more diffuse compared to the Syntaxin 1A staining.

Thus, we can conclude that the difference in visual appearance in the STED-micrographs is not based on different spectral properties of the fluorophores.

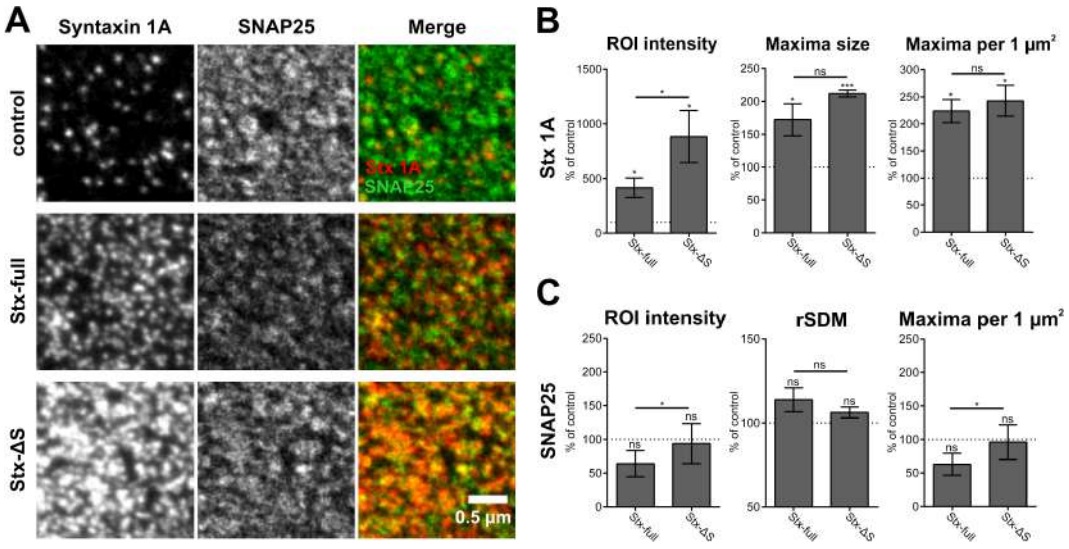

FIGURE 5.12: **Exchanging spectral properties of Syntaxin 1A and SNAP25 staining. (A)** Images from membrane sheets after exchanging the spectral properties of the fluorophores used in the different channels. SNAP25 is now visualized with an αGFP-nanobody coupled with ATTO594, Syntaxin 1A with the αHPC-1 antibody coupled with an ATTO647 secondary antibody. **(B and C)** As in Figure 5.9, detailed analysis of Syntaxin 1A and SNAP25 parameters describing their lateral distribution in the plasma membrane. All values given as mean ±SD, related to control set to 100 % (n = 3 experiments, 20 membrane sheets were imaged per condition and experiment. Two-tailed student´s t-test compare (i) control to Stx-full/Stx-ΔS and (ii) Stx-full to Stx-ΔS; ns = not significant, $p > 0.05$; *$p < 0.05$; **$p < 0.01$; ***$p < 0.001$.) (Figure taken an modified from: Mertins et al., 2021).

5.1.7 Role of SNAP25 SNARE-motifs in the mesoscale organization

So far, experiments show that Syntaxin 1A with a complete SNARE-motif (Stx-full) seems to be able to influence the lateral organization of SNAP25. Compared to Syntaxin 1A, SNAP25 has two SNARE-motifs. They are both involved in the formation of the ternary SNARE-complex during membrane fusion (Stein et al., 2009). We were wondering if both SNARE-motifs are also required for the mesoscale organization or whether one is sufficient. Hence, we compared three SNAP25 deletion constructs where either the C-terminal (SNAP25-ΔC), N-terminal (SNAP25-ΔN) or both SNARE-motifs (SNAP25-ΔN/C) are deleted and that were co-expressed with Stx-full. As a control, SNAP25-GFP with both SNARE-motifs (SNAP25-WT) was used. The control condition is identical to the "Stx-full" condition in Figure 5.9.

Comparing the mean ROI intensities (data not shown), SNAP25-WT shows the

lowest of all constructs with a gradual increase with a deletion from the N- to C-terminal domain or both (see also Figure 5.13 A, upper row). The inversed tendency is also seen for the PCC and the rSDM (5.13 B and C).

Deleting one or more SNARE-motifs of SNAP25 leads to a more homogeneous distribution of the protein. When plotting the rSDM against the mean ROI intensity of single membrane sheets (Figure 5.13 D), at the same ROI intensity, SNAP25-WT show a higher clustering degree (black regression line), compared to SNAP25-ΔN/C (grey regression line, see magnification in Figure 5.13 D and compare top left and top right images in A). This implicates that in SNAP25-ΔN/C the SNAP25-crowds are less tightly packed with a better accessibility to the GFP-tag (see Figure 5.7). Deletion of the N-terminal motif (SNAP25-ΔN) leads to similar looking membrane sheets, deletion of the C-terminal motif leads to membrane sheets looking more similar to the control (SNAP25-WT). Figure 5.13 E visualizes the radial pair distribution function (RPDF; as g(r)). This analysis describes the probability to find a syntaxin-cluster in a shell (15 nm) around a SNAP25-crowd at a certain radius (r(nm)). We find SNAP25-WT closer to syntaxin-clusters than all the other SNAP25 constructs. Deleting the C-terminal domain leads to less syntaxin-clusters in the proximity of SNAP25, yet it does not show such a drastic decrease as the other two deletion variants.

This leads us to the conclusion that SNAP25´s N-terminal SNARE-motif is more important for the mesoscale organization on the plasma membrane and primarily interacts with syntaxin´s SNARE-motif.

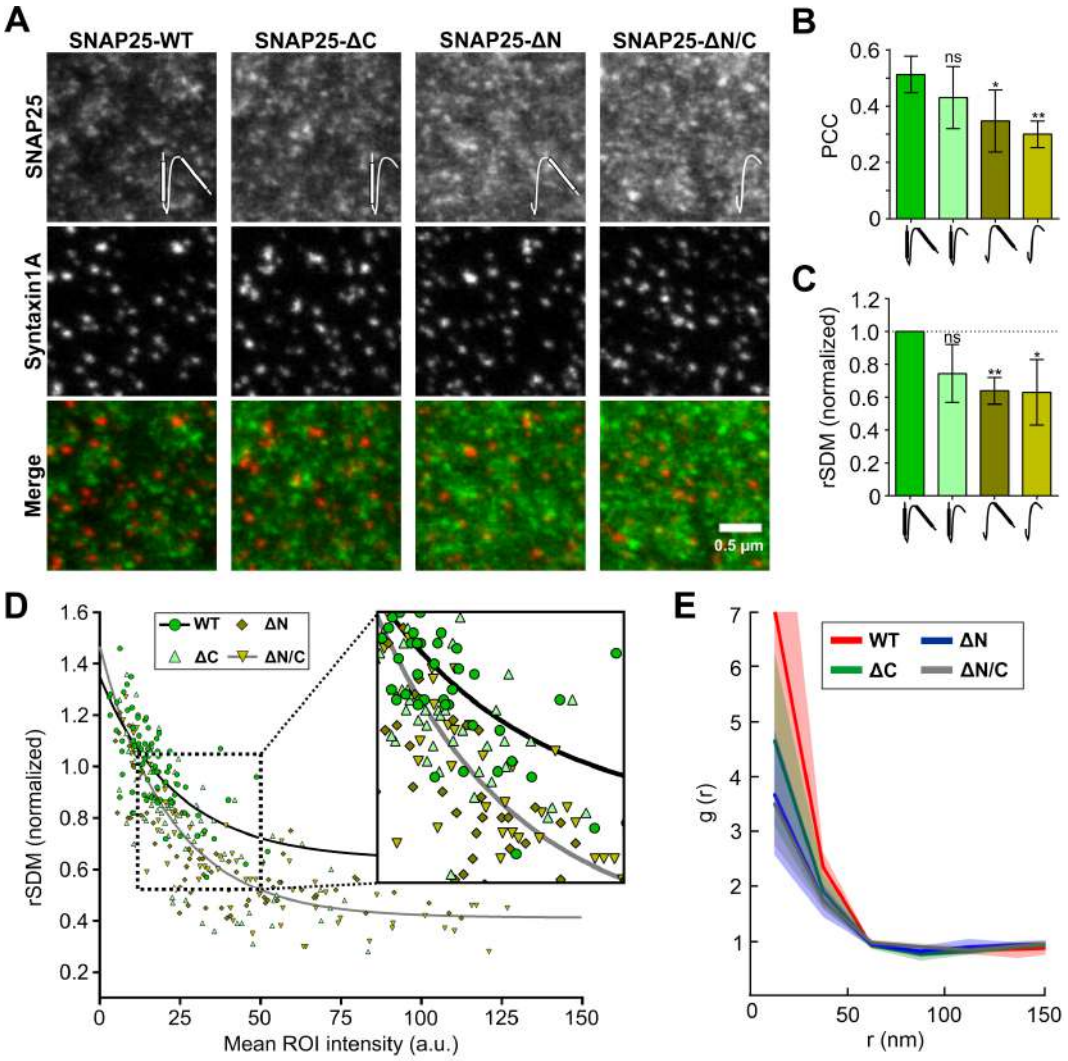

FIGURE 5.13: **Analysis of SNAP25-deletion constructs to identify the SNARE-motif responsible for Syntaxin 1A mediated mesoscale organization. (A)** Example images from membrane sheets of PC12 cells expressing Stx-full in combination with either GFP-SNAP25 (SNAP25-WT), a GFP-SNAP25 construct lacking the C-terminal motif (SNAP25-ΔC), the N-terminal motif (SNAP25-ΔN) or both motifs (SNAP25-ΔN/C). **(B)** PCC between Stx-full and each GFP-SNAP25-construct. **(C)** rSDM of GFP-SNAP25 normalized to the WT, set to 100 %. **(D)** rSDM from individual membrane sheets of GFP-SNAP25 constructs plotted against their mean ROI intensity. **(E)** Radial pair distribution function (RPDF; as g(r)). SNAP25 is the reference maxima, shown is the probability to find a syntaxin maxima in a shell (15 nm) around a SNAP25 maxima at a certain radius (r(nm)). Analysis of RDF contributed by Prof. Jan Hasenauer. Parts of transfection, immunostaining and imaging was done by Jérôme Finke (Figure and legend modified from: Mertins et al., 2021).

5.2 Influence of regulatory factors on the mesoscale organization

So far, this study could show that Syntaxin 1A is capable of influencing SNAP25-crowds via a SNARE-SNARE-motif interaction. Furthermore, it was shown that the N-terminal domain of SNAP25 is the main interaction partner for syntaxin´s SNARE-motif. Re-organization in the plasma membrane might be a way to ensure proper formation of the acceptor-complex (see section 6).
A follow up question is, whether Syntaxin 1A and SNAP25 are the only two proteins involved in the regulation of the mesoscale organization or if other regulatory proteins might play a role in this. For example, Munc18-1 or Complexin are important proteins that interact with SNARE-proteins / SNARE-complexes before membrane fusion (Rizo et al., 2015).

5.2.1 Munc18-1

The SNARE-cycle (see section 2.3.5) includes several regulatory proteins which influence and orchestrate this process. Looking at the proteins involved, one promising candidate that might be able to change the organization of SNAREs at the plasma membrane is Munc18-1. It has been shown to tightly interact with Syntaxin 1A, dominantly by stabilizing its closed conformation (Misura et al., 2000; Chen et al., 2008), yet it is also able to bind to the open conformation (Burkhardt et al., 2008) as well as to assembled t-SNARE-complexes (Dulubova et al., 2007; Shen et al., 2007). Furthermore, high-resolution imaging data and Co-IP show a tripartite interaction of Munc18-1-Syntaxin 1A-SNAP25, where Syntaxin 1A is the connecting link between Munc18-1 and SNAP25 (Pertsinidis et al., 2013).
Therefore, to test the influence of Munc18-1 on the mesoscale organization of Syntaxin 1A (and/or SNAP25), we incubated plasma membrane sheets with Munc18-1. Previously, we tested whether plasma membrane sheets possess free binding sites for Munc18-1 and whether it binds efficiently to Syntaxin 1A.

5.2.1.1 Munc18-1 recruitment to the plasma membrane depends on the full SNARE-motif of Syntaxin 1A

To study whether Munc18-1 binds to Syntaxin 1A, we used an approach based on HepG2 cells which do not express neuronal SNARE-proteins like Syntaxin 1A and SNAP25. HepG2 cells were transfected with Munc18-1-GFP together with Stx-full or Stx-ΔS. Stx-ΔS was used as a control because it lacks part of the SNARE-motif and therefore an important point of interaction (Merklinger et al., 2017). In this co-expression system we can study the influence of syntaxin´s-SNARE motif on the recruitment of Munc18-1 to the plasma membrane .

Studies show that Syntaxin 1A alone is able to traffic to the cell membrane (Toonen et al., 2005; Merklinger et al., 2017). In PC12 cells, Munc18-1 localization to the plasma membrane depends on direct interaction with Syntaxin 1A (Schütz et al., 2005). Here, we wanted to validate this hypothesis with our own syntaxin-deletion construct with a truncated SNARE-motif. We would expect less binding of Munc18-1 to the plasma membrane compared to Stx-full. Munc18-1-GFP fluorescence was amplified with an αGFP-nanobody coupled to ATTO488, whereas syntaxin-constructs were visualized via their 3xmyc-tag (αMyc-tag visualized with a secondary antibody coupled to AF594). Here, we switched from the previously used HPC-1 antibody (visualizing endogenous Syntaxin 1A and Stx-full/Stx-ΔS) to labelling the C-terminal 3xmyc-tag localized at the extracellular side. Switching the labelling strategy was necessary, because after Munc18-1 is bound to Syntaxin 1A at the plasma membrane, the epitope for the HPC-1 antibody is probably masked and therefore inaccessible.

Employing epifluorescence imaging, we analyse single membrane sheets (representative images in Figure 5.14 A), plotting the Munc18-1 staining against the Stx-myc staining intensity (Figure 5.14 B). The more Stx-myc staining we observe, the more Munc18-1 is recruited to the plasma membrane. However, we see a strong difference in Munc18-1 plasma membrane localization depending on the SNARE-motif. Red circles indicate plasma membrane sheets shown for illustration. For better comparison, a 2-times brighter sheet from the Stx-ΔS-condition was chosen

as Stx-ΔS is better accessible for the antibody and thus yields a several-fold stronger staining at the same molecule number . Comparison of the dependency of recruited Munc18-1 from Stx/Stx-ΔS constructs indicates that Stx-ΔS almost completely has lost its ability to recruit Munc18-1.

We conclude that Syntaxin 1A with the complete SNARE-domain (Stx-full) is able to recruit Munc18-1 to the plasma membrane in a very efficient manner, compared to Stx-ΔS, where we observe almost no staining at the plasma membrane anymore.

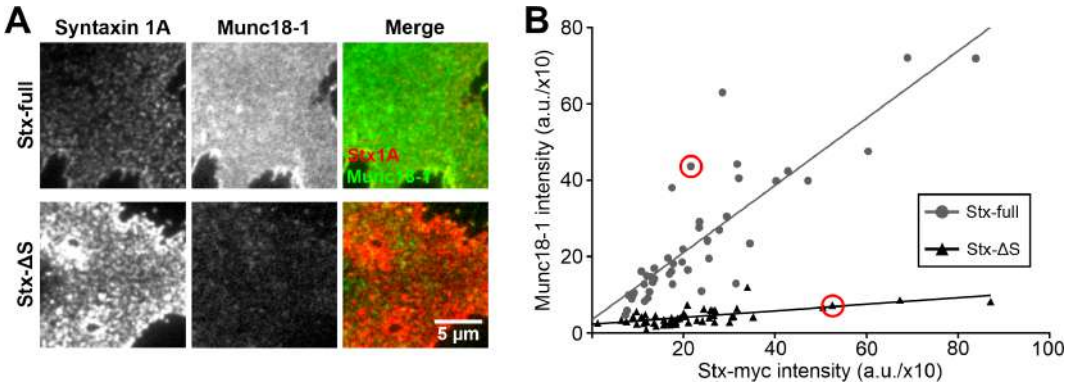

FIGURE 5.14: **Munc18-1 needs an intact SNARE-motif for membrane recruitment by Syntaxin 1A. (A)** Representative HepG2 membrane sheets from cells transfected with Munc18-1-GFP in combination with either Stx-full (upper row) or Stx-ΔS (lower row). Images in one channel are displayed with the same intensity scaling employing a linear LUT. Syntaxin 1A constructs are stained with an αMyc-antibody (visualized with a secondary antibody coupled to AF594), GFP-signal intensity of Munc18-1 is enhanced with an αGFP-nanobody (coupled to ATTO488). **(B)** Single membrane sheet intensities in both channels are plotted against each other and a linear regression line (employing a least square´s fit) is fitted through the data points. Red circles indicate the two membrane sheets shown in (A) (membrane sheets collected from n = 3 independent experiments, at least 15 sheets were imaged per condition and experiment).

5.2.1.2 Free Munc18-1 binding sites on PC12 membrane sheets overexpressing Stx-full-myc

Next, PC12 cells were used to characterize the binding of recombinant Munc18-1 to free binding sites. To assess the binding, we turned to only overexpressing Stx-full-myc alone and incubated the membrane sheets with recombinant Munc18-1. We had to overexpress Stx-full-myc to be able to stain the myc-tag because we can not use the HPC-1 antibody (see also previous section 5.2.1.1). Still, we wanted to

test to which degree the binding of Munc18-1 is dependent on the amount of available Syntaxin 1A. Stx-full is labelled with an αMyc-tag antibody visualized with a secondary antibody coupled to AF594, Munc18-1 with an antibody raised against the protein itself and visualized with a StarGreen coupled secondary antibody. It needs to be mentioned that we might deal with an unphysiological ratio between Syntaxin 1A and SNAP25 that may also affect the Munc18-1 binding sites, but because we were trying to proof the principle, this was ignored in this experiment.

Representative epifluorescence images in Figure 5.15 A show the six conditions that were compared. After sonication, membrane sheets were either incubated with buffer only to determine any incubation effects or with four different Munc18-1 concentrations: 0.5, 1, 2 and 4 µM. Control is defined as the directly fixed condition, with no further incubation. Signal in the StarGreen-channel in the control and buffer condition is arising from endogenous Munc18-1 in PC12 cells. We assume that not all Munc18-1 binding sites are occupied before addition of recombinant Munc18-1, because both proteins bind in a 1:1 stoichiometry (Misura et al., 2000) and Syntaxin 1A is present in a roughly 20-fold excess over Munc18-1 in PC12 cells (Schütz et al., 2005) already without syntaxin overexpression. Overexpression of Stx-myc should lead to a further increase in available binding sites.

As expected, the Munc18-1/green signal intensity rises when recombinant Munc18-1 is added (Figure 5.15 B). Upon incubation with only buffer, the signal intensity decreases slightly, most likely due to Munc18-1 dissociating from the membrane. Interestingly, we can not observe a correlation between the average ROI intensity of overexpressed Stx-full and Munc18-1 concentration (Figure 5.15 C). However, when plotting the Stx-myc expression level against the Munc18-1-intensity on the level of single membrane sheets, it is clear that the binding is dependent on the syntaxin level (Figure 5.15 C). Hence, even adding only 0.5 µM of Munc18-1 increases the staining intensity to almost the same level as 4 µM Munc18-1 does.

This suggests that already the lowest concentration of 0.5 µM is able to saturate most of the available Munc18-1 binding sites, even after overexpression of Stx-full.

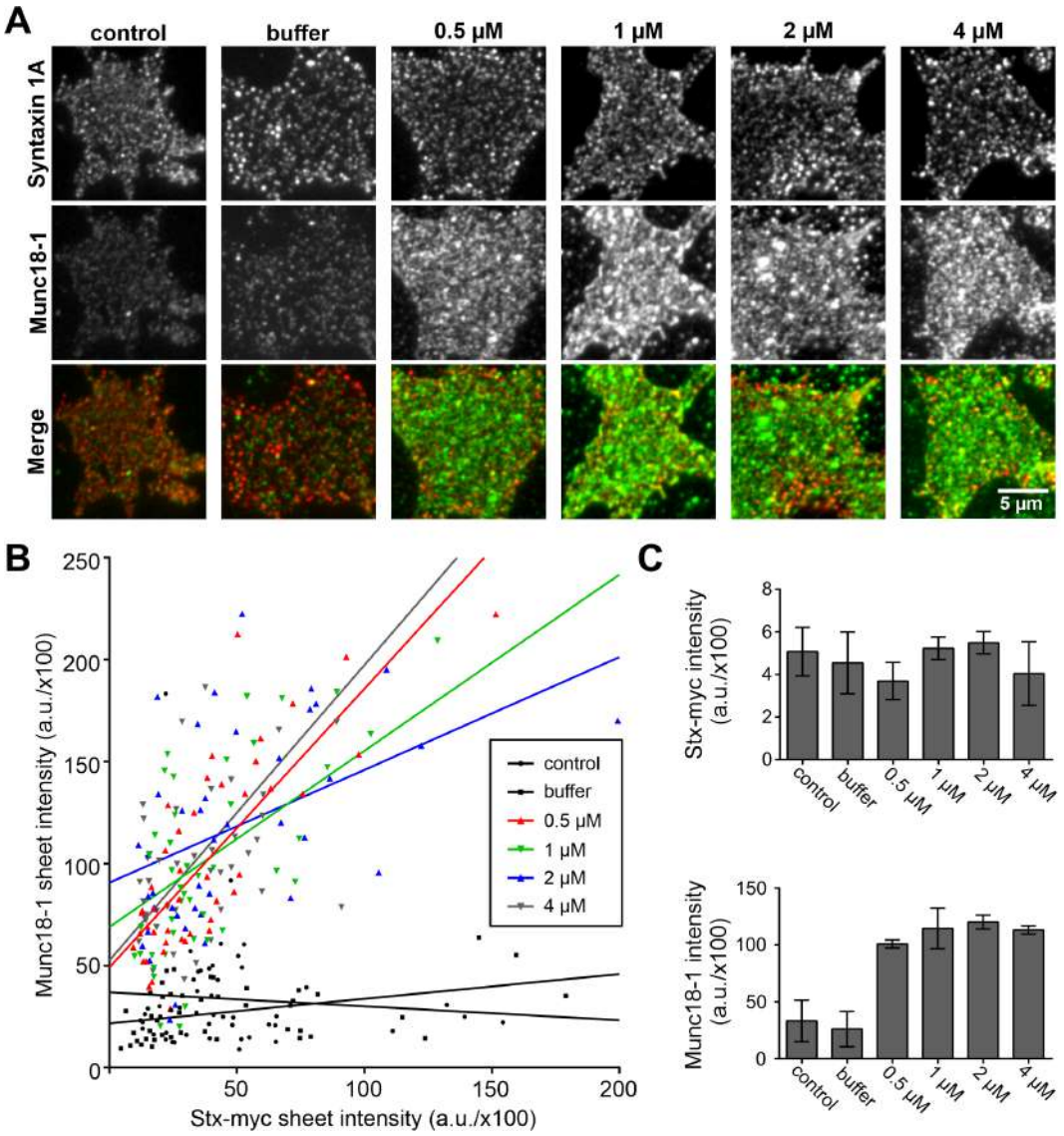

FIGURE 5.15: **Munc18-1 binding to PC12 membrane sheets overexpressing Stx-myc.** PC12 plasma membrane sheets directly fixed or incubated with different buffers to characterize binding capacity of Munc18-1. **(A)** Representative images from all conditions. Upper row shows Stx-full-myc, where the myc-tag (αMyc-tag antibody visualized with a secondary antibody coupled to AF594) is immunostained. Membrane sheets were chosen representing a similar Stx-myc expression level to compare Munc18-1 binding. Middle row shows membrane sheet staining against Munc18-1 (αMunc18 antibody visualized with a secondary antibody coupled to StarGreen). Control and buffer condition show endogenous Munc18-1. Lower row shows the merged image. Membrane sheets from one channel are displayed with the same scaling employing a linear LUT, to showcase the increase in Munc18-1-staining upon addition of recombinant protein. **(B)** Both staining´s from single membrane sheet are plotted against each other with a linear regression line fitted through (employing least squares fit). They show a positive correlation between Syntaxin 1A expression level and Munc18-1 staining intensity. **(C)** Bar graphs showing mean ROI intensity for Syntaxin 1A (top panel) and Munc18-1 (lower panel). All values given as mean ±SD. (n = 2 independent experiments, at least 18 sheets were imaged per condition and experiment).

5.2.1.3 Influence of Munc18-1 on the SNARE-mesoscale organization

To test the influence of recombinant Munc18-1 on the mesoscale organization of Syntaxin 1A and/or SNAP25, PC12 cells were used. For visualization purposes, GFP-SNAP25 was overexpressed and visualized with an αGFP-nanobody coupled with ATTO647. Endogenous Syntaxin 1A was visualized using the previously mentioned HPC-1 antibody in combination with a secondary antibody coupled with AF594. If Munc18-1 is a positive regulator of the mesoscale distribution of SNARE-proteins, we would expect parameters to change in a way that indicates more clustering of Syntaxin 1A and/or SNAP25, this means less maxima per μm^2, an increase in the rSDM and a decrease in ROI intensity. PC12 cells expressing GFP-SNAP25 were either directly fixed (control), incubated for 15 min with control buffer or with 6 µM Munc18-1.

Comparing directly fixed membrane sheets (control) with membrane sheets incubated for 15 min without Munc18-1 (0 µM Munc18), it appears that Syntaxin 1A starts patching together (compare Syntaxin 1A staining in upper and middle row in Figure 5.16 A). This is confirmed in a trend towards a lower number of maxima. This phenomenon has already been described before (Zilly et al., 2011). In contrast to that, SNAP25 maxima density do not change upon incubation with recombinant Munc18-1. None of the analysed parameter change significantly in the presence of additional Munc18-1. For SNAP25, there is only a tendency towards a higher clustering degree upon addition of 6 µM Munc18-1, which is accompanied by a very slight drop in ROI intensity (Figure 5.16 C).

However, none of the observed effects are significant. Consequently, we reason that Munc18-1 has no influence on the lateral distribution of neither Syntaxin 1A nor SNAP25.

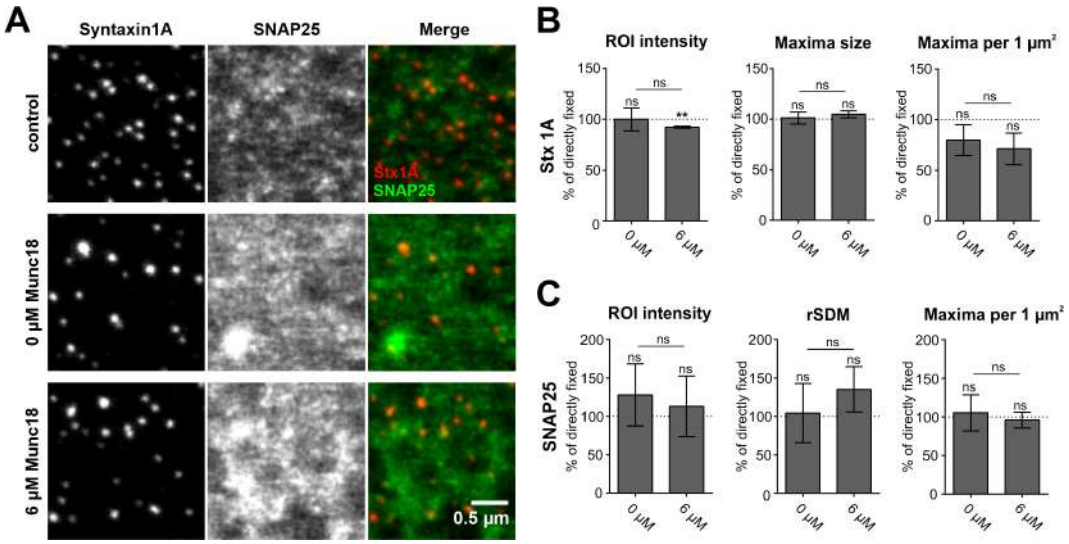

FIGURE 5.16: **Munc18-1 does not influence the distribution of SNAREs.** Membrane sheets from PC12 cells expressing GFP-SNAP25 were directly fixed or incubated with buffer only (0 µM Munc18-1) or with 6 µM Munc18-1 . **(A)** Example images illustrating the three conditions. Endogenous Syntaxin 1A is visualized by the HPC-1 antibody coupled with AF594, GFP-SNAP25 is visualized by an αGFP-nanobody coupled to ATTO647. **(B)** Analysis of Syntaxin 1A average ROI intensity, maxima size and maxima per µm2, related to the average of directly fixed membrane sheets (set to 100 %). **(C)** Analysis of SNAP25 average ROI intensity, clustering degree (rSDM) and maxima density, related to directly fixed membrane sheets. Values are given as means ±SD (n = 3 experiments, at least 10 sheets were imaged per condition and experiment). Two-tailed student´s t-test compare (i) control to 0 µM Munc18-1/6 µM Munc18-1 and (ii) 0 µM Munc18-1 to 6 µM Munc18-1 ; ns = not significant, $p > 0.05$, $^{**}p < 0.01$. (Figure and legend modified from: Mertins et al., 2021).

6 Discussion

In this study, the mesoscale organization of the two classical SNARE-proteins Syntaxin 1A and SNAP25 was investigated. Before neuronal exocytosis takes place, the two proteins can be found at the plasma membrane of neuroendocrine cells as well as in the presynaptic membrane of neurons. But they are not randomly scattered, yet show a specific organization on the mesoscale. Especially the nanoclustering behaviour of Syntaxin 1A has been studied intensively. SNAP25 is also involved in the SNARE nanocluster organization.

This study shows that syntaxin-clusters are able to redistribute the more widespread and abundant SNAP25 on the plasma membrane using conventional (Figure 5.7) and high-resolution microscopy (Figure 5.9) in combination with the plasma membrane sheeting technique. To further characterize the interaction, deletion constructs of Syntaxin 1A and SNAP25 were examined (Figure 5.1). Using Co-Immunoprecipitation (Figure 5.8) and assessing the specific distribution in the plasma membrane using a custom written macro (Figure 5.9 and Figure 5.13), it was determined that the heterophilic protein-protein interactions are mainly facilitated via the SNARE-motif.

Several regulatory proteins help to facilitate the complex process of neuronal exocytosis. One very interesting protein here is the S/M-protein Munc18-1. It binds tightly to Syntaxin 1A, yet its specific function in neuronal exocytosis is not elucidated in detail. Here, we used recombinant Munc18-1 on membrane sheets (Figure 5.15 and Figure 5.16). The results of this study suggest that Munc18-1 has no role in the regulation of the mesoscale distribution of Syntaxin 1A and/or SNAP25 at the plasma membrane.

6.1 Challenges of labeling proteins in a cluster

To visualize the organization of proteins at the plasma membrane, fluorescent labeling is inevitable. Already labeling of single proteins using traditional immunocytochemistry presents challenges, such as unwanted background or unspecific staining. Visualizing proteins in a tight cluster presents the additional challenge that the important epitope might be buried within the cluster, thus hindering correct fluorescent labeling. To characterize the composition of a protein cluster, we would ideally need a stoichiometric staining where each protein is labeled with one fluorophore.

A study from 2019 compared antibody and nanobody labeling of Syntaxin 1A and SNAP25 employing high-resolution microscopy on cultured primary hippocampal neurons (Maidorn et al., 2019). For this, the group developed specific nanobody-probes in their own lab, via immunization of alpacas and subsequent phage-display. The nanobodies were then coupled with an ATTO647-fluorophore. Both nanobodies detected the same populations as the conventional antibodies, yet showed a more "smooth" distribution. Furthermore, they revealed a previously unknown population of SNARE-proteins outside of synapses. They also tested their nanobodies in PC12 cells, where they support our assumption that conventional antibodies have difficulties reaching all epitopes in a cluster (Maidorn et al., 2019).

When Syntaxin 1A is engaged in tight homophilic clusters, we most likely deal with a sub-stoichiometric labeling, meaning that not every single protein copy inside a cluster is recognized by a primary antibody. The primary antibody which we use for Syntaxin 1A detection is raised against the HPC-1 epitope (located at the N-terminal domain of Syntaxin 1A). Once the single proteins are tightly engaged in a cluster, it is practically impossible for the relatively bulky primary antibody ($\sim$150 kDa; $\sim$15 nm x $\sim$5 nm (San Paulo et al., 2000)) to reach every epitope (Figure 6.1). Yet, we can use this fact to our advantage because, as already shown in a study by Merklinger et al. (Merklinger et al., 2017) and this study, a sub-stoichiometric labeling allows us to draw conclusions from the cluster staining intensity onto the

cluster packing density. A decrease in staining intensity points to a tighter packing of molecules inside the cluster which makes epitopes inaccessible for staining probes (as seen here in Figure 5.6, epifluorescence imaging in Figure 5.7 and high-resolution imaging in Figure 5.9).

On the other hand, for SNAP25, we do not have a reliable primary antibody available. Previous studies employing conventional antibodies show very precise, punctuate staining patterns (as seen in Rickman et al., 2010 and Saka et al., 2014). On the other hand, genetic labeling of SNAP25 leads to a more widespread, less pronounced distribution. Immunostaining of PC12 membrane sheets which also overexpressed YFP-SNAP25, show that not every YFP-SNAP25 molecule is also positive for an antibody (Zilly et al., 2011). Further studies have also raised serious doubts concerning these spotted staining patterns which are often seen in high-resolution images employing conventional antibodies (Opazo et al., 2012; Reshetniak et al., 2020).

Because of that inconclusive staining, for this study a SNAP25-construct with a N-terminal GFP-tag was moderately overexpressed in PC12 cells. The GFP-tag itself is rather large in comparison to SNAP25 (27 kDa vs. 25 kDa, respectively). the rigidtiy and size of the GFP-tag could theoretically influence the behaviour of SNAP25. But first, it was shown that the expression of GFP-tagged SNAP25 is able to rescue synaptic transmission in SNAP25-knockout mice, hence it is fully functional even with this rather large tag. Second, results shown in Figure **??** B confirm that we raise the overall concentration of SNAP25 by a maximum of 4-fold, the majority is raised between 2- and 3-fold. Especially for high-resolution imaging in Figure 5.9, sheets in the middle expression range were chosen, because over a certain threshold of expression, it was not possible anymore to resolve single protein clusters. So we assume that around half of all SNAP25 molecules are labeled with a GFP-tag which should not interfere with clustering mechanisms. Thus we assume that this approach represents the distribution of SNAP25 in the plasma membrane best.

Because the GFP-tag itself is not suitable for high-resolution STED-microscopy, we labeled the GFP-tag with an αGFP-nanobody ($\sim$15 kDa; $\sim$2-5 nm) coupled with

ATTO647. Stainings for high-resolution microscopy employing a nanobody coupled with an organic dye showed very good results in the past (Ries et al., 2012). The nanobody used in this study exhibits a 1:1 binding towards GFP, and each nanobody is labeled with one fluorophore (Degree of labeling; DOL = 0.8-1.2). The epitope-label displacement is minimized in this approach, but we do not have the signal amplification which we observe using conventional antibodies. This might explain some of the lower signal-to-noise ratios observed in Figure 5.9.

6.2 Staining patterns and implications on clustering density

As already mentioned before, in tightly clustered proteins we can observe the effect that we encounter different staining intensities due to the protein´s packing density. Here, we do not only observe this for Syntaxin 1A (as already shown in Merklinger et al., 2017), but also for SNAP25. Epifluorescence images in Figure 5.7 show a lower GFP-SNAP25 signal intensity upon overexpression of Stx-full. The lower intensity from the GFP-tag itself raised the question whether we might deal with a lower expression level at the membrane. This was excluded by verifying the trafficking of GFP-SNAP25 to the membrane in the absence or presence of additional syntaxin-constructs (Figure 5.4). If we have a similar amount of GFP-SNAP25 at the plasma membrane, then what is the reason for the decrease in intensity of the GFP-tag and the ATTO647-fluorophore? Previous studies showed that if two fluorophores come in close proximity ($\sim$5 nm or less), this can lead to self-quenching effects (Schneider et al., 2021). A study from 2016 observed a similar effect of GFP-self-quenching after oligomerization/aggregation of single amyloid-β-GFP-fusion proteins (Ochiishi et al., 2016). Thus, we attribute this change in the observed staining intensity to a tighter packing of GFP-SNAP25.

The decrease in nanobody-intensity might be explained that upon close contact of both molecules, the accessibility of the nanobody towards its GFP-epitope is hindered, which leads to less binding and consequently a lower signal intensity. We argue that this is most likely due to shielding of the epitope from syntaxin´s

rather large N-terminal domain (see Figure 6.1). Yet, we can not rule out any self-quenching effects if two ATTO647-fluorophores come in close contact.

However, the lateral changes of SNAP25 in the plasma membrane can not be explained by distortions in the imaging process, it is rather likely a consequence of a tighter packing and decreased epitope accessibility. So we assume that the GFP-SNAP25 signal decreases because SNAP25-crowds are recruited towards syntaxin-clusters.

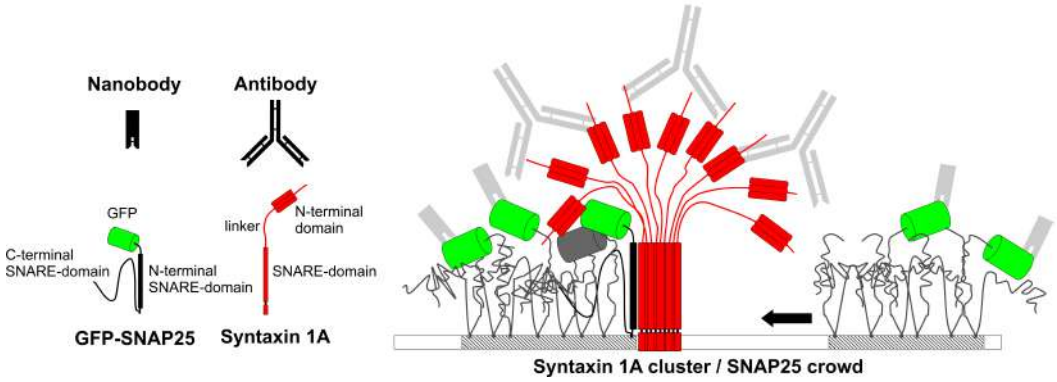

FIGURE 6.1: **Schematic model of the mesoscale re-organization of SNAP25-crowds via Syntaxin 1A-clusters. Left side:** In this study, GFP-SNAP25 is labeled with an αGFP-nanobody coupled to ATTO647, whereas Syntaxin 1A (and Stx-full/Stx-ΔS) is labeled with a conventional antibody (αHPC-1) coupled to AF594 (sizes not to scale). **Right side:** Integrating the results from this study with previous literature, we propose the following model: Syntaxin 1A molecules are able to form tightly packed clusters on their own, resembling a bunch of flowers. (GFP-)SNAP25 molecules exist either as an unbound or bound crowd. In an unbound crowd, every GFP-SNAP25 can be detected with a nanobody, due to loosely packing and the existence of endogenous, untagged SNAP25. Here, GFP-self quenching is less likely because the GFP-tags are more spaced out and able to move freely. This is very different in a bound crowd. In this instance, we assume that (GFP-)SNAP25 molecules come closer together. SNAP25´s N-terminal motif interacts with syntaxin´s SNARE-motif pulling the SNAP25-crowd towards the cluster. Consequently, some GFP-tags are shielded under syntaxin´s rather larger N-terminal domain which renders them inaccessible for a nanobody. Furthermore, due to the closer packing of the molecules and being immobilized under the cluster´s roof, we observe self-quenching. One syntaxin-clusters is able to interact with several SNAP25-crowds, because we can observe that Syntaxin 1A influences a surplus of SNAP25 (Figure 5.9). Dashed part of the membrane illustrates cholesterol lipid phases. Upon interaction with Syntaxin 1A, SNAP25's SNARE-motif becomes alpha helical (black rectangle), prior to that its unstructured (Fasshauer et al., 1997a) (Figure modified from: Mertins et al., 2021).

6.3 SNARE-protein ratios of PC12 cells

Since Syntaxin 1A and SNAP25 were overexpressed for most of the experiments (either alone or together), it was crucial to make sure that we always kept SNAP25 in a surplus especially at the plasma membrane, to not invert the physiological ratio in PC12 cells.

First, we determined the overall endogenous and overexpressed protein amount in whole PC12 cells using western bot analysis (Figure 5.2). Furthermore, we specifically determined the endogenous ratio of Syntaxin 1A and SNAP25 in our PC12 cells (Figure 5.3). To do this, we used a quantitative approach employing GFP-tagged constructs of both proteins. The GFP-tag can be stained with the same antibody and thus with the same affinity which allows us to calculate a conversion factor from overexpressed to endogenous protein, to determine the endogenous protein ratio. At an endogenous level in PC12 whole cells, SNAP25 is around 12-times more abundant than Syntaxin 1A (we observe a range in ratio in all three experiments from 9-fold up to 15-fold more SNAP25, single experimental data not shown here, Figure 5.3). This is on average slightly less than the previously reported value of a 17-fold excess of SNAP25 in PC12 cells (Knowles et al., 2010). This variety is probably a result of the difference in approach, ours averaging the ratio in the whole population of cells versus employing quantitative WB.

After conformation of similar trafficking rates of GFP-SNAP25 towards the plasma membrane in all three conditions (Figure 5.4), we looked directly at the ratio of Syntaxin 1A to SNAP25 at the plasma membrane (Figure 5.5). After overexpression of Stx-myc constructs alone or in combination with GFP-SNAP25, we push the ratio further towards Syntaxin 1A, still the estimated ratio at the plasma membrane of Stx1A:SNAP25 is roughly 1:5. Consequently, we would argue that we do not invert the ratio of Stx1A:SNAP25 in whole cells or at the plasma membrane.

A lower Syntaxin 1A amount seems to be important, because an elevated Syntaxin 1A level impairs the glucose-related insulin release in mouse pancreatic β-cells (Nagamatsu et al., 1996) and also restricts movement of SNAP25 at the plasma membrane ().

Interestingly, this massive surplus of SNAP25 is not reported consistently in all cell lines. In isolated rat boutons, studies found only 1.3-fold more SNAP25 than Syntaxin 1A (Wilhelm et al., 2014). Another study used an adipocyte cell line to determine the ratio of Syntaxin 4 (65 % aa identity with Syntaxin 1A; Bennett et al., 1993) and SNAP23 (60.5 % homology with SNAP25; expasy homology calculator), which together are important for insulin-dependent Glut4 translocation. They report a 3-fold excess of SNAP23 over Syntaxin 4 (Hickson et al., 2000). Ratio-values specifically at the AZ of neurons have not been reported yet, which might be due to its very small size (200-500 nm in diameter; Südhof, 2012) making it harder to investigate.

6.4 Essential anatomy of the Syntaxin 1A-SNAP25 mesoscale network

The fact that proteins organize into clusters at the plasma membrane is a well known phenomenon which can be observed in a variety of different membrane proteins. The term "mesoscale organization" describes the lateral organization of protein clusters in relation to one another (Saka et al., 2014; Lillemeier et al., 2006). Research shows that the two SNARE-proteins Syntaxin 1A and SNAP25 are distributed in-homogeneously in the plasma membrane. Each protein forms a cluster or crowd (referring to Syntaxin 1A or SNAP25, respectively) on its own. In this study we observe the already described pronounced Syntaxin 1A-clusters (Sieber et al., 2007; Knowles et al., 2010; Rickman et al., 2010), while SNAP25 on the other hand tends to form diffuse crowds which are more widespread on the membrane. Upon raising the syntaxin-concentration, we observe more clusters which also tend to be slightly bigger, simultaneously pulling SNAP25 with it, which is noticed in dimmer crowds and a higher degree of clustering (Figure 5.9). This recruitment of SNAP25 is facilitated via the full-length SNARE-motif of Syntaxin 1A, because experiments using the Stx-ΔS deletion construct did not show the same results.

We further identified the specific interaction from the perspective of SNAP25, employing different SNAP25-deletion constructs, deleting either only one or both SNARE-domains at the same time. By doing this, we could identify that the N-terminal SNARE-motif of SNAP25 plays a more important role in the interaction with syntaxin´s SNARE-motif (Figure 5.13). Deleting the C-terminal SNARE-motif exhibits no significant effect, yet it still shows a trend towards a lower rSDM (Figure 5.13 C). This observation is in accordance with the literature, because SNAP25-constructs where the N-terminal SNARE-motif was still present, showed decreased diffusion in FRAP-experiments when Syntaxin 1A was present as well (Halemani et al., 2010). The results presented in this study together with FRAP-data from Halemani et al., show that the C-terminal SNARE-motif does not interact with syntaxin´s SNARE-motif in the same way as the N-terminal SNARE-motif does. Interestingly, also the position of the motif within SNAP25 plays a role, because placing the N-terminal motif at SNAP25´s C-terminus did not slow down the diffusion of SNAP25 as mentioned before.

The influence of syntaxin-clusters onto SNAP25-crowds is also visible when looking at the maxima size distribution (Figure 5.11). When raising the concentration of Stx-full in the plasma membrane, we see that syntaxin-cluster sizes rise up around 20 nm (from 60-70 nm up to 70-80 nm). SNAP25 crowd sizes decrease from 120-130 nm down to 60-70 nm, so almost half in size. This is no bleed-through artefact (which was also tested once with n=18 sheets, data not shown here), because then we would expect that this bleed through effect is even more prominent with the Stx-ΔS variant which shows several-fold brighter staining intensities, which is not the case. SNAP25-crowds are rather large (peak at 150-160 nm) when Stx-ΔS is present. The signal-to-noise ratio is another important point that should be considered when talking about maxima sizes. GFP-SNAP25 shows a lower staining intensity and signal-to-noise ratio than Syntaxin 1A. Smaller and darker crowds might not be detected which leads to an overestimation of crowd-sizes. Yet if we overestimate all sizes, this should not influence the overall trend.

Taken together, the data presented here points to the fact that SNARE-SNARE-interactions are not only involved in driving neuronal exocytosis, but also generally

organize Syntaxin 1A and SNAP25 on the mesoscale at the plasma membrane.

6.5 What is the internal structure of a Syntaxin 1A-SNAP25 cluster?

The spatial localization and organization of Syntaxin 1A and SNAP25 at the plasma membrane has been studied employing different high-resolution microscopy techniques in the past.

In our study, we do not observe a complete overlap or mixing of Syntaxin 1A and SNAP25 in one cluster (Figure 5.10). Yet, we can not decisively conclude the internal structure, because the resolution of the here used STED-microscope setup is only ∼70 nm (calculated PSF for 594 and 647 channels are 67 nm and 66 nm, respectively; see Mertins et al., 2021), which is not enough to resolve single molecules. From the here presented data, we assume that we might deal with one of the following interaction scenarios:

One possibility would be that only molecules at the border of the entities interact. In single-molecule localization experiments, the molecule concentration thins out towards the periphery, both in Syntaxin 1A and SNAP25 entities, which is why Syntaxin 1A-SNAP25 complexes could form in areas of lower packing around the core of syntaxin clusters (Bar-On et al., 2012). In a simplified view, in this scenario we deal with two syntaxin cluster phases, a pure cluster core and a cluster-annulus containing heteromeric complexes. However, there may be no annulus. Instead, the syntaxin-cluster trunk could constitute a tight oligomeric bundle of alpha-helical SNARE-domains, serving as a binding surface for SNAP25. The SNARE-domain of SNAP25 could zipper into one of the grooves of the trunk, becoming alpha-helical as well (Figure 6.1), similar to the SNARE-zippering reaction upon SNARE-complex assembly (Brunger et al., 2019; Sutton et al., 1998). This model is supported by the finding that in the above-mentioned FRAP measurement, SNAP25 mobility increases after introducing helix breakers into the N-terminal SNARE-domain (Halemani et al., 2010). An alternative scenario would be clustering of binary Syntaxin 1A-SNAP25 complexes, in other words, there are no longer distinguishable Syntaxin 1A and SNAP25 entities. This interpretation is challenged by the following arguments. First, microscopic overlap between

syntaxin clusters and SNAP25 crowds is only partial in the sense that they do not overlap concentrically (Figure 5.10; see also Halemani et al., 2010). In single molecule imaging experiments, the majority of SNARE molecules are located in clusters and about half of the clustered Syntaxin 1A or SNAP25 molecules overlap with the nearest SNAP25 or syntaxin cluster, respectively (Pertsinidis et al., 2013). Regarding the high abundancy of SNAP25 in PC12 cells, one may not expect half of the SNAP25 crowds in close proximity to syntaxin clusters. However, it should be noted that in Pertsinidis et al. mouse hippocampal neurons were used and that in a similar sample (rat synaptosomes) SNAP25 is only slightly more abundant than Syntaxin 1A (Wilhelm et al., 2014). Moreover, as Pertsinidis et al. point out, not all molecules present may be detected, because steric hindrance does not allow binding of an antibody to every molecule in the cluster (Pertsinidis et al., 2013). Finally, the large fraction of SNAP25 being close to syntaxin clusters can also be explained by several SNAP25 crowds gathering around one syntaxin cluster. In any case, analysing overlap between two types of densely packed molecules is technically limited and provides no definite answer. For this reason, the following second argument is more conclusive. SNAP25 exceeds the concentration of Syntaxin 1A, in the condition Stx-full roughly still about 5-fold (see Figure 5.9). If clusters would be large oligomers of syntaxin-SNAP25 complexes, in the condition Stx-full, 80 % of SNAP25 should not respond to Syntaxin 1A overexpression. The strong effect we observe suggests that only a few molecules from the SNAP25 crowds directly interact with syntaxin clusters. Therefore, SNAP25 and Syntaxin 1A entities may largely preserve their identities, interacting only at their peripheries. However, under certain conditions the excess of SNAP25 may be just too large to be controlled by Syntaxin 1A. For instance, in the control of Figure 5.9, in which only SNAP25 is elevated, the cellular SNAP25:Syntaxin 1A ratio is expected to increase from 20- up to 30-fold (the 10-fold physiological ratio doubles/triples using membrane sheets from the middle expression range, Figure 5.5). Under this condition, the endogenous Syntaxin 1A is no longer capable of re-organizing the majority of SNAP25, explaining why SNAP25 is spread all over the membrane, also in areas lacking any Syntaxin 1A (Figure 5.9 A, upper row). [1]

[1] passage in italics taken from: Mertins et al., 2021

6.6 Functional relevance of SNARE-clustering on the membrane

Given the nature of SNARE-proteins, it is easy to come to the conclusion that clustering of SNARE-proteins might be important for neuronal exocytosis. Yet, the question remains whether functionally active complexes form inside or outside of SNARE-clusters.

Clustering of Syntaxin 1A molecules might also be a way to avoid unwanted complexes in the plasma membrane, which have been found to occur in solution when looking at isolated proteins. Clustering could be a mechanism to reduce the available Syntaxin 1A binding sites for SNAP25. It might inhibit the formation of the so-called "dead-end-complex", where one SNAP25 molecule is bound by two Syntaxin 1A molecules, as found in experiments using isolated proteins (Fasshauer et al., 2004). There is no definitive proof for the "dead-end-complex" in native membranes, which might be due to the bulk methods used for investigation or due to effective prevention of the complex.

Another thought might be that high local concentrations of SNARE-proteins at the plasma membrane might provide the necessary amount of interaction partners for the formation of SNARE-complexes needed for fast and constitutive exocytosis. Syntaxin-clusters especially could represent a "storage solution" for molecules that are being recruited to the place where they are needed. In notion with that, syntaxin-clusters themselves have been described as very dynamic entities, constantly assembling and dis-assembling or exchanging syntaxin -molecules between clusters (Barg et al., 2010; Sieber et al., 2007). Syntaxin-clusters present an internal density gradient, decreasing towards the edge. It has been shown that around a third of the whole syntaxin-population exists as freely moving, single molecules (Bar-On et al., 2012; Rickman et al., 2010). Looking at the NMJ from *Drosophila*, we can find syntaxin molecules also organized in defined clusters, the average cluster size was determined to be slightly larger compared to clusters found in cells. Upon synaptic activity, Syntaxin 1A clusters in NMJs decrease in size and single molecules increase in mobility (Bademosi et al., 2016). The same group also found

that the anesthetic "propofol" decreases Syntaxin 1A mobility in the membrane (combined with a decrease in neurotransmitter release) and traps them in nanoclusters on the pre-synaptic membrane. Cluster size, cluster number and molecule density inside the cluster increased significantly (employing single molecule localization in unstimulated PC12 cells). After abolishing the interaction with SNAP25 (by deleting syntaxin´s SNARE-motif almost completely), syntaxin´s mobility did not decrease as before. The requirement for an interaction with SNAP25 suggests that nanoclusters could be comprised of Syntaxin 1A/SNAP25 heterodimers which are important for neurotransmitter release (Bademosi et al., 2018).
Regarding the functional aspect, early studies proposed SNARE-clusters as direct sites of vesicle docking and fusion (Lang et al., 2001; Ohara-Imaizumi et al., 2004). Results from these studies could be interpreted that fusion takes place in close proximity next to/around a syntaxin-cluster, because the spatial resolution of resolution-limited microscopy would not have been able to differentiate between fusion directly at the cluster or next to it. Fusion of vesicles was localized to membrane parts which are enriched in PI(4,5)P2 (Milosevic et al., 2005), which coincides with syntaxin-clustering (Aoyagi et al., 2005). A more recent study also emphasizes syntaxin-clusters as a site of vesicle docking, not vesicle fusion (Gandasi et al., 2014).

6.7 Possible role of Munc18-1 on the network organization

Most, if not all research regarding the binding of Munc18-1 towards Syntaxin 1A (whether it is alone in the open or closed confirmation or engaged in a SNARE-complex) was done using isolated proteins employing biophysical approaches. There are little studies employing in-situ or in-vivo approaches specifically examining the binding modes of Munc18-1 towards single or complexed Syntaxin 1A. Regarding the controversy between results, it is questionable how far we can transfer results from studies with isolated proteins onto the actual behaviour of Munc18-1 and Syntaxin 1A in the densely crowded and highly dynamic environment of the plasma membrane.

In this study, we tried to elucidate the effect of recombinant Munc18-1 directly on plasma membranes sheets of PC12 cells. First, we confirmed that Munc18-1 binds to Syntaxin 1A. We can show that Munc18-1 locates to the plasma membrane when syntaxin´s SNARE-motif is present. Compared to that, the deletion construct Stx-ΔS is not able to facilitate trafficking of Munc18-1 to the plasma membrane (Figure 5.14). Those experiments were done in HepG2 cells, which do not endogenously express neuronal SNARE-proteins, showing that no other factors are required for the plasma membrane localization of Munc18-1 than the interaction with Syntaxin 1A. Syntaxin 1A constructs tagged with GFP are able to traffic to the plasma membrane without additional Munc18-1, as shown in experiments in a study from 2017 (Merklinger et al., 2017), in contrary to a previous study that claimed Syntaxin 1A needs Munc18-1 for efficient plasma membrane localization in non-neuronal cells (Rowe et al., 1999).

Establishing the approach to study the influence of recombinant Munc18-1 on the mesoscale organization of SNARE-proteins, we showed that recombinant Munc18-1 binds to the plasma membrane with a high affinity in PC12 cells. Upon overexpression of Stx-full-myc, adding 0.5 µM recombinant Munc18-1 saturated almost all of the available Syntaxin 1A binding sites (Figure 5.15). The binding of Munc18-1 showed a positive correlation with the Stx-full-myc expression level.

Investigating the role of Munc18-1 directly on the mesoscale organization SNARE-proteins showed no significant change in the lateral distribution of neither Syntaxin 1A nor SNAP25 (Figure 5.16). Admittedly, we observe a tendency of SNAP25 towards decreased ROI intensity and a slightly higher clustering degree (Figure 5.16 C), in combination with a decrease in ROI intensity of endogenous Syntaxin 1A. As we showed previously in this study, Syntaxin 1A influences the distribution of SNAP25 (Figure 5.9), thus after a certain point we would also expect changes in SNAP25´s distribution. Concluding from this, a slight decrease of the ROI intensity of Syntaxin 1A/SNAP25 could point to a regulatory function of Munc18-1. But especially due to the diffuse nature of the GFP-SNAP25 staining, we might not be able to pick up on such a small change.

There could also be other reasons why we cannot detect any significant changes of

Syntaxin 1A/SNAP25 upon increase of Munc18-1: One possibility might be that there is actually no change on the mesoscale, but only on the nanoscale. Single Munc18-1 molecules might form complexes with single Syntaxin 1A molecules at the periphery of the cluster, where syntaxin-molecules are less clustered (Bar-On et al., 2012). Syntaxin-molecules (most likely in their closed conformation) bound by Munc18-1 would exit the cluster, which could be detected as slightly smaller and darker syntaxin-clusters. One question remains, how many syntaxin-molecules would need to exit the cluster to result in a nanometer-size change? Different staining or detection methods need to be utilized to quantify these small changes on the nanoscale.

Another possibility would be that only upon stimulation of neuronal exocytosis we could see a change in the mesoscale distribution, dependent on Munc18-1. Syntaxin-clusters decrease in size upon exocytosis (Bademosi et al., 2016), this might be due to Munc18-1 releasing syntaxin-molecules from the periphery to supply the cell with further reactive Syntaxin 1A/Munc18-1 complexes (theoretically as the starting point for the SNARE-cycle). In this theory, Munc18-1 would displace SNAP25 from Syntaxin 1A (Ma et al., 2013). On the other hand, Munc18-1 can bind to Syntaxin 1A/SNAP25 complexes (Dawidowski et al., 2016), hence a triple complex consisting of Syntaxin 1A/SNAP25/Munc18-1 would be established (that acts as an acceptor for Synaptobrevin; Jakhanwal et al., 2017). Another group employed live-cell imaging of PC12 cells transfected with Stx-GFP to determined the requirements of Syntaxin 1A to be recruited into on-granule clusters. Via introducing different mutations into Syntaxin 1A, they found that mutations that abolished Stx1A/Munc18-1 binding in-vitro (Δ29-258 and ΔHabc; Yin et al., 2018) also diminished inclusion in on-granule clusters. Thus they propose a strong association between granules, Syntaxin 1A and Munc18-1.

Taken together, if Munc18-1 has any influence on the mesoscale distribution of Syntaxin 1A and/or SNAP25, then we are unable to detect these change with the here used methods, using recombinant Munc18-1 on PC12 membrane sheets visualized with high-resolution microscopy. Single-molecule fluorescence microscopy in live

PC12 cells could be an approach to study the mesoscale organization and potentially also dynamics on the plasma membrane of SNARE-proteins. One of the major problems for live-cell super-resolution microscopy is the availability of specific chemical binding probes for the protein of interest (here: Syntaxin 1A, SNAP25 and Munc18-1). Labeling of biomolecules with tags such as SNAP-tag, Halo-tag or Clip-tag have already been used (Wang et al., 2019), yet we still deal with the endogenous amount of the protein of interest. Stains for endogenous biomolecules are commercially only available for cytoskeletal-structures such as actin or tubulin. Until specific probes are available, a moderate overexpression system with GFP-tagged proteins is the best chance to gain more insight into the mesoscale organization of SNARE-proteins at the plasma membrane.

7 Supplementary information

7.1 Suppl. for 4.1.6.1: Whole analysed range of maxima

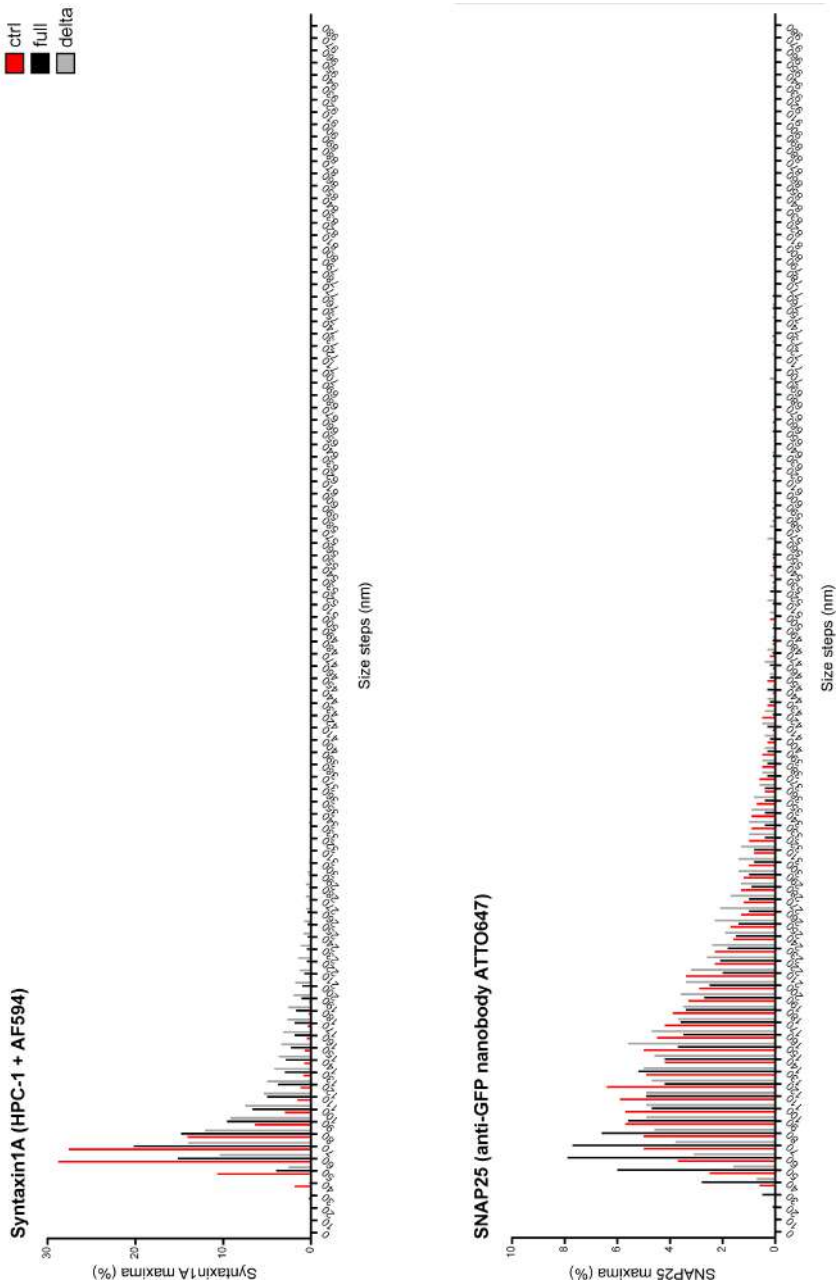

FIGURE 7.1: **Whole range of maxima size distribution of Syntaxin 1A and SNAP25.**

Bibliography

Aikawa, Yoshikatsu, Xiaofeng Xia, and Thomas F.J. Martin (Feb. 2006). "SNAP25, but not syntaxin 1A, recycles via an ARF6-regulated pathway in neuroendocrine cells". In: *Molecular Biology of the Cell* 17.2, pp. 711–722. ISSN: 10591524.

Antoku, Yasuko, Peter Dedecker, Paulo S Pinheiro, Tom Vosch, and Jakob Balslev Sørensen (2015). "Spatial distribution and temporal evolution of DRONPA-fused SNAP25 clusters in adrenal chromaffin cells †". In: *Photochem. Photobiol. Sci* 14, p. 1005. DOI: 10.1039/c4pp00423j.

Aoyagi, Kyota, Tsukiko Sugaya, Masato Umeda, Seiji Yamamoto, Susumu Terakawa, and Masami Takahashi (Apr. 2005). "The Activation of Exocytotic Sites by the Formation of Phosphatidylinositol 4,5-Bisphosphate Microdomains at Syntaxin Clusters". In: *Journal of Biological Chemistry* 280.17, pp. 17346–17352. ISSN: 0021-9258. DOI: 10.1074/JBC.M413307200.

Archbold, Julia K., Andrew E. Whitten, Shu Hong Hu, Brett M. Collins, and Jennifer L. Martin (Dec. 2014). "SNARE-ing the structures of Sec1/Munc18 proteins". In: *Current opinion in structural biology* 29, pp. 44–51. ISSN: 1879-033X. DOI: 10.1016/J.SBI.2014.09.003.

Arora, Swati, Ingrid Saarloos, Robbelien Kooistra, Rhea Van De Bospoort, Matthijs Verhage, and Ruud F Toonen (2017). "SNAP-25 gene family members differentially support secretory vesicle fusion". In: DOI: 10.1242/jcs.201889.

Avery, Julia, Darren J. Ellis, Thorsten Lang, Phillip Holroyd, Dietmar Riedel, Robert M. Henderson, J. Michael Edwardson, and Reinhard Jahn (Jan. 2000). "A Cell-Free System for Regulated Exocytosis in Pc12 Cells". In: *The Journal of Cell Biology* 148.2, p. 317. ISSN: 00219525. DOI: 10.1083/JCB.148.2.317.

Bacia, Kirsten, Christina G. Schuette, Nicoletta Kahya, Reinhard Jahn, and Petra Schwille (Sept. 2004). "SNAREs Prefer Liquid-disordered over "Raft" (Liquid-ordered) Domains When Reconstituted into Giant Unilamellar Vesicles". In:

Journal of Biological Chemistry 279.36, pp. 37951–37955. ISSN: 0021-9258. DOI: 10.1074/JBC.M407020200.

Bademosi, Adekunle T., Elsa Lauwers, Pranesh Padmanabhan, Lorenzo Odierna, Ye Jin Chai, Andreas Papadopulos, Geoffrey J. Goodhill, Patrik Verstreken, Bruno Van Swinderen, and Frédéric A. Meunier (Dec. 2016). "In vivo single-molecule imaging of syntaxin1A reveals polyphosphoinositide- and activity-dependent trapping in presynaptic nanoclusters". In: *Nature Communications 2017 7:1* 7.1, pp. 1–17. ISSN: 2041-1723. DOI: 10.1038/ncomms13660.

Bademosi, Adekunle T., James Steeves, Shanker Karunanithi, Oressia H. Zalucki, Rachel S. Gormal, Shu Liu, Elsa Lauwers, Patrik Verstreken, Victor Anggono, Frederic A. Meunier, and Bruno van Swinderen (Jan. 2018). "Trapping of Syntaxin1a in Presynaptic Nanoclusters by a Clinically Relevant General Anesthetic". In: *Cell Reports* 22.2, pp. 427–440. ISSN: 2211-1247. DOI: 10.1016/J.CELREP.2017.12.054.

Baker, Richard W. and Frederick M. Hughson (June 2016). "Chaperoning SNARE assembly and disassembly". In: *Nature Reviews Molecular Cell Biology 2016 17:8* 17.8, pp. 465–479. ISSN: 1471-0080. DOI: 10.1038/nrm.2016.65.

Bar-On, Dana, Ulrike Winter, Esther Nachliel, Menachem Gutman, Dirk Fasshauer, Thorsten Lang, and Uri Ashery (Oct. 2008). "Imaging the assembly and disassembly kinetics of cis-SNARE complexes on native plasma membranes". In: *FEBS letters* 582.23-24, pp. 3563–3568. ISSN: 0014-5793. DOI: 10.1016/J.FEBSLET.2008.08.040.

Bar-On, Dana, Steve Wolter, Sebastian Van De Linde, Mike Heilemann, German Nudelman, Esther Nachliel, Menachem Gutman, Markus Sauer, and Uri Ashery (Aug. 2012). "Super-resolution imaging reveals the internal architecture of nano-sized syntaxin clusters". In: *The Journal of biological chemistry* 287.32, pp. 27158–27167. ISSN: 1083-351X. DOI: 10.1074/JBC.M112.353250.

Barg, S., M. K. Knowles, X. Chen, M. Midorikawa, and Wolfhard Almers (Nov. 2010). "Syntaxin clusters assemble reversibly at sites of secretory granules in live cells". In: *Proceedings of the National Academy of Sciences of the United States of America* 107.48, pp. 20804–20809. ISSN: 1091-6490. DOI: 10.1073/PNAS.1014823107.

Bark, I. Christina and Michael C. Wilson (Feb. 1994). "Human cDNA clones encoding two different isoforms of the nerve terminal protein SNAP-25". In: *Gene* 139.2, pp. 291–292. ISSN: 0378-1119. DOI: 10.1016/0378-1119(94)90773-0.

Batoulis, Helena, Thomas H Schmidt, Pascal Weber, Jan-Gero Schloetel, Christian Kandt, and Thorsten Lang (2016). "Concentration Dependent Ion-Protein Interaction Patterns Underlying Protein Oligomerization Behaviours OPEN". In: DOI: 10.1038/srep24131.

Bennett, Mark K., Nicole Calakos, and Richard H. Scheller (1992). "Syntaxin: A synaptic protein implicated in docking of synaptic vesicles at presynaptic active zones". In: *Science* 257.5067, pp. 255–259. ISSN: 00368075. DOI: 10.1126/SCIENCE.1321498.

Bennett, Mark K., JoséE E. Garcia-Arrarás, Lisa A. Elferink, Karen Peterson, Anne M. Fleming, Christopher D. Hazuka, and Richard H. Scheller (Sept. 1993). "The syntaxin family of vesicular transport receptors". In: *Cell* 74.5, pp. 863–873. ISSN: 00928674. DOI: 10.1016/0092-8674(93)90466-4.

Block, M. R., B. S. Glick, C. A. Wilcox, F. T. Wieland, and J. E. Rothman (1988). "Purification of an N-ethylmaleimide-sensitive protein catalyzing vesicular transport". In: *Proceedings of the National Academy of Sciences of the United States of America* 85.21, pp. 7852–7856. ISSN: 0027-8424. DOI: 10.1073/PNAS.85.21.7852.

Block, Stephan (2018). "biomolecules Brownian Motion at Lipid Membranes: A Comparison of Hydrodynamic Models Describing and Experiments Quantifying Diffusion within Lipid Bilayers". In: *Biomolecules*. DOI: 10.3390/biom8020030.

Bock, Jason B, Hugo T Matern, Andrew A Peden, and Richard H Scheller (2001). "A genomic perspective on membrane compartment organization". In: *analysis NATURE* | 409.

Bogaart, Geert van den, Thorsten Lang, and Reinhard Jahn (2013). "Microdomains of SNARE proteins in the plasma membrane". In: *Current topics in membranes* 72, pp. 193–230. ISSN: 1063-5823. DOI: 10.1016/B978-0-12-417027-8.00006-4.

Boschert, Ursula, Celestine O'shaughnessy, Robin Dickinson, Michela Tessari, Caterina Bendotti, and Stefan Catsicas (1996). "Developmental and Plasticity-Related Differential Expression of Two SNAP-25 Isoforms in the Rat Brain". In: *THE*

JOURNAL OF COMPARATIVE NEUROLOGY 367.177, p. 193. DOI: 10.1002/(SICI)1096-9861(19960401)367:2.

Brunger, Axel T., Ucheor B. Choi, Ying Lai, Jeremy Leitz, Kristopher Ian White, and Qiangjun Zhou (Feb. 2019). "The pre-synaptic fusion machinery". In: *Current opinion in structural biology* 54, pp. 179–188. ISSN: 1879-033X. DOI: 10.1016/J.SBI.2019.03.007.

Burkhardt, Pawel, Douglas A. Hattendorf, William I. Weis, and Dirk Fasshauer (Apr. 2008). "Munc18a controls SNARE assembly through its interaction with the syntaxin N-peptide". In: *The EMBO Journal* 27.7, p. 923. ISSN: 02614189. DOI: 10.1038/EMBOJ.2008.37.

Calovi, Stefano, Federico N. Soria, and Jan Tønnesen (Aug. 2021). "Super-resolution STED microscopy in live brain tissue". In: *Neurobiology of Disease* 156, p. 105420. ISSN: 0969-9961. DOI: 10.1016/J.NBD.2021.105420.

Campbell, Biology, Jane B. Reece, Lisa A. Urry, Michael L. Cain, Steven A. Wasserman, Peter V. Minorsky, and Robert B. Jackson (Oct. 2010). *Campbell Biology*. Vol. 9. Benjamin Cummings.

Chamberlain, Luke H., Robert D. Burgoyne, and Gwyn W. Gould (May 2001). "SNARE proteins are highly enriched in lipid rafts in PC12 cells: implications for the spatial control of exocytosis". In: *Proceedings of the National Academy of Sciences of the United States of America* 98.10, pp. 5619–5624. ISSN: 0027-8424. DOI: 10.1073/PNAS.091502398.

Chamberlain, Luke H. and Gwyn W. Gould (Dec. 2002). "The vesicle- and target-SNARE proteins that mediate Glut4 vesicle fusion are localized in detergent-insoluble lipid rafts present on distinct intracellular membranes". In: *The Journal of biological chemistry* 277.51, pp. 49750–49754. ISSN: 0021-9258. DOI: 10.1074/JBC.M206936200.

Chebotareva, N. A., B. I. Kurganov, and N. B. Livanova (2004). "Biochemical effects of molecular crowding". In: *Biochemistry. Biokhimiia* 69.11, pp. 1239–1251. ISSN: 0006-2979. DOI: 10.1007/S10541-005-0070-Y.

Chen, Xiaocheng, Jun Lu, Irina Dulubova, and Josep Rizo (May 2008). "NMR Analysis of the Closed Conformation of Syntaxin-1". In: *Journal of biomolecular NMR* 41.1, p. 43. ISSN: 09252738. DOI: 10.1007/S10858-008-9239-1.

Chintagari, Narendranath Reddy, Nili Jin, Pengcheng Wang, Telugu Akula Narasaraju, Jiwang Chen, and Lin Liu (June 2006). "Effect of cholesterol depletion on exocytosis of alveolar type II cells". In: *American journal of respiratory cell and molecular biology* 34.6, pp. 677–687. ISSN: 1044-1549. DOI: 10.1165/RCMB.2005-0418OC.

Colbert, Karen N., Douglas A. Hattendorf, Thomas M. Weiss, Pawel Burkhardt, Dirk Fasshauer, and William I. Weis (July 2013). "Syntaxin1a variants lacking an N-peptide or bearing the LE mutation bind to Munc18a in a closed conformation". In: *Proceedings of the National Academy of Sciences of the United States of America* 110.31, pp. 12637–12642. ISSN: 00278424.

Dawidowski, Damian and David S. Cafiso (Mar. 2016). "Munc18-1 and the Syntaxin-1 N Terminus Regulate Open-Closed States in a t-SNARE Complex". In: *Structure* 24.3, pp. 392–400. ISSN: 0969-2126. DOI: 10.1016/J.STR.2016.01.005.

Delgado Cruz, Mariel and Kyoungtae Kim (2019). "The inner workings of intracellular heterotypic and homotypic membrane fusion mechanisms". In: *J Biosci*. DOI: 10.1007/s12038-019-9913-3.

Delgado-Martínez, Ignacio, Ralf B. Nehring, and Jakob B. Sørensen (Aug. 2007). "Differential abilities of SNAP-25 homologs to support neuronal function". In: *Journal of Neuroscience* 27.35, pp. 9380–9391. ISSN: 02706474. DOI: 10.1523/JNEUROSCI.5092-06.2007.

Dulubova, Irina, Mikhail Khvotchev, Siqi Liu, Iryna Huryeva, Thomas C. Südhof, and Josep Rizo (Feb. 2007). "Munc18-1 binds directly to the neuronal SNARE complex". In: *Proceedings of the National Academy of Sciences of the United States of America* 104.8, pp. 2697–2702. ISSN: 00278424.

Dulubova, Irina, Shuzo Sugita, Sandra Hill, Masahiro Hosaka, Imma Fernandez, Thomas C. Südhof, and Josep Rizo (Aug. 1999). "A conformational switch in syntaxin during exocytosis: role of munc18". In: *The EMBO journal* 18.16, pp. 4372–4382. ISSN: 0261-4189. DOI: 10.1093/EMBOJ/18.16.4372.

Dulubova, Irina, Tomohiro Yamaguchi, Demet Araç, Hongmei Li, Iryna Huryeva, Sang Won Min, Josep Rizo, and Thomas C. Südhof (Jan. 2003). "Convergence and divergence in the mechanism of SNARE binding by Sec1/Munc18-1ike proteins". In: *Proceedings of the National Academy of Sciences of the United States of America* 100.1, pp. 32–37. ISSN: 00278424.

Fasshauer, Dirk, Dieter Bruns, Betty Shen, Reinhard Jahn, and Axel T. Brünger (1997a). "A structural change occurs upon binding of syntaxin to SNAP-25". In: *The Journal of biological chemistry* 272.7, pp. 4582–4590. ISSN: 0021-9258. DOI: 10.1074/JBC.272.7.4582.

Fasshauer, Dirk, R Bryan Sutton, Axel T Brunger † ‡, and Reinhard Jahn (1998). "Conserved structural features of the synaptic fusion complex: SNARE proteins reclassified as Q-and R-SNAREs (membrane fusionneurotransmissionclostridial neurotoxins)". In: *Neurobiology* 95, pp. 15781–15786.

Fasshauer, Dirk and Martin Margittai (Feb. 2004). "A Transient N-terminal Interaction of SNAP-25 and Syntaxin Nucleates SNARE Assembly". In: *Journal of Biological Chemistry* 279.9, pp. 7613–7621. ISSN: 00219258. DOI: 10.1074/JBC.M312064200.

Fasshauer, Dirk, Henning Otto, William K. Eliason, Reinhard Jahn, and Axel T. Brünger (Oct. 1997b). "Structural changes are associated with soluble N-ethylmaleimide-sensitive fusion protein attachment protein receptor complex formation". In: *The Journal of biological chemistry* 272.44, pp. 28036–28041. ISSN: 0021-9258. DOI: 10.1074/JBC.272.44.28036.

Fernandez, Imma, Josep Ubach, Irina Dulubova, Xiangyang Zhang, Thomas C. Südhof, and Josep Rizo (Sept. 1998). "Three-dimensional structure of an evolutionarily conserved N-terminal domain of syntaxin 1A". In: *Cell* 94.6, pp. 841–849. ISSN: 0092-8674. DOI: 10.1016/S0092-8674(00)81742-0.

Fernández-Chacón, Rafael, Andreas Königstorfer, Stefan H. Gerber, Jesús García, Maria F. Matos, Charles F. Stevens, Nils Brose, Josep Rizo, Christian Rosenmund, and Thomas C. Südhof (Mar. 2001). "Synaptotagmin I functions as a calcium regulator of release probability". In: *Nature* 410.6824, pp. 41–49. ISSN: 0028-0836. DOI: 10.1038/35065004.

Fowler, Philip W., John J. Williamson, Mark S.P. Sansom, and Peter D. Olmsted (Sept. 2016). "Roles of Interleaflet Coupling and Hydrophobic Mismatch in Lipid Membrane Phase-Separation Kinetics". In: *Journal of the American Chemical Society* 138.36, pp. 11633–11642. ISSN: 15205126.

Frick, Manfred, Katja Schmidt, and Benjamin J. Nichols (Mar. 2007). "Modulation of Lateral Diffusion in the Plasma Membrane by Protein Density". In: *Current Biology* 17.5, pp. 462–467. ISSN: 09609822. DOI: 10.1016/J.CUB.2007.01.069.

Fujimoto, Toyoshi and Ingela Parmryd (Jan. 2017). "Interleaflet coupling, pinning, and leaflet asymmetry-major players in plasma membrane nanodomain formation". In: *Frontiers in Cell and Developmental Biology* 4.JAN, p. 155. ISSN: 2296634X.

Gandasi, Nikhil R. and Sebastian Barg (May 2014). "Contact-induced clustering of syntaxin and munc18 docks secretory granules at the exocytosis site". In: *Nature communications* 5. ISSN: 2041-1723. DOI: 10.1038/NCOMMS4914.

Goodsell, David S. (1992). *The Machinery of Life*. Springer New York. DOI: 10.1007/978-0-387-84925-6.

Grant, Nancy J., Regine Hepp, Winfried Krause, Dominique Aunis, Peter Oehme, and Keith Langley (1999). "Differential expression of SNAP-25 isoforms and SNAP-23 in the adrenal gland". In: *Journal of neurochemistry* 72.1, pp. 363–372. ISSN: 0022-3042. DOI: 10.1046/J.1471-4159.1999.0720363.X.

Greene, L. A. and A. S. Tischler (July 1976). "Establishment of a noradrenergic clonal line of rat adrenal pheochromocytoma cells which respond to nerve growth factor." In: *Proceedings of the National Academy of Sciences* 73.7, pp. 2424–2428. ISSN: 00278424. DOI: 10.1073/PNAS.73.7.2424.

Halemani, Nagaraj D., Ioanna Bethani, Silvio O. Rizzoli, and Thorsten Lang (Mar. 2010). "Structure and Dynamics of a Two-Helix SNARE Complex in Live Cells". In: *Traffic* 11.3, pp. 394–404. ISSN: 1600-0854. DOI: 10.1111/J.1600-0854.2009.01020.X.

Han, Liping, Tiandan Jiang, Gayoung A. Han, Nancy T. Malintan, Li Xie, Li Wang, Frederick W. Tse, Herbert Y. Gaisano, Brett M. Collins, Frederic A. Meunier, and Shuzo Sugita (Oct. 2009). "Rescue of Munc18-1 and -2 double knockdown

reveals the essential functions of interaction between Munc18 and closed syntaxin in PC12 cells". In: *Molecular Biology of the Cell* 20.23, pp. 4962–4975. ISSN: 10591524.

Hanson, Phyllis I., John E. Heuser, and Reinhard Jahn (1997). "Neurotransmitter release - four years of SNARE complexes". In: *Current opinion in neurobiology* 7.3, pp. 310–315. ISSN: 0959-4388. DOI: 10.1016/S0959-4388(97)80057-8.

He, Enqi, Keimpe Wierda, Rhode Van Westen, Jurjen H. Broeke, Ruud F. Toonen, L. Niels Cornelisse, and Matthijs Verhage (June 2017). "Munc13-1 and Munc18-1 together prevent NSF-dependent de-priming of synaptic vesicles". In: *Nature communications* 8. ISSN: 2041-1723. DOI: 10.1038/NCOMMS15915.

Heerklotz, H. (Nov. 2002). "Triton promotes domain formation in lipid raft mixtures." In: *Biophysical Journal* 83.5, p. 2693. ISSN: 00063495. DOI: 10.1016/S0006-3495(02)75278-8.

Heo, Paul, Jeff Coleman, Jean Baptiste Fleury, James E. Rothman, and Frederic Pincet (Feb. 2021). "Nascent fusion pore opening monitored at single-SNAREpin resolution". In: *Proceedings of the National Academy of Sciences of the United States of America* 118.5. ISSN: 1091-6490. DOI: 10.1073/PNAS.2024922118.

Hess, Douglas T, Ted M Slater, Michael C Wilson, and J H Pate Skene' (1992). "The 25 kDa Synaptosomal-associated Protein SNAP-25 Is the Major Methionine-Rich Polypeptide in Rapid Axonal Transport and a Major Substrate for Palmitoylation in Adult CNS". In: *The Journal of Neuroscience* 12, p. 46344641.

Heumann, R, V Kachel, and H Thoenen (Apr. 1983). "Relationship between NGF-mediated volume increase and "priming effect" in fast and slow reacting clones of PC12 pheochromocytoma cells. Role of cAMP." In: *Experimental cell research* 145.1, pp. 179–90. ISSN: 0014-4827. DOI: 10.1016/s0014-4827(83)80019-6.

Hickson, Gilles R.X., Luke H. Chamberlain, Valerie H. Maier, and Gwyn W. Gould (Apr. 2000). "Quantification of SNARE protein levels in 3T3-L1 adipocytes: implications for insulin-stimulated glucose transport". In: *Biochemical and biophysical research communications* 270.3, pp. 841–845. ISSN: 0006-291X. DOI: 10.1006/BBRC.2000.2525.

Holroyd, Phillip, Thorsten Lang, Dirk Wenzel, Pietro De Ramilli, and Reinhard Jahn (Dec. 2002). "Imaging direct, dynamin-dependent recapture of fusing secretory granules on plasma membrane lawns from PC12 cells". In: *Proceedings of the National Academy of Sciences of the United States of America* 99.26, pp. 16806–16811. ISSN: 00278424.

Jahn, Reinhard and Dirk Fasshauer (Oct. 2012). "Molecular machines governing exocytosis of synaptic vesicles". In: *Nature* 490.7419, pp. 201–207. ISSN: 1476-4687. DOI: 10.1038/NATURE11320.

Jahn, Reinhard and Richard H. Scheller (Aug. 2006). "SNAREs — engines for membrane fusion". In: *Nature Reviews Molecular Cell Biology 2006 7:9* 7.9, pp. 631–643. ISSN: 1471-0080. DOI: 10.1038/nrm2002.

Jakhanwal, Shrutee, Chung-Tien Lee, Henning Urlaub, and Reinhard Jahn (June 2017). " An activated Q- SNARE / SM protein complex as a possible intermediate in SNARE assembly ". In: *The EMBO Journal* 36.12, pp. 1788–1802. ISSN: 0261-4189. DOI: 10.15252/EMBJ.201696270.

Kádková, Anna, Julika Radecke, and Jakob B. Sørensen (Nov. 2019). "The SNAP-25 Protein Family". In: *Neuroscience* 420, pp. 50–71. ISSN: 1873-7544. DOI: 10.1016/J.NEUROSCIENCE.2018.09.020.

Knowles, M. K., S. Barg, L. Wan, M. Midorikawa, X. Chen, and Wolfhard Almers (Nov. 2010). "Single secretory granules of live cells recruit syntaxin-1 and synaptosomal associated protein 25 (SNAP-25) in large copy numbers". In: *Proceedings of the National Academy of Sciences of the United States of America* 107.48, pp. 20810–20815. ISSN: 10916490. DOI: 10.1073/pnas.1014840107.

Kusumi, A., Y. Sako, and M. Yamamoto (1993). "Confined lateral diffusion of membrane receptors as studied by single particle tracking (nanovid microscopy). Effects of calcium-induced differentiation in cultured epithelial cells". In: *Biophysical Journal* 65.5, pp. 2021–2040. ISSN: 00063495. DOI: 10.1016/S0006-3495(93)81253-0.

Kusumi, Akihiro, Yuki M. Shirai, Ikuko Koyama-Honda, Kenichi G.N. Suzuki, and Takahiro K. Fujiwara (May 2010). "Hierarchical organization of the plasma membrane: Investigations by single-molecule tracking vs. fluorescence correlation

spectroscopy". In: *FEBS Letters* 584.9, pp. 1814–1823. ISSN: 0014-5793. DOI: 10.1016/J.FEBSLET.2010.02.047.

Lafont, Frank, Paul Verkade, Thierry Galli, Christian Wimmer, Daniel Louvard, and Kai Simons (Mar. 1999). "Raft association of SNAP receptors acting in apical trafficking in Madin-Darby canine kidney cells". In: *Proceedings of the National Academy of Sciences of the United States of America* 96.7, pp. 3734–3738. ISSN: 00278424.

Lang, Thorsten, Dieter Bruns, Dirk Wenzel, Dietmar Riedel, Phillip Holroyd, Christoph Thiele, and Reinhard Jahn (May 2001). "SNAREs are concentrated in cholesterol-dependent clusters that define docking and fusion sites for exocytosis". In: *The EMBO Journal* 20.9, p. 2202. ISSN: 02614189. DOI: 10.1093/EMBOJ/20.9.2202.

Lang, Thorsten, Martin Margittai, Helmut Hölzler, and Reinhard Jahn (Aug. 2002). "SNAREs in native plasma membranes are active and readily form core complexes with endogenous and exogenous SNAREs". In: *The Journal of cell biology* 158.4, pp. 751–760. ISSN: 0021-9525. DOI: 10.1083/JCB.200203088.

Lillemeier, Björn F., Janet R. Pfeiffer, Zurab Surviladze, Bridget S. Wilson, and Mark M. Davis (Dec. 2006). "Plasma membrane-associated proteins are clustered into islands attached to the cytoskeleton". In: *Proceedings of the National Academy of Sciences of the United States of America* 103.50, pp. 18992–18997. ISSN: 0027-8424. DOI: 10.1073/PNAS.0609009103.

Lindén, M, P Sens, and R Phillips (2012). "Entropic Tension in Crowded Membranes". In: *PLoS Comput Biol* 8.3, p. 1002431. DOI: 10.1371/journal.pcbi.1002431.

Littleton, J. Troy (July 2000). "A Genomic Analysis of Membrane Trafficking and Neurotransmitter Release in Drosophila". In: *Journal of Cell Biology* 150.2, F77–F82. ISSN: 0021-9525. DOI: 10.1083/JCB.150.2.F77.

Loranger, Stephanie S. and Maurine E. Linder (Sept. 2002). "SNAP-25 traffics to the plasma membrane by a syntaxin-independent mechanism". In: *Journal of Biological Chemistry* 277.37, pp. 34303–34309. ISSN: 00219258. DOI: 10.1074/JBC.M202125200.

Low, Seng Hui, Amit Vasanji, Jayasri Nanduri, Min He, Nikunj Sharma, Michelle Koo, Judith Drazba, and Thomas Weimbs (Feb. 2006). "Syntaxins 3 and 4 Are Concentrated in Separate Clusters on the Plasma Membrane before the Establishment of Cell Polarity". In: *Molecular Biology of the Cell* 17.2, p. 977. ISSN: 10591524. DOI: 10.1091/MBC.E05-05-0462.

Ma, Cong, Lijing Su, Alpay B. Seven, Yibin Xu, and Josep Rizo (Jan. 2013). "Reconstitution of the vital functions of Munc18 and Munc13 in neurotransmitter release". In: *Science (New York, N.Y.)* 339.6118, pp. 421–425. ISSN: 1095-9203. DOI: 10.1126/SCIENCE.1230473.

Maidorn, Manuel, Aurélien Olichon, Silvio O. Rizzoli, and Felipe Opazo (Feb. 2019). "Nanobodies reveal an extra-synaptic population of SNAP-25 and Syntaxin 1A in hippocampal neurons". In: *mAbs* 11.2, p. 305. ISSN: 19420870. DOI: 10.1080/19420862.2018.1551675.

Malintan, Nancy T., Tam H. Nguyen, Liping Han, Catherine F. Latham, Shona L. Osborne, Peter J. Wen, Siew Joo Tiffany Lim, Shuzo Sugita, Brett M. Collins, and Frederic A. Meunier (Aug. 2009). "Abrogating Munc18-1-SNARE complex interaction has limited impact on exocytosis in PC12 cells". In: *The Journal of biological chemistry* 284.32, pp. 21637–21646. ISSN: 0021-9258. DOI: 10.1074/JBC.M109.013508.

Margittai, M., J. Widengren, E. Schweinberger, G. F. Schröder, S. Felekyan, E. Haustein, M. König, D. Fasshauer, H. Grubmüller, R. Jahn, and C. A.M. Seidel (Dec. 2003). "Single-molecule fluorescence resonance energy transfer reveals a dynamic equilibrium between closed and open conformations of syntaxin 1". In: *Proceedings of the National Academy of Sciences of the United States of America* 100.26, pp. 15516–15521. ISSN: 00278424. DOI: 10.1073/PNAS.2331232100.

Marrink, Siewert J., Valentina Corradi, Paulo C.T. Souza, Helgi I. Ingólfsson, D. Peter Tieleman, and Mark S.P. Sansom (May 2019). "Computational Modeling of Realistic Cell Membranes". In: *Chemical Reviews* 119.9, pp. 6184–6226. ISSN: 15206890.

Merklinger, Elisa, Jan-Gero Schloetel, Pascal Weber, Helena Batoulis, Sarah Holz, Nora Karnowski, Jé Rô Me Finke, and Thorsten Lang (2017). "The packing density of a supramolecular membrane protein cluster is controlled by cytoplasmic interactions". In: DOI: 10.7554/eLife.20705.001.

Mertins, Jasmin, Jérôme Finke, Ricarda Sies, Kerstin M Rink, Jan Hasenauer, and Thorsten Lang (2021). "The mesoscale organization of syntaxin 1A and SNAP25 is determined by SNARE-SNARE interactions". In: 10, p. 69236. DOI: 10.7554/eLife.

Milosevic, Ira, Jakob B. Sørensen, Thorsten Lang, Michael Krauss, Gábor Nagy, Volker Haucke, Reinhard Jahn, and Erwin Neher (Mar. 2005). "Plasmalemmal phosphatidylinositol-4,5-bisphosphate level regulates the releasable vesicle pool size in chromaffin cells". In: *The Journal of neuroscience : the official journal of the Society for Neuroscience* 25.10, pp. 2557–2565. ISSN: 1529-2401. DOI: 10.1523/JNEUROSCI.3761-04.2005.

Milovanovic, Dragomir, Alf Honigmann, Seiichi Koike, Fabian Göttfert, Gesa Pähler, Meike Junius, Stefan Müllar, Ulf DIederichsen, Andreas Janshoff, Helmut Grubmüller, Herre J. Risselada, Christian Eggeling, Stefan W. Hell, Geert Van Den Bogaart, and Reinhard Jahn (Jan. 2015). "Hydrophobic mismatch sorts SNARE proteins into distinct membrane domains". In: *Nature Communications 2015 6:1* 6.1, pp. 1–10. ISSN: 2041-1723. DOI: 10.1038/ncomms6984.

Misura, Kira M.S., Richard H. Scheller, and William I. Weis (Mar. 2000). "Three-dimensional structure of the neuronal-Sec1–syntaxin 1a complex". In: *Nature 2000 404:6776* 404.6776, pp. 355–362. ISSN: 1476-4687. DOI: 10.1038/35006120.

Mohrmann, Ralf, Heidi De Wit, Matthijs Verhage, Erwin Neher, and Jakob B. Sørensen (Oct. 2010). "Fast vesicle fusion in living cells requires at least three SNARE complexes". In: *Science* 330.6003, pp. 502–505. ISSN: 00368075.

Monk, Peter and Lynda Partridge (July 2012). "Tetraspanins: gateways for infection". In: *Infectious disorders drug targets* 12.1, pp. 4–17. ISSN: 2212-3989. DOI: 10.2174/187152612798994957.

Munch, Anders S., Girish H. Kedar, Jan R.T. van Weering, Sonia Vazquez-Sanchez, Enqi He, Timon André, Thimo Braun, Thomas H. Söllner, Matthijs Verhage,

and Jakob B. Sørensen (June 2016). "Extension of Helix 12 in Munc18-1 Induces Vesicle Priming". In: *Journal of Neuroscience* 36.26, pp. 6881–6891. ISSN: 0270-6474. DOI: 10.1523/JNEUROSCI.0007-16.2016.

Munro, Sean (Nov. 2003). "Lipid rafts: elusive or illusive?" In: *Cell* 115.4, pp. 377–388. ISSN: 0092-8674. DOI: 10.1016/S0092-8674(03)00882-1.

Murray, David H. and Lukas K. Tamm (Oct. 2011). "Molecular mechanism of cholesterol- and polyphosphoinositide-mediated syntaxin clustering". In: *Biochemistry* 50.42, pp. 9014–9022. ISSN: 00062960.

Nagamatsu, Shinya, Tomonori Fujiwara, Yoko Nakamichi, Takashi Watanabe, Hiroshi Katahira, Hiroki Sawa, and Kimio Akagawa (Jan. 1996). "Expression and Functional Role of Syntaxin 1/HPC-1 in Pancreatic β Cells: SYNTAXIN 1A, BUT NOT 1B, PLAYS A NEGATIVE ROLE IN REGULATORY INSULIN RELEASE PATHWAY". In: *Journal of Biological Chemistry* 271.2, pp. 1160–1165. ISSN: 0021-9258. DOI: 10.1074/JBC.271.2.1160.

Nickels, Jonathan D., Jeremy C. Smith, and Xiaolin Cheng (Nov. 2015). "Lateral organization, bilayer asymmetry, and inter-leaflet coupling of biological membranes". In: *Chemistry and Physics of Lipids* 192, pp. 87–99. ISSN: 0009-3084. DOI: 10.1016/J.CHEMPHYSLIP.2015.07.012.

Novick, Peter, Charles Field, and Randy Schekman (1980). "Identification of 23 complementation groups required for post-translational events in the yeast secretory pathway". In: *Cell* 21.1, pp. 205–215. ISSN: 0092-8674. DOI: 10.1016/0092-8674(80)90128-2.

Ochiishi, Tomoyo, Motomichi Doi, Kazuhiko Yamasaki, Keiko Hirose, Akira Kitamura, Takao Urabe, Nobutaka Hattori, Masataka Kinjo, Tatsuhiko Ebihara, and Hideki Shimura (Mar. 2016). "Development of new fusion proteins for visualizing amyloid-β oligomers in vivo". In: *Scientific Reports 2016 6:1* 6.1, pp. 1–15. ISSN: 2045-2322. DOI: 10.1038/srep22712.

Ohara-Imaizumi, Mica, Chiyono Nishiwaki, Toshiteru Kikuta, Konosuke Kumakura, Yoko Nakamichi, and Shinya Nagamatsu (Feb. 2004). "Site of docking and fusion of insulin secretory granules in live MIN6 beta cells analyzed by TAT-conjugated anti-syntaxin 1 antibody and total internal reflection fluorescence

microscopy". In: *The Journal of biological chemistry* 279.9, pp. 8403–8408. ISSN: 0021-9258. DOI: 10.1074/JBC.M308954200.

Opazo, Felipe, Matthew Levy, Michelle Byrom, Christina Schäfer, Claudia Geisler, Teja W. Groemer, Andrew D. Ellington, and Silvio O. Rizzoli (Sept. 2012). "Aptamers as potential tools for super-resolution microscopy". In: *Nature Methods 2012 9:10* 9.10, pp. 938–939. ISSN: 1548-7105. DOI: 10.1038/nmeth.2179.

Ossig, Rainer, Hans Dieter Schmitt, Bert De Groot, Dietmar Riedel, Sirkka Keränen, Hans Ronne, Helmut Grubmüller, and Reinhard Jahn (Nov. 2000). "Exocytosis requires asymmetry in the central layer of the SNARE complex". In: *The EMBO Journal* 19.22, p. 6000. ISSN: 02614189. DOI: 10.1093/EMBOJ/19.22.6000.

Oyler, G. A., G. A. Higgins, R. A. Hart, E. Battenberg, M. Billingsley, F. E. Bloom, and M. C. Wilson (1989). "The identification of a novel synaptosomal-associated protein, SNAP-25, differentially expressed by neuronal subpopulations". In: *The Journal of cell biology* 109.6 Pt 1, pp. 3039–3052. ISSN: 0021-9525. DOI: 10.1083/JCB.109.6.3039.

Pertsinidis, Alexandros, Konark Mukherjee, Manu Sharma, Zhiping P. Pang, Sang Ryul Park, Yunxiang Zhang, Axel T. Brunger, Thomas C. Südhof, and Steven Chu (July 2013). "Ultrahigh-resolution imaging reveals formation of neuronal SNARE/Munc18 complexes in situ". In: *Proceedings of the National Academy of Sciences of the United States of America* 110.30, E2812–E2820. ISSN: 10916490.

Pevsner, Jonathan, Shu Chan Hsu, Janice E.A. Braun, Nicole Calakos, Anthony E. Ting, Mark K. Bennett, and Richard H. Scheller (1994). "Specificity and regulation of a synaptic vesicle docking complex". In: *Neuron* 13.2, pp. 353–361. ISSN: 0896-6273. DOI: 10.1016/0896-6273(94)90352-2.

Pike, Linda J. (July 2006). "Rafts defined: a report on the Keystone symposium on lipid rafts and cell function". In: *Journal of Lipid Research* 47.7, pp. 1597–1598. ISSN: 0022-2275. DOI: 10.1194/JLR.E600002-JLR200.

Predescu, Sanda A., Dan N. Predescu, Kayo Shimizu, Irene K. Klein, and Asrar B. Malik (Nov. 2005). "Cholesterol-dependent syntaxin-4 and SNAP-23 clustering regulates caveolar fusion with the endothelial plasma membrane". In:

The Journal of biological chemistry 280.44, pp. 37130–37138. ISSN: 0021-9258. DOI: 10.1074/JBC.M505659200.

Prinslow, Eric A., Karolina P. Stepien, Yun Zu Pan, Junjie Xu, and Josep Rizo (Jan. 2019). "Multiple factors maintain assembled trans-SNARE complexes in the presence of NSF and αSNAP". In: *eLife* 8. ISSN: 2050084X. DOI: 10.7554/ELIFE.38880.

Ramadurai, Sivaramakrishnan, Andrea Holt, Victor Krasnikov, Geert Van Den Bogaart, J Antoinette Killian, and Bert Poolman (2009). "Lateral Diffusion of Membrane Proteins". In: *ACS Publications*. DOI: 10.1021/ja902853g.

Reshetniak, Sofiia, Rubén Fernández-Busnadiego, Marcus Müller, Silvio O. Rizzoli, and Christian Tetzlaff (Oct. 2020). "Quantitative Synaptic Biology: A Perspective on Techniques, Numbers and Expectations". In: *International Journal of Molecular Sciences 2020, Vol. 21, Page 7298* 21.19, p. 7298. ISSN: 1422-0067. DOI: 10.3390/IJMS21197298.

Ribrault, Claire, Jürgen Reingruber, Maja Petkovic´ Petkovic´, Thierry Galli, Noam E Ziv, David Holcman, and Antoine Triller (2011). "Syntaxin1A Lateral Diffusion Reveals Transient and Local SNARE Interactions". In: *JNEUROSCI*. DOI: 10.1523/JNEUROSCI.4065-11.2011.

Richmond, Janet E. and Kendal S. Broadie (Oct. 2002). "The synaptic vesicle cycle: exocytosis and endocytosis in Drosophila and C. elegans". In: *Current Opinion in Neurobiology* 12.5, pp. 499–507. ISSN: 0959-4388. DOI: 10.1016/S0959-4388(02)00360-4.

Rickman, Colin, Claire N. Medine, Alison R. Dun, David J. Moulton, Ondřej Mandula, Nagaraj D. Halemani, Silvio O. Rizzoli, Luke H. Chamberlain, and Rory R. Duncan (Apr. 2010). "t-SNARE Protein Conformations Patterned by the Lipid Microenvironment". In: *Journal of Biological Chemistry* 285.18, pp. 13535–13541. ISSN: 0021-9258. DOI: 10.1074/JBC.M109.091058.

Ries, Jonas, Charlotte Kaplan, Evgenia Platonova, Hadi Eghlidi, and Helge Ewers (Apr. 2012). "A simple, versatile method for GFP-based super-resolution microscopy via nanobodies". In: *Nature Methods 2012 9:6* 9.6, pp. 582–584. ISSN: 1548-7105. DOI: 10.1038/nmeth.1991.

Rizo, Josep and Junjie Xu (June 2015). "The Synaptic Vesicle Release Machinery". In: *Annual review of biophysics* 44, pp. 339–367. ISSN: 1936-1238. DOI: 10.1146/ANNUREV-BIOPHYS-060414-034057.

Rowe, Joanna, Nicoletta Corradi, Maria Luisa Malosio, Elena Taverna, Philippe Halban, Jacopo Meldolesi, and Patrizia Rosa (June 1999). "Blockade of membrane transport and disassembly of the Golgi complex by expression of syntaxin 1A in neurosecretion-incompetent cells: prevention by rbSEC1". In: *Journal of Cell Science* 112.12, pp. 1865–1877. ISSN: 0021-9533. DOI: 10.1242/JCS.112.12.1865.

Ryan, T. A., J. Myers, D. Holowka, B. Baird, and W. W. Webb (1988). "Molecular crowding on the cell surface". In: *Science (New York, N.Y.)* 239.4835, pp. 61–64. ISSN: 0036-8075. DOI: 10.1126/SCIENCE.2962287.

Sahl, Steffen J, Stefan W Hell, and Stefan Jakobs (2017). "Fluorescence nanoscopy in cell biology". In: *Nature Publishing Group* 18. DOI: 10.1038/nrm.2017.71.

Saka, Sinem K., Alf Honigmann, Christian Eggeling, Stefan W. Hell, Thorsten Lang, and Silvio O. Rizzoli (July 2014). "Multi-protein assemblies underlie the mesoscale organization of the plasma membrane". In: *Nature Communications 2014 5:1* 5.1, pp. 1–14. ISSN: 2041-1723. DOI: 10.1038/ncomms5509.

Salaün, Christine, Gwyn W. Gould, and Luke H. Chamberlain (May 2005). "Lipid Raft Association of SNARE Proteins Regulates Exocytosis in PC12 Cells". In: *The Journal of biological chemistry* 280.20, p. 19449. ISSN: 00219258. DOI: 10.1074/JBC.M501923200.

San Paulo, Alvaro and Ricardo García (Mar. 2000). "High-Resolution Imaging of Antibodies by Tapping-Mode Atomic Force Microscopy: Attractive and Repulsive Tip-Sample Interaction Regimes". In: *Biophysical Journal* 78.3, pp. 1599–1605. ISSN: 0006-3495. DOI: 10.1016/S0006-3495(00)76712-9.

Scheffer, Konstanze D., Alexander Gawlitza, Gilles A. Spoden, Xin A. Zhang, Carsten Lambert, Fedor Berditchevski, and Luise Florin (Mar. 2013). "Tetraspanin CD151 mediates papillomavirus type 16 endocytosis". In: *Journal of virology* 87.6, pp. 3435–3446. ISSN: 1098-5514. DOI: 10.1128/JVI.02906-12.

Schneider, Falk, Taras Sych, Christian Eggeling, and Erdinc Sezgin (Jan. 2021). "Influence of nanobody binding on fluorescence emission, mobility, and organization of GFP-tagged proteins". In: *iScience* 24.1, p. 101891. ISSN: 2589-0042. DOI: 10.1016/J.ISCI.2020.101891.

Schuck, Sebastian, Masanori Honsho, Kim Ekroos, Andrej Shevchenko, and Kai Simons (May 2003). "Resistance of cell membranes to different detergents". In: *Proceedings of the National Academy of Sciences of the United States of America* 100.10, pp. 5795–5800. ISSN: 0027-8424. DOI: 10.1073/PNAS.0631579100.

Schütz, Dagmar, Felipe Zilly, Thorsten Lang, Reinhard Jahn, and Dieter Bruns (May 2005). "A dual function for Munc-18 in exocytosis of PC12 cells". In: *The European journal of neuroscience* 21.9, pp. 2419–2432. ISSN: 0953-816X. DOI: 10.1111/J.1460-9568.2005.04095..

Sezgin, Erdinc, Ilya Levental, Satyajit Mayor, and Christian Eggeling (Mar. 2017). "The mystery of membrane organization: composition, regulation and roles of lipid rafts". In: *Nature Reviews Molecular Cell Biology 2017 18:6* 18.6, pp. 361–374. ISSN: 1471-0080. DOI: 10.1038/nrm.2017.16.

Shen, Jingshi, Shailendra S. Rathore, Lavan Khandan, and James E. Rothman (July 2010). "SNARE bundle and syntaxin N-peptide constitute a minimal complement for Munc18-1 activation of membrane fusion". In: *Journal of Cell Biology* 190.1, pp. 55–63. ISSN: 0021-9525. DOI: 10.1083/JCB.201003148.

Shen, Jingshi, David C. Tareste, Fabienne Paumet, James E. Rothman, and Thomas J. Melia (Jan. 2007). "Selective activation of cognate SNAREpins by Sec1/Munc18 proteins". In: *Cell* 128.1, pp. 183–195. ISSN: 0092-8674. DOI: 10.1016/J.CELL.2006.12.016.

Sieber, Jochen, K. I. Willig, C. Kutzner, C. Gerding-Reimers, B. Harke, G. Donnert, B. Rammner, C. Eggeling, S. W. Hell, H. Grubmüller, and et al. (2007). "Anatomy and Dynamics of a Supramolecular Membrane Protein Cluster". In: *Science* 317.

Sieber, Jochen J, Katrin I Willig, Rainer Heintzmann, Stefan W Hell, and Thorsten Lang (Apr. 2006). "The SNARE motif is essential for the formation of syntaxin clusters in the plasma membrane." In: *Biophysical journal* 90.8, pp. 2843–51. ISSN: 0006-3495. DOI: 10.1529/biophysj.105.079574.

Simons, Kai and Elina Ikonen (1997). "Functional rafts in cell membranes". In: *Nature* 387, pp. 569–572.

Singer, S J and Garth L Nicolson (1972). "The Fluid Mosaic Model of the Structure of Cell Membranes". In: *Science*.

Söllner, Thomas, Sidney W. Whiteheart, Michael Brunner, Hediye Erdjument-Bromage, Scott Geromanos, Paul Tempst, and James E. Rothman (Mar. 1993). "SNAP receptors implicated in vesicle targeting and fusion". In: *Nature 1993 362:6418* 362.6418, pp. 318–324. ISSN: 1476-4687. DOI: 10.1038/362318a0.

Stein, Alexander, Gert Weber, Markus C. Wahl, and Reinhard Jahn (July 2009). "Helical extension of the neuronal SNARE complex into the membrane". In: *Nature 2009 460:7254* 460.7254, pp. 525–528. ISSN: 1476-4687. DOI: 10.1038/nature08156.

Stone, Matthew B., Sarah A. Shelby, Marcos F. Nńñez, Kathleen Wisser, and Sarah L. Veatch (Feb. 2017). "Protein sorting by lipid phase-like domains supports emergent signaling function in b lymphocyte plasma membranes". In: *eLife* 6. ISSN: 2050084X. DOI: 10.7554/ELIFE.19891.

Stone, Matthew B. and Sarah L. Veatch (June 2015). "Steady-state cross-correlations for live two-colour super-resolution localization data sets". In: *Nature Communications 2015 6:1* 6.1, pp. 1–10. ISSN: 2041-1723. DOI: 10.1038/ncomms8347.

Südhof, Thomas C. (July 2012). "The Presynaptic Active Zone". In: *Neuron* 75.1, p. 11. ISSN: 08966273. DOI: 10.1016/J.NEURON.2012.06.012.

Sutton, R. Bryan, Dirk Fasshauer, Reinhard Jahn, and Axel T. Brunger (Sept. 1998). "Crystal structure of a SNARE complex involved in synaptic exocytosis at 2.4Å resolution". In: *Nature 1998 395:6700* 395.6700, pp. 347–353. ISSN: 1476-4687. DOI: 10.1038/26412.

Teng, Felicia Yu Hsuan, Ya Wang, and Bor Luen Tang (2001). "The syntaxins". In: *Genome Biology* 2.11, reviews3012.1. ISSN: 14656906. DOI: 10.1186/GB-2001-2-11-REVIEWS3012.

Toonen, Ruud F., Olexiy Kochubey, Heidi De Wit, Attila Gulyas-Kovacs, Bas Konijnenburg, Jakob B. Sørensen, Jurgen Klingauf, and Matthijs Verhage (Aug. 2006). "Dissecting docking and tethering of secretory vesicles at the target membrane".

In: *The EMBO journal* 25.16, pp. 3725–3737. ISSN: 0261-4189. DOI: 10.1038/SJ.EMBOJ.7601256.

Toonen, Ruud F.G., Klaas Jan De Vries, Robbert Zalm, Thomas C. Südhof, and Matthijs Verhage (June 2005). "Munc18-1 stabilizes syntaxin 1, but is not essential for syntaxin 1 targeting and SNARE complex formation". In: *Journal of Neurochemistry* 93.6, pp. 1393–1400. ISSN: 00223042. DOI: 10.1111/J.1471-4159.2005.03128.X.

Toonen, Ruud F.G. and Matthijs Verhage (Apr. 2003). "Vesicle trafficking: pleasure and pain from SM genes". In: *Trends in Cell Biology* 13.4, pp. 177–186. ISSN: 0962-8924. DOI: 10.1016/S0962-8924(03)00031-X.

Torregrosa-Hetland, Cristina J., José Villanueva, Virginia Garcia-Martínez, Giovanna Expósito-Romero, Maria Del Mar Francés, and Luis M. Gutiérrez (Mar. 2013). "Cortical F-actin affects the localization and dynamics of SNAP-25 membrane clusters in chromaffin cells". In: *The International Journal of Biochemistry & Cell Biology* 45.3, pp. 583–592. ISSN: 1357-2725. DOI: 10.1016/J.BIOCEL.2012.11.021.

Ullrich, Alexander, Mathias A Böhme, Johannes Schöneberg, Harald Depner, Stephan J Sigrist, and Frank Noé (2015). "Dynamical Organization of Syntaxin-1A at the Presynaptic Active Zone". In: *PLoS Comput Biol* 11.9, p. 1004407. DOI: 10.1371/journal.pcbi.1004407.

Vacquier, Victor D. (Mar. 1975). "The isolation of intact cortical granules from sea urchin eggs: Calcium ions trigger granule discharge". In: *Developmental Biology* 43.1, pp. 62–74. ISSN: 0012-1606. DOI: 10.1016/0012-1606(75)90131-1.

Van Den Bogaart, Geert, Karsten Meyenberg, H. Jelger Risselada, Hayder Amin, Katrin I. Willig, Barbara E. Hubrich, Markus Dier, Stefan W. Hell, Helmut Grubmüller, Ulf Diederichsen, and Reinhard Jahn (Oct. 2011). "Membrane protein sequestering by ionic protein–lipid interactions". In: *Nature 2011 479:7374* 479.7374, pp. 552–555. ISSN: 1476-4687. DOI: 10.1038/nature10545.

Verhage, Matthijs, Ascanio S. Maia, Jaap J. Plomp, Arjen B. Brussaard, Joost H. Heeroma, Hendrika Vermeer, Ruud F. Toonen, Robert E. Hammer, Timo K. Van Den Berg, Markus Missler, Hans J. Geuze, and Thomas C. Südhof (Feb. 2000). "Synaptic assembly of the brain in the absence of neurotransmitter secretion".

In: *Science (New York, N.Y.)* 287.5454, pp. 864–869. ISSN: 0036-8075. DOI: 10.1126/SCIENCE.287.5454.864.

Voets, Thomas, Ruud F. Toonen, Elisabeth C. Brian, Heidi De Wit, Tobias Moser, Jens Rettig, Thomas C. Südhof, Erwin Neher, and Matthijs Verhage (Aug. 2001). "Munc18-1 promotes large dense-core vesicle docking". In: *Neuron* 31.4, pp. 581–592. ISSN: 0896-6273. DOI: 10.1016/S0896-6273(01)00391-9.

Wang, Lu, Michelle S. Frei, Aleksandar Salim, and Kai Johnsson (Feb. 2019). "Small-Molecule Fluorescent Probes for Live-Cell Super-Resolution Microscopy". In: *Journal of the American Chemical Society* 141.7, pp. 2770–2781. ISSN: 15205126. DOI: 10.1021/JACS.8B11134/ASSET/IMAGES/LARGE/JA-2018-11134C{_}0008.JPEG.

Watanabe, Michitoshi, Kazushige Nomura, Akihiro Ohyama, Ryoki Ishikawa, Yoshiaki Komiya, Kohei Hosaka, Emiko Yamauchi, Hisaaki Taniguchi, Nobuyuki Sasakawa, Konosuke Kumakura, Tatsuo Ushiki, Osamu Sato, Mitsuo Ikebe, and Michihiro Igarashi (Oct. 2005). "Myosin-Va regulates exocytosis through the submicromolar Ca 2+-dependent binding of syntaxin-1A". In: *Molecular Biology of the Cell* 16.10, pp. 4519–4530. ISSN: 10591524.

Weber, Thomas, Boris V. Zemelman, James A. McNew, Benedikt Westermann, Michael Gmachl, Francesco Parlati, Thomas H. Söllner, and James E. Rothman (Mar. 1998). "SNAREpins: Minimal Machinery for Membrane Fusion". In: *Cell* 92.6, pp. 759–772. ISSN: 0092-8674. DOI: 10.1016/S0092-8674(00)81404-X.

Weidman, P. J., P. Melancon, M. R. Block, and J. E. Rothman (1989). "Binding of an N-ethylmaleimide-sensitive fusion protein to Golgi membranes requires both a soluble protein(s) and an integral membrane receptor". In: *The Journal of cell biology* 108.5, pp. 1589–1596. ISSN: 0021-9525. DOI: 10.1083/JCB.108.5.1589.

Wichmann, Jan and Stefan W. Hell (June 1994). "Breaking the diffraction resolution limit by stimulated emission: stimulated-emission-depletion fluorescence microscopy". In: *Optics Letters, Vol. 19, Issue 11, pp. 780-782* 19.11, pp. 780–782. ISSN: 1539-4794. DOI: 10.1364/OL.19.000780.

Wilhelm, Benjamin G., Sunit Mandad, Sven Truckenbrodt, Katharina Kronert, Christina Schäfer, Burkhard Rammner, Seong Joo Koo, Gala A. Claßen, Michael Krauss,

Volker Haucke, Henning Urlaub, and Silvio O. Rizzoli (2014). "Composition of isolated synaptic boutons reveals the amounts of vesicle trafficking proteins". In: *Science (New York, N.Y.)* 344.6187, pp. 1023–1028. ISSN: 1095-9203. DOI: 10.1126/SCIENCE.1252884.

Wu, Mark N., Karen L. Schulze, Thomas E. Lloyd, and Hugo J. Bellen (2001). "The ROP-Syntaxin interaction inhibits neurotransmitter release". In: *European Journal of Cell Biology* 80.2, pp. 196–199. ISSN: 01719335. DOI: 10.1078/0171-9335-00143.

Yin, Peng, Nikhil R. Gandasi, Swati Arora, Muhmmad Omar-Hmeadi, Jan Saras, and Sebastian Barg (Nov. 2018). "Syntaxin clusters at secretory granules in a munc18-bound conformation". In: *Molecular Biology of the Cell* 29.22, p. 2700. ISSN: 19394586. DOI: 10.1091/MBC.E17-09-0541.

Zhou, Huan Xiang, Germán Rivas, and Allen P. Minton (2008). "Macromolecular crowding and confinement: biochemical, biophysical, and potential physiological consequences". In: *Annual review of biophysics* 37, pp. 375–397. ISSN: 1936-122X. DOI: 10.1146/ANNUREV.BIOPHYS.37.032807.125817.

Zilly, Felipe E, Nagaraj D Halemani, David Walrafen, Luis Spitta, Arne Schreiber, Reinhard Jahn, and Thorsten Lang (Apr. 2011). "Ca2+ induces clustering of membrane proteins in the plasma membrane via electrostatic interactions." In: *The EMBO journal* 30.7, pp. 1209–20. ISSN: 1460-2075. DOI: 10.1038/emboj.2011.53.

Acknowledgements

First and foremost I would like to thank my supervisor Prof. Dr. Thorsten Lang for giving me the opportunity to work in his group and many fruitful discussions. I am grateful for his encouragement and steady support throughout my project.
I also want to thank Thomas Söllner and Kerstin M. Rink who provided me with recombinant Munc18-1 and the overall collaboration. Many thanks for their support and input regarding the project.
Prof. Dr. Jan Hasenauer has to be acknowledged for providing me with the analysis of the RDF (Figure 5.13 E and in my publication) and overall very nice discussions.
I want to thank Jérôme Finke who helped me a lot with the experiments (Figure 5.6; 5.8; 5.13), especially during the time of paper revisions and thereafter.
Thanks to Niko Reppert for cloning of Munc18-1-GFP as well as Ricarda Sies regarding Munc18-1 experiments (Figure 5.16).
I am further grateful for the TRR83 of the DFG who provided me with the necessary funding for this research.
I want to thank the people from AG Burgdorf and AG Thiele for sharing valuable advice and knowledge as well as lab equipment and chemicals.
I want to thank all the current and former lab members, especially Ricarda Sies and Vivien Averesch who helped me in the beginning to get accustomed to the lab.
Many thanks to Dominik Sons, Sara Schmidt, Niko Reppert, Annika Massenberg, Jérôme Finke and Lisa Hitschler for your patient help and the great atmosphere inside and outside of the lab!
My deepest gratitude to Michael Lutter, who has been there in the beginning, yet not at the end.
Thank you so much to Daria Flack, for always being a valuable friend and ally during the good and bad times during my PhD.
For my mother. Even though you have no clue what i did during my PhD, you always supported me.